Springer Theses
Recognizing Outstanding Ph.D. Research

Ting Lei

Design, Synthesis, and Structure-Property Relationship Study of Polymer Field-Effect Transistors

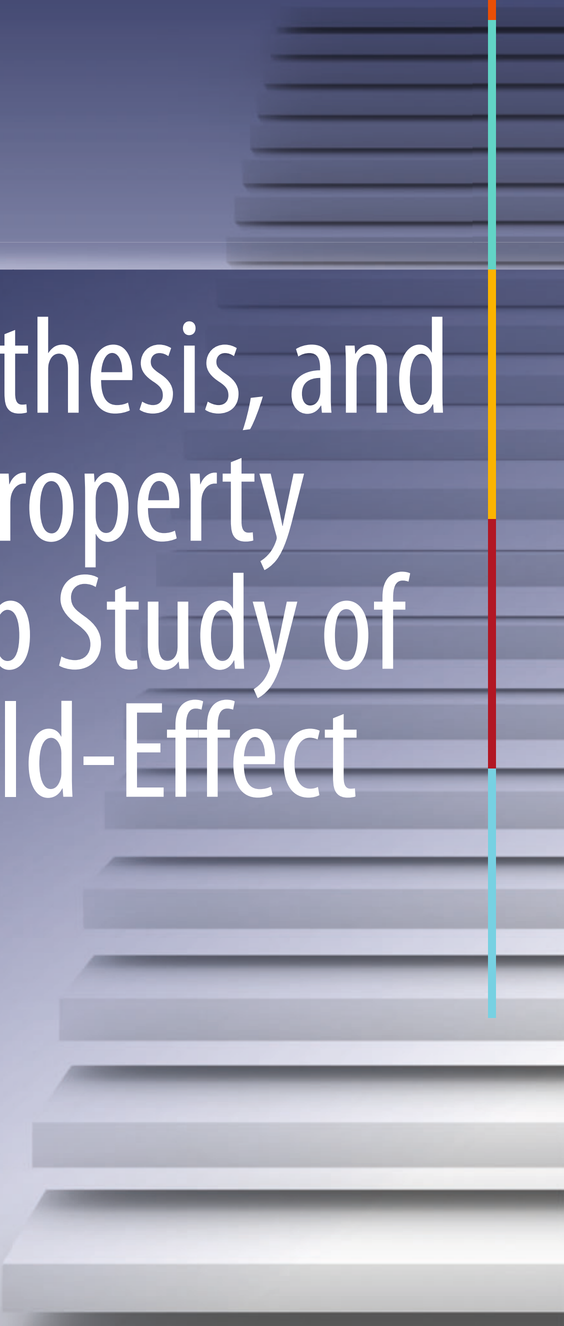

Springer

Springer Theses

Recognizing Outstanding Ph.D. Research

Aims and Scope

The series "Springer Theses" brings together a selection of the very best Ph.D. theses from around the world and across the physical sciences. Nominated and endorsed by two recognized specialists, each published volume has been selected for its scientific excellence and the high impact of its contents for the pertinent field of research. For greater accessibility to non-specialists, the published versions include an extended introduction, as well as a foreword by the student's supervisor explaining the special relevance of the work for the field. As a whole, the series will provide a valuable resource both for newcomers to the research fields described, and for other scientists seeking detailed background information on special questions. Finally, it provides an accredited documentation of the valuable contributions made by today's younger generation of scientists.

Theses are accepted into the series by invited nomination only and must fulfill all of the following criteria

- They must be written in good English.
- The topic should fall within the confines of Chemistry, Physics, Earth Sciences, Engineering and related interdisciplinary fields such as Materials, Nanoscience, Chemical Engineering, Complex Systems and Biophysics.
- The work reported in the thesis must represent a significant scientific advance.
- If the thesis includes previously published material, permission to reproduce this must be gained from the respective copyright holder.
- They must have been examined and passed during the 12 months prior to nomination.
- Each thesis should include a foreword by the supervisor outlining the significance of its content.
- The theses should have a clearly defined structure including an introduction accessible to scientists not expert in that particular field.

More information about this series at http://www.springer.com/series/8790

Ting Lei

Design, Synthesis, and Structure-Property Relationship Study of Polymer Field-Effect Transistors

Doctoral Thesis accepted by
Peking University, Beijing, China

Springer

Author
Dr. Ting Lei
Department of Chemical Engineering
Stanford University
Stanford, CA
USA

Supervisor
Prof. Jian Pei
College of Chemistry and Molecular Engineering
Peking University
Beijing
People's Republic of China

ISSN 2190-5053 ISSN 2190-5061 (electronic)
Springer Theses
ISBN 978-3-662-45666-8 ISBN 978-3-662-45667-5 (eBook)
DOI 10.1007/978-3-662-45667-5

Library of Congress Control Number: 2014956869

Springer Heidelberg New York Dordrecht London

Printed on acid-free paper

Springer-Verlag GmbH Berlin Heidelberg is part of Springer Science+Business Media
(www.springer.com)

Parts of this thesis have been published in the following journal articles:

1. T. Lei, J.-Y. Wang, and J. Pei, "Design, Synthesis, and Structure-Property Relationship of Isoindigo-Based Conjugated Polymers", *Acc. Chem. Res.* **2014**, *47*, 1117.
2. T. Lei, X. Xia, J.-Y. Wang, C.-J. Liu, and J. Pei, "Conformation Locked" Strong Electron-Deficient Poly(*p*-Phenylene Vinylene) Derivatives for Ambient-Stable n-Type Field-Effect Transistors: Synthesis, Properties, and Effects of Fluorine Substitution Position", *J. Am. Chem. Soc.***2014**. *136*, 2135.
3. T. Lei, J.-Y. Wang, and J. Pei, "Roles of Flexible Chains in Organic Semiconducting Materials", *Chem. Mater.* **2014**, *26*, 594.
4. T. Lei, J.-H. Dou, X.-Y. Cao, J.-Y. Wang, and J. Pei, "Electron-Deficient Poly (*p*-Phenylene Vinylene) Provides Electron Mobility over 1 cm^2 V^{-1} s^{-1} under Ambient Conditions", *J. Am. Chem. Soc.* **2013**, *135*, 12168.
5. T. Lei, J.-H. Dou, X.-Y. Cao, J.-Y. Wang, and J. Pei, "A BDOPV-based Donor–Acceptor Polymer for High-Performance n-Type and Oxygen-Doped Ambipolar Field-Effect Transistors", *Adv. Mater.* **2013**, *25*, 6589.
6. T. Lei, J.-H. Dou, Z.-J. Ma, C.-J. Liu, and J. Pei, "Chlorination as a Useful Method to Modulate Conjugated Polymers: Balanced and Ambient-Stable Ambipolar Field-Effect Transistors and Inverters Based on Chlorinated Isoindigo Polymers", *Chem. Sci.* **2013**, *4*, 2447.
7. T. Lei, J.-H. Dou, Z.-J. Ma, C.-H. Yao, C.-J. Liu, and J. Pei, "Ambipolar Polymer Field-Effect Transistors Based on Fluorinated Isoindigo: High Performance and Improved Ambient Stability", *J. Am. Chem. Soc.* **2012**, *134,* 20025.
8. T. Lei, J.-H. Dou, and J. Pei, "Influence of Alkyl Chain Branched Positions on the Hole Mobilities of Polymer Thin-Film Transistors", *Adv. Mater.* **2012**, *24*, 6451.
9. T. Lei, Y. Cao, X. Zhou, Y. Peng, J. Bian, J. Pei, "Systematic Investigation of Isoindigo-Based Polymeric Field-Effect Transistors: Design Strategy and Impact of Polymer Symmetry and Backbone Curvature", *Chem. Mater.* **2012**, *24*, 1762.
10. T. Lei, Y. Cao, Y. Fan, C.-J. Liu, S.-C. Yuan, and J. Pei, "High-Performance Air-Stable Organic Field-Effect Transistors: Isoindigo-Based Conjugated Polymers", *J. Am. Chem. Soc.* **2011**, *133,* 6099.

Supervisor's Foreword

Solution-processable semiconducting polymers are emerging as a promising candidate for next generation electronics applications; they are lightweight and flexible, and have low production cost. Polymer field-effect transistors (FETs), in particular, are fundamental components for polymer-based electronics. They are also used as a tool for fundamental understanding of charge transport capability of polymer semiconductors.

Aimed at developing high-mobility and high-stability polymer FETs, Dr. Ting Lei first unearthed "isoindigo" for polymer FETs. Starting with the investigation of side chain effects, Ting demonstrated the great values and bright vista of isoindigo for polymer FETs and proposed a novel design strategy "molecular docking." To further improve the device performance and ambient stability, several other design strategies, such as using farther branched alkyl chains, modulating polymer energy levels, and locking polymer backbone conformations, have been proposed. The development of high election-mobility polymers has always been a challenging issue. Based on the concept of π-extended isoindigo, Ting developed a new strong electron-deficient building block—BDOPV. By applying the strategies successfully used in isoindigo polymers, BDOPV-based polymers exhibited high electron mobilities and outstanding stability for both n-type and ambipolar FETs, demonstrating their broad applications in organic electronics.

This thesis is highly original and its results not only significantly deepen our understanding of polymer FETs but also provide a series of materials with great practical values. I feel very lucky to have Ting as one of my Ph.D. students because he is a highly self-motivated and creative student. He taught me something new during his Ph.D. study. This thesis has paved a way for further development of high-performance conjugated polymers and better understanding of the structure–property relationship in polymer semiconductors.

Beijing, July 2014 Prof. Jian Pei

Acknowledgments

I would like to express the deepest appreciation to my advisor, Prof. Jian Pei. It has been eight years since I joined his group when I was a sophomore. I feel privileged to have been able to receive Prof. Pei's instructions during the most important years in my life. From the great fondness for chemistry to the completion of this thesis, my every step and every achievement would not have been possible without the guidance and efforts of Prof Pei. When I suffered from depression in the face of difficulties, Prof. Pei's support and encouragement gave me strength and confidence. His diligence, vast knowledge, rigorous scholarship, and keen insight into the science frontier has had a profound influence on me.

I would like to thank Prof. Yuguo Ma and Prof. Dahui Zhao for their guidance and help during my doctorate study period. I also want to thank all the professors in Institute of Organic Chemistry. The positive academic atmosphere and various teaching and communication platforms enriched my knowledge. I thank Prof. Jiang Bian and Yang Peng for providing help in theoretical calculation, Prof. Dehai Liang and Dr. Cui Zheng for assistance in dynamic light scattering.

I am also especially indebted to Dr. Jia Luo for mentoring me on organic synthesis, Dr. Yan Zhou for guiding me on device fabrication, Dr. Yue Cao and Jin-Hu Dou for their great helps in compound synthesis, and all my colleagues for their helps in both work and life. My special appreciation goes to Prof. Xiao-Yu Cao for his fruitful discussion and help in paper writing.

Thanks to my parents for everything they have given to me. You support me with your love and considerate care. You are my strong backing! I am also grateful to my wife, Li Wang. You make my life colorful and give me strong support and encouragement.

Finally, loving thanks to all my teachers, classmates, friends, and relatives.

Stanford, July 2014 Dr. Ting Lei

Contents

Abbreviations

AFM	Atomic force microscope
AMOLED	Active matrix organic light emitting diode
BBT	Benzobisthiadiazole
BDOPV	Benzodifurandione-based oligo(*p*-phenylene vinylene)
BDPPV	Benzodifurandione-based poly(*p*-phenylene vinylene)
BHJ	Bulk heterojunction
BT	Benzothiadiazole
DFT	Density functional theory
DPP	Diketopyrrolopyrrole
DSC	Differential scanning calorimetry
ESI	Electrospray ionization
GIXD	Grazing-incident X-ray diffraction
GPC	Gel permeation chromatography
HOMO	Highest occupied molecular orbital
HT-GPC	High-temperature gel permeation chromatography
II or IID	Isoindigo
LCD	Liquid crystal display
LUMO	Lowest unoccupied molecular orbital
MOSFET	Metal oxide semiconductor field-effect transistor
MS	Mass spectrometry
NDI	Naphthalene diimide
NMR	Nuclear magnetic resonance
OFET	Organic field-effect transistor
OLED	Organic light-emitting diode
OPV	Organic photovoltaic
OSC	Organic solar cells
P3HT	Poly(3-hexylthiophene)
PCE	Power conversion efficiency
PES	Photoemission spectroscopy
PPV	Poly(*p*-phenylene vinylene)
PR-TRMC	Pulse-radiolysis time-resolved microwave conductivity

PT	Polythiophene
RFID	Radio frequency identification
TFT	Thin film transistors
TGA	Thermogravimetric analysis
XRD	X-ray diffraction

Chapter 1
Introduction

1.1 Research Background

Materials, energy, and information technology are widely considered as the three pillars of modern civilization. Materials science provides the basic platform for the exploration of new energy and the development of information technology, becoming one of the most important impetus for the development of human society. From the functional perspective, materials can be categorized into structural and functional materials. Structural materials are those that bear load. The key properties of materials in relation to bearing load are mechanical properties. They are broadly applied to construction, packaging, industrial production, etc. Functional materials display physical and chemical properties, such as optical, electrical, and magnetic proprieties which are of use. They are mainly used in high-tech industries, such as microelectronics, biology, and medicine. Because functional materials have played a key role in many cutting-edge technologies, they are currently becoming the core of materials science research. All materials are categorized as either organic or inorganic. For inorganic materials, atoms first form chemical bonds (e.g., ionic bond, covalent bond, and metallic bond), and then form solid materials by arranging themselves orderly. Inorganic materials are stable and have exhibited a lot of electronic properties. Conventional inorganic materials such as silicon-based semiconductors have been well developed and become the basis of new energy and information technology. Reduction in size often does more than simply make things smaller. In the last two decades, inorganic nanomaterials, including zero-dimensional quantum dots, one-dimensional nanowires and carbon nanotubes, and two-dimensional graphene, have experienced enormously growth. Apart from simply miniaturization, electronic, optical, magnetic, and mechanical properties will change significantly below certain size scale due to quantum confinement of electrons or Wannier excitons [1]. Because of their interesting physical and chemical properties, nanomaterials have attracted broad interdisciplinary interests in areas ranging from physical, chemical, and biological sciences to medical and engineering fields [2]. Unlike inorganic

T. Lei, *Design, Synthesis, and Structure-Property Relationship Study of Polymer Field-Effect Transistors*, Springer Theses, DOI 10.1007/978-3-662-45667-5_1

materials, organic materials are formed by molecules via weak van der Waals interactions. This difference makes organic materials less stable than inorganic materials and not suitable for charge carrier transport. At the present time, organic materials, particularly polymers, are mainly used as structural materials. Compared with inorganic materials, organic materials are light-weight, low-cost, flexible, and suitable for large-area solution process. In addition, organic materials can be readily modified and provide great opportunities for diverse functions and applications.

Organic materials are generally considered as insulating materials because they are mainly formed through van der Waals interactions. In the 1970, Heeger et al. discovered that under certain doping conditions the polyacetylene can be highly conductive, comparable to some inorganic conductors [3, 4]. This breakthrough changed the traditional view on organic materials and opened up a new research field named organic electronics. In the late 1980s, several optoelectronic applications of organic semiconducting materials, such as organic light-emitting diodes (OLED) [5], organic photovoltaics (OPV) [6], and organic field-effect transistors (OFET) [7] etc. were successfully developed, demonstrating a bright vista for diverse applications of organic materials. Currently the investigation of organic semiconductors is a research hotspot in both academia and industry.

OLED is a light-emitting diode (LED) in which the emissive electroluminescent layer is a film of organic compound which transforms electric energy to optical energy under electricity. In an applied electric field, electrons and holes are injected into organic compounds to form excitons, which will go back to ground state along with emitting light. Compared with liquid crystal display (LCD), OLED can significantly reduce power consumption and achieve lightweight, ultra-thin, and flexible displays. Samsung has already applied OLED display to mobile phones, and LG also launched 55-in. AMOLED (Active Matrix OLED) TV in 2013.

OPV or organic solar cell (OSC), is a type of electronic device that uses organic polymers or small molecules for light absorption and charge transport to produce electricity from sunlight by the photovoltaic effect. Under incident light, organic materials can be excited to produce excitons which will be separated into electrons and holes at the interface between two different materials. In a built-in electric field, electrons and holes move toward two electrodes to generate electricity. In the 1980s, Tang developed the first OSC based on a bilayer device structure and demonstrated a power conversion efficiency (PCE) of 1 % [6]. In order to avoid the disadvantages in bilayer OPVs, such as weak absorption and low exciton dissociation efficiency, Heeger et al. mixed conjugated polymer Poly[2-methoxy-5-(2-ethylhexyloxy)-1, 4-phenylenevinylene] (**MEH-PPV**) with C_{60} derivative and developed bulk heterojunction (BHJ) solar cell structure [8, 9]. In the last few years, BHJ solar cell has experienced a rapid development with PCE increasing rapidly from 5 % to over 10 % [10, 11].

OFET is one of the most basic component for logic circuits, which can be used in radio frequency identification (RFID) tags, electronic papers, and flat-panel displays. They are also used as a tool for the characterization of charge transport capability of organic semiconductors. Charge carrier mobility is a key parameter for organic semiconductors, which represents the velocity of charge carrier moving through the channel of an OFET under an applied electrical field. In 1983, Ebisawa et al. reported a FET device using polyacetylene as the semiconducting layer [12], but the device only showed very weak switching features. In 1986, Tsumura et al. reported an OFET device based on polythiophene that displayed typical output characteristics, which is considered as the first OFET [7]. Since then, this field has received increasing attention and thousands of papers concerning both small molecule and polymer FETs have been published. The charge carrier mobility increased from 10^{-5} to over 30 $\mathrm{cm^2\ V^{-1}\ s^{-1}}$ [13], surpassing that of amorphous silicon and comparable to that of polycrystalline silicon.

Besides the above three main fields, organic semiconducting materials have also been widely used as active materials in photodetectors [14], light pumped lasers [15, 16], non-linear optics [17], bio/chemical sensor [18], etc. These applications also utilize the optoelectronic properties of organic materials to realize certain functions, but the chemical structures and device fabrications are different. In all these field, structure-property relationship is always an essential issue, which requires significant efforts on exploring the complex relationships among molecule structure, aggregation behavior, and device performance.

1.2 Polymer Field-Effect Transistors

1.2.1 Introduction of OFET

Field-effect transistors (FETs) is one of the most important and basic components in semiconducting devices. They have been widely used in computers, communications, and information technologies. Inorganic single-crystal FETs [e.g., metal-oxide-semiconductor field-effect transistor (MOSFET)] are fabricated using conventional inorganic semiconducting materials such as Si and GaAs. They have become the mainstream technology of semiconducting industry. However, the fabrication process of such transistors usually needs high temperature (>1,000 °C), which cannot be used on heat-sensitive substrates such as glass and plastics [19]. In order to use FETs on these substrates, thin film transistors (TFTs) were developed and have been widely applied to the control circuits of flat panel display (e.g., LCD). The fabrication process of TFTs generally needs the deposition of several thin layers, including electrode layer, dielectric layer, and semiconducting layer. The most widely used TFTs in LCD is hydrogenated amorphous silicon (α-Si:H), which can be deposited in thin films at low temperatures onto a variety of substrates. However, α-Si is not transparent with low mobility (0.1–1 $\mathrm{cm^2\ V^{-1}\ s^{-1}}$) and poor flexibility. Therefore it cannot be used for high performance AMOLED display and flexible or transparent devices.

OFET has broad applications for the next generation logic circuits, displays, and RFIDs due to its low-cost, light-weight, mechanical flexibility, and compatibility with heat-sensitive substrates [20]. Furthermore, one of the most important process

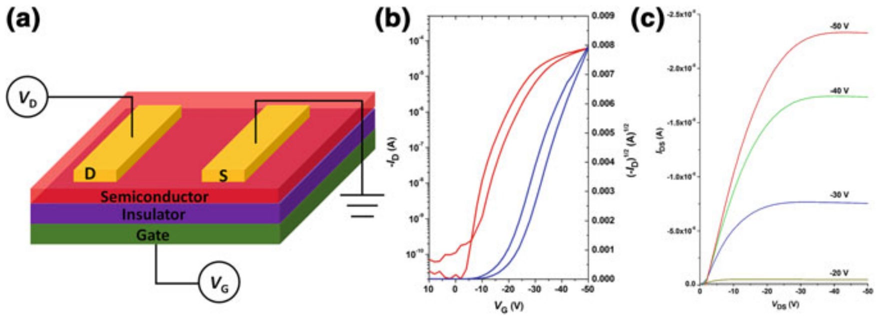

Fig. 1.1 **a** Schematic diagram of an OFET device structure. A typical OFET **b** transfer and **c** output characteristics

in OLEDs and OPVs is charge carrier transport in organic compounds [21]. Charge carrier mobility is a key parameter to investigate the charge transport process and can be determined by several methods, such as Hall effect (suitable for high-mobility materials), space-charge limited current (SCLC, only for low-mobility materials), surface-charge decay, transient current measurement, time of flight, and field-effect method [22]. Field-effect method is realized by fabricating FET devices. Thus OFET study is meaningful for both practical applications and deep understanding of the carrier transport mechanism.

An OFET is a three-terminal device, which consists of three electrodes (gate, source (S), and drain (D)), one insulating layer (or dielectric layer), and one semiconducting layer (Fig. 1.1a). When the gate electrode does not apply voltage, there is no induced charge carriers in the semiconducting layer, and no current passes through the channel between source and drain electrodes. When applying a voltage on the gate electrode, the dielectric layer can capacitively induce charges in the semiconducting layer, and electrical current is generated under voltage bias between drain and source electrodes. FET can be divided into three categories based on the majority charge carriers, namely p-type (holes), n-type (electrons), and ambipolar FETs. Ambipolar FETs can transport both holes and electrons under different gate voltages. OFETs generally need two electrical characterizations: (1) apply constant drain–source voltage (V_{DS} or V_D), scan gate voltage (V_{GS} or V_G) and measure the drain–source current (I_{DS}) to obtain transfer characteristics (Fig. 1.1b); (2) apply constant gate voltage (V_{GS}), scan drain–source voltage (V_{DS}) and measure drain–source current (I_{DS}) at the same time to obtain output characteristics (Fig. 1.1c). The key parameters to evaluate the performance of an OFET device is charge carrier mobility (μ), current on/off ratio (I_{ON}/I_{OFF}), threshold voltage (V_T), and subthreshold swing (S).

Similar to inorganic MOSFETs, the output curves of OFETs also have linear and saturation regimes. While devices working in linear region ($V_{DS} < V_G - V_T$), charge carrier mobility (μ_{lin}) can be calculated by the following formula:

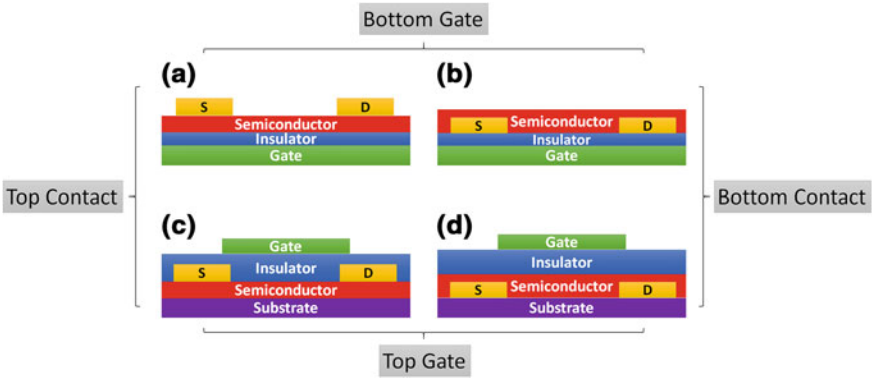

Fig. 1.2 Four device architectures for OFET: **a** bottom-gate top-contact structure; **b** bottom-gate bottom-contact structure; **c** top-gate top-contact structure; **d** top-gate bottom-contact structure

$$I_{DS} = \frac{W}{L}\mu_{\text{lin}} C_{\text{i}} (V_{\text{G}} - V_{\text{T}}) V_{DS} \tag{1.1}$$

While device working in saturation region ($V_{DS} > V_G - V_T$), charge carrier mobility (μ_{sat}) can be calculated by the following formula:

$$I_{DS} = \frac{W}{2L}\mu_{\text{sat}} C_{\text{i}} (V_{\text{G}} - V_{\text{T}})^2 \tag{1.2}$$

where W is channel width, L is channel length, C_i is the capacitance of the dielectric layer. The mobility in the saturation regime can be directly extracted from the slope of linear fitting of ${I_{DS}}^{1/2}$ versus V_G. In general, the saturation mobility is higher than that in the linear regime, because more charge traps have been filled. In this book, all the mobilities are characterized using the saturation region mobility, unless otherwise mentioned.

Different deposition orders of the device layers lead to different device architectures of OFETs (Fig. 1.2). According to the gate electrode position and the contact between drain/source electrode and semiconductor, there are four possible device structures: bottom-gate top-contact (BGTC), bottom-gate bottom-contact (BGBC), top-gate top-contact (TGTC), and top-gate bottom-contact (TGBC). Although the device performance is mainly determined by semiconductors, device structures can greatly affect the charge injection and contact resistance. For p-type materials, BGTC and BGBC structures are often used, whereas TGBC structures are mostly used for ambipolar and n-type OFETs to reduce the oxygen and water influences. Because of the different device injection pathways, BGBC and TGBC structures are generally considered to have smaller injection barriers [23]. In this book, we use the BGTC structure to fabricate p-type OFETs and the TGBC structure for ambipolar and n-type OFETs.

Small molecule FET materials are well developed in the last decades, because they usually have high purity with ordered crystal packing and their crystal structures can be readily resolved. In 2011, Hasegawa et al. reported a solution-processed small molecule thin film device by inkjet printing and they obtained very high hole mobility surpassing 30 cm^2 V^{-1} s^{-1}, very promising for large-area low-cost applications [13]. However, to achieve high-mobility in small molecule materials, a highly crystalized semiconducting layer is usually required. It is hard to realize flexible devices for small molecule materials. Moreover, single crystals are often brittle and temperature sensitive, which limits the applications of OFETs. Compared with small molecules, polymer materials are usually in amorphous or semi-crystalline states, enabling better solution-processability, mechanical flexibility, and temperature stability. The past few years have witnessed momentous changes in the mobility of conjugated polymers and a number of polymers have exhibited mobilities over 1 cm^2 V^{-1} s^{-1} with notably improved ambient stability. Before the discussion of different conjugated polymers, some theoretical considerations of charge carrier transport in conjugated polymers are discussed for better understanding the structure-property relationships in conjugated polymers.

1.2.2 Charge Transport Mechanism in Conjugated Polymers

Charge transport in polymer films generally contains two processes: intrachain and interchain transport (Fig. 1.3a). Intrachain transport (Fig. 1.3a, route 1) is realized by π-electron delocalization along polymer backbones, providing high carrier mobility according to theoretical prediction. The intrachain transport is largely determined by the effective conjugation length of the polymer, which is limited by the torsional disorder along polymer backbone and the presence of chemical defects [24]. Using pulse-radiolysis time-resolved microwave conductivity (PR-TRMC) measurement, Prins et al. reported that the intrachain mobility of a ladder-type poly

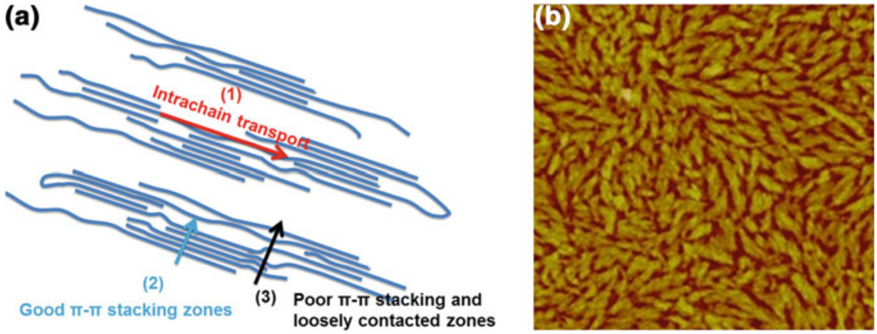

Fig. 1.3 **a** Charge transport process in polymer FETs and **b** a typical AFM height image of polymer films

(p-phenylene) polymer can be as high as 600 $\mathrm{cm}^2\ \mathrm{V}^{-1}\ \mathrm{s}^{-1}$ [25], considerably higher than the mobilities found for small-molecule single crystals. Therefore, reducing the torsional angles or using shape-persistent backbones might improve the effective conjugation length and thereby increase the intrachain transport. Furthermore, because the intrachain transport is much faster than the interchain one, polymers with higher molecular weight usually display higher mobilities, which has been demonstrated in many polymers [26, 27].

In polymer films, there are generally crystallized and amorphous zones, as indicated by the atomic force microscopy (AFM) image in Fig. 1.3b. Thus interchain transport is generally classified into two pathways: (i) transport at ordered packing zones, which may adopt a hopping mechanism like orderly packed small molecules (Fig. 1.3a, route 2); (ii) transport at loosely contacted zones, where carrier transport is slow (Fig. 1.3a, route 3). Thus ordered molecular packing in film will reduce the loosely contact zones, thereby improving interchain transport.

For route 2, charge transport mechanism is similar to the "hopping mechanism" of small molecules. According to the charge transport theory developed by Brédas et al. [22], the charge carrier transport in organic materials can be described by Marcus electron transfer theory (Eq. 1.3). In organic crystals, the ΔG^0 is 0 because the electron transfer happens in a same kind of molecules. Thus the Eq. 1.3 formula can be simplified into Eq. 1.4 as follows:

$$k = \frac{2\pi}{\hbar} V^2 \sqrt{\frac{1}{4\pi k_{\mathrm{B}} T \lambda}} \exp\left[-\left(\Delta G^0 + \lambda\right)^2 / 4\lambda k_{\mathrm{B}} T\right] \tag{1.3}$$

$$k = \frac{V^2}{\hbar} \left(\frac{\pi}{\lambda k_{\mathrm{B}} T}\right)^{\frac{1}{2}} \exp\left(-\frac{\lambda}{4 k_{\mathrm{B}} T}\right) \tag{1.4}$$

where T designates temperature, k_{B} is Boltzmann's constant. So there are two key parameters that determine charge carrier transport speed (k): reorganization energy (λ) and electronic coupling (V). From their mathematical relationship, we can see that the smaller the reorganization energy and the larger electronic coupling, the faster the carrier can transport.

In the process of charge carrier transport, organic molecules change between neutral state and charged state constantly. Reorganization energy reflects the energy that organic molecule needs to change its structure after electron transfer (Fig. 1.4): It contains two relaxation energies: (1) one molecule changes from neutral state to charged state (λ^1) and (2) the other molecule changes from charged state to neutral state (λ^2). Large structure changes in charge transfer process generally result in high reorganization energy. Thus a rigid molecule with a shape-persistent backbone usually has lower reorganization energy. Electronic coupling (or charge transfer integral) is determined by the relative position and frontier orbital distribution of organic molecules. Generally, the closer the π–π distance between two molecules, the stronger the electron coupling. Brédas et al. investigated the evolution of the hole and electron transfer integrals in cofacial dimers when one of the tetracene

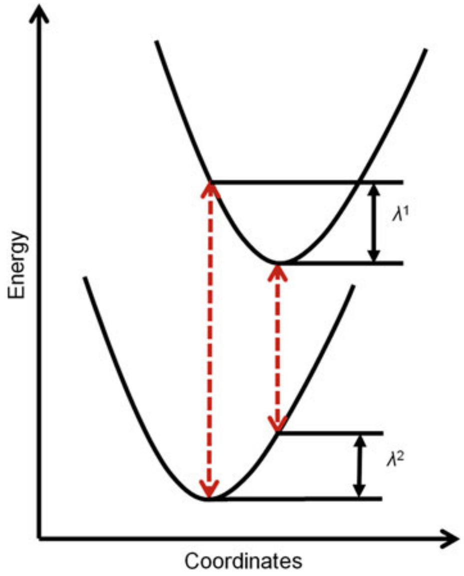

Fig. 1.4 Sketch of the potential energy surfaces for neutral state and charged molecule state, showing the vertical transitions. The reorganization energy equals the sum of all the relaxation energies $\lambda^1 + \lambda^2$

molecules is translated along its long or short axis [22]. As expected, the overall effect of such displacements is to reduce the wavefunction overlap and thus the electronic coupling. However, the most interesting result is the appearance of oscillations in the values of the couplings for translations along the long molecular axis. As a consequence, even small translations can lead to significantly different electronic coupling for both holes and electrons. In practical problems, the calculation of the intermolecular electron coupling is almost based on already known molecular single crystal structures because of the inability to predict molecular single crystal arrangement by computational method. Similar to small molecule, the interchain charge carrier transport of conjugated polymers can also be evaluated by the above theory. Recently, a few papers reported qualitative investigation on the intrachain transport of conjugated polymers [28]. However, quantitatively predicting the interchain transport seems impossible due to the great difficulty in resolving the polymer packing structures in solid state.

Briefly, to increase the carrier mobility of conjugated polymers in film, several molecular design strategies are always employed: (1) decrease the defects in polymer chain and increase the efficient conjugation length; (2) increase molecular weight of polymers; (3) improve π–π stacking interactions and polymer packing order in film; (4) decrease intrachain π–π stacking distance and modulate the interchain packing conformations to achieve large electronic coupling.

1.2.3 Recent Development of Polymer Field-Effect Transistors

In 1986, Tsumura et al. reported the first OFET using polythiophene (**PT**) as the semiconducting layer [7]. The **PT** was obtained by electrochemical polymerization with poor film quality and low mobility of ~10^{-5} $cm^2\ V^{-1}\ s^{-1}$. Because of the low mobility of conjugated polymers, polymer based OFETs did not attract many attentions. Recently, the development of novel building blocks and fabrication processes have led to significant progress of polymer semiconductors and a number of conjugated polymers have displayed high mobilities of over 1 $cm^2\ V^{-1}\ s^{-1}$.

The introduction of alkyl side chains can significantly increase the solubility of **PT** and improve the film quality of the semiconducting layer. The most successful example is poly(3-hexylthiophene) (**P3HT**) system. **P3HT** was first synthesized by random polymerization. The asymmetry of 3-substituted thiophenes results in three possible couplings (Fig. 1.5): head-to-head (HH), tail-to-tail (TT), and head-to-tail (HT). HH connection produces great steric hindrance and large dihedral angles in polymer backbone, leading to weak π–π stacking interactions and less ordered molecular packing in film. Using regioselective synthetic strategy, regioregular **P3HT** (**rr-P3HT**) with HT connection was obtained [29, 30], and **rr-P3HT** with regioselectivity of over 98 % can be readily obtained from many commercial source. High regioselectivity is essential to achieve high mobility for **P3HT** [29, 30]. Furthermore, polymer molecular packing also affects the carrier transport. In thin film, **rr-P3HT** has two types of molecular packing on substrate: edge-on packing and face-on packing. **rr-P3HT** with edge-on packing displayed hole mobility of up to 0.1 $cm^2\ V^{-1}\ s^{-1}$, which is two orders of magnitude higher than that of **rr-P3HT** with face-on packing [31].

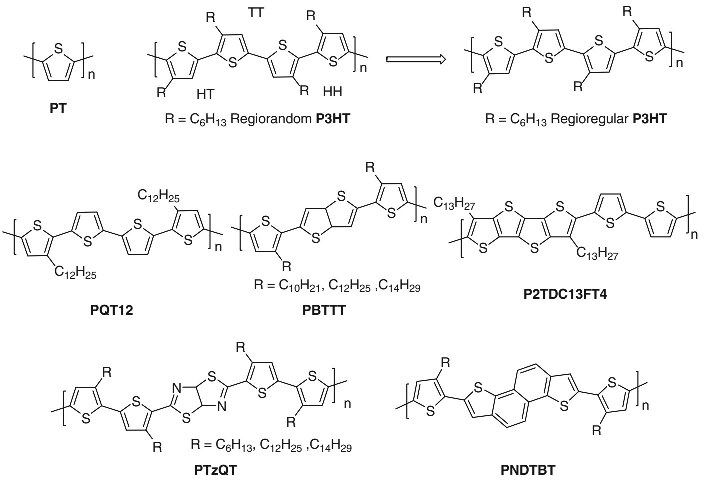

Fig. 1.5 Thiophene-based polymer FET materials

To avoid regioselectivity problem in **P3HT**, Ong et al. developed **PQT12** for polymer FETs [32]. They chose longer dodecyl chains to ensure the good solubility of the polymer. **PQT12** was synthesized by $FeCl_3$ catalyzed oxidative polymerization and displayed similar lamellar packing to **P3HT** with good crystallinity. By using BG/TC device structure, **PQT12** exhibited the highest hole mobility of 0.14 $cm^2\ V^{-1}\ s^{-1}$ and good air stability. Another important method to improve polymer mobility is introducing fused rings in polymer backbone, which may increase the rigidity of polymer backbone and lead to ordered molecular packing. McCulloch et al. reported **PBTTT** system using thienothiophene as a building block and investigated the influence of the alkyl side chain lengths on device performance [33]. Because of the long alkyl chains, these polymers exhibited liquid crystal phase under certain temperature. All the **PBTTT** with different alkyl chain lengths showed mobilities of 0.2–0.6 $cm^2\ V^{-1}\ s^{-1}$, and **PBTTT** with $C_{14}H_{29}$ side chains displayed the highest hole mobility of 0.72 $cm^2\ V^{-1}\ s^{-1}$. After introducing thienothiophene, **PBTTT** showed a HOMO level of –5.1 eV, 0.3 eV lower than that of **P3HT**, which provided this polymer with much better ambient stability than **P3HT** under low-humidity ($R_H = \sim 4\ \%$) air. Besides thienothiophene unit, other large fused aromatics, such as dithieno[3,2-*b*:2′3′-*d*]thiophene [34], tetrathienoacene [35], and pentathienoacene [36], were also used as building blocks for polymer FET materials. He et al. used a tetrathienoacene derivative as building block and synthesized polymer **P2TDC13FT4**. This polymer showed high hole mobilities of up to 0.33 $cm^2\ V^{-1}\ s^{-1}$ [37]. Furthermore, they also synthesized larger fused aromatics for polymer FETs. However, they found that a larger fused aromatics did not necessarily mean a higher mobility; instead, the symmetry of a molecule played a significant role in device performance and molecules with C_2-symmetry usually had higher mobility.

Although many thiophene-based polymers were reported with mobilities over 0.5 $cm^2\ V^{-1}\ s^{-1}$ and on/off ratios over 10^6 [33], their stability is unsatisfactory under ambient conditions. An effective approach to improve the stability is to introduce electron-deficient aromatic rings into the backbone of polythiophene to lower the HOMO level of the polymer. Osaka et al. reported conjugated polymers based on thiazolothiazole (e.g. polymer **PTzQT**) [38] and benzobisthiazole [39]. Because of the non-bonding interactions between nitrogen atoms in the thiazole rings and sulfur atoms in the thiophene rings, the introduction of thiazole efficiently improved the rigidity and planarity of polymer backbones, which ensured good intrachain conjugation and interchain π–π stacking. These polymers all exhibited highly ordered lamellar packing, in which **PTzQT** with $C_{14}H_{29}$ side chains showed the maximum mobility of 0.3 $cm^2\ V^{-1}\ s^{-1}$. Similar polymers based on benzobisthiazole also showed good mobilities of up to 0.26 $cm^2\ V^{-1}\ s^{-1}$. Furthermore, the electron-deficient thiazole provided the polymers with lower HOMO levels. For example, the benzobisthiazole-based polymers displayed good stability for over 2 months under high-humidity air ($R_H = 75\ \%$) [39]. Osaka and Takemiya et al. also reported a polymer FET material using naphthodithiophene as a building block (**PNDTBT**), which showed high hole mobilities of up to 0.54 $cm^2\ V^{-1}\ s^{-1}$. The introduction of the electron-deficient naphthalene ring endowed this polymer with good stability under medium humidity condition [40].

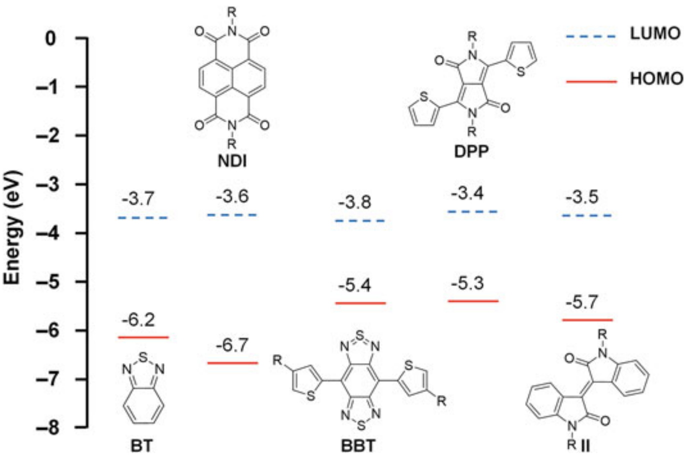

Fig. 1.6 Chemical structures and HOMO/LUMO levels of several electron-deficient building blocks used for high-performance polymer FETs [43]

Heralded as the third generation of semiconducting conjugated polymers, donor–acceptor (D-A) polymers have significantly boosted the development of polymer-based electronic materials [41]. D-A polymers are conjugated polymers containing a combination of electron-rich (donor) and electron-deficient (acceptor) units. This type of polymers are generally obtained via cross-coupling reactions (e.g., Stille and Susuki reactions) between donor and acceptor units. Using D-A polymers, BHJ solar cells with efficiency over 9 % [10], and polymer FETs with mobility over 10 $cm^2 V^{-1} s^{-1}$ [42] have been reported. Because of the abundance of donors, the development of strong electron-deficient building blocks remains essential to advancing D-A conjugated polymers. Recently, electron-deficient fused aromatic rings such as diketopyrrolopyrrole (**DPP**), benzothiadiazole (**BT**), naphthalene diimide (**NDI**), benzobisthiadiazole (**BBT**), and isoindigo (**II**) have been used as acceptors to construct donor–acceptor polymers (Fig. 1.6), leading to the significant development of polymer FETs [43].

Figure 1.6 displays the chemical structures of several important electron-deficient building blocks and the energy levels of their highest occupied molecular orbitals (HOMOs) and lowest unoccupied molecular orbitals (LUMOs) [43]. The HOMO levels of the building blocks range from –5.3 to –6.3 eV, and their LUMO levels are obviously lower than traditional polymer building blocks in the range from –3.4 to –3.8 eV. From the structure perspective, the introduction of strong electron-deficient groups, such as ketone and thiadiazole groups, has efficiently lowered their LUMO energy levels. Polymer FETs based on isoindigo and its derivatives is the main content of this book and we will discuss it in detail in the following chapters.

2,1,3-Benzothiadiazole are cheap and easy to synthesize, making them widely used in donor-acceptor polymers [44]. Müllen et al. reported the first high-

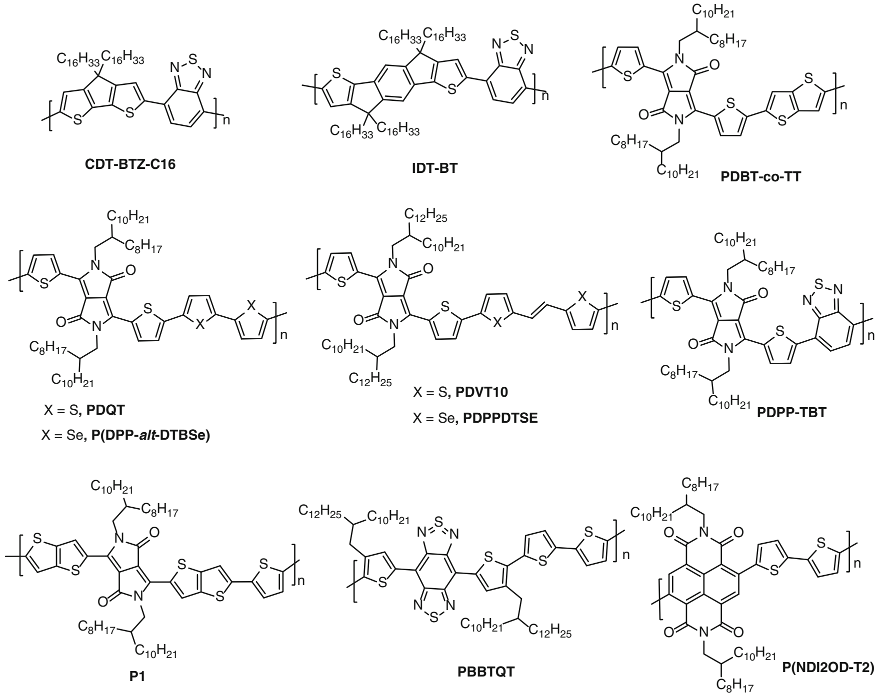

Fig. 1.7 Donor-accepter polymers with charge carrier mobility approaching or surpassing 1 cm^2 V^{-1} s^{-1}

performance **BT** based polymer **BTZ-CDT-C16** (Fig. 1.7), which showed hole mobility of 0.17 cm^2 V^{-1} s^{-1} [45]. By increasing molecular weight of the polymer and using dip-coating method to prepare polymer film, the polymer packing order in film was improved, leading to significantly improved hole mobility of 1.4 cm^2 V^{-1} s^{-1} [46]. Further increasing molecular weight of **BTZ-CDT-C16** led to even higher hole mobility of up to 3.3 cm^2 V^{-1} s^{-1} [26]. Nanowires based on this polymer were also obtained through solution process and a higher hole mobility of up to 5.5 cm^2 V^{-1} s^{-1} was obtained [47]. Selected area electron diffraction (SAED) showed that the π–π stacking direction of the polymer is perpendicular to the nanowire direction, indicating that the polymer backbones were aligned parallel to the direction of nanowire, which is considered to be favorable for the charge carrier transport. This series of research demonstrate that the molecular weight of polymer and good polymer chain alignment are crucial to obtain high device performance. Rigid backbone structure is good for reducing the disorder of polymer chains and thereby increasing mobility [48]. McCulloch et al. reported polymer **IDT-BT** with a ladder-shape donor unit [49]. This polymer adopted a face-on packing mode in thin film with π–π stacking distance of 4.1 Å. The maximum hole mobility of the polymer reached 1.2 cm^2 V^{-1} s^{-1} when TG/BC device structure was used. By using high molecular weight **IDT-BT**, the mobility of the polymer was further increased to 3.6 cm^2 V^{-1} s^{-1} [50]. In this paper, the authors proposed that the charge transport in high-mobility semiconducting polymers is predominantly occurring along the backbone and requires only occasional intermolecular hopping. This finding is consistent with the aforementioned charge transport mechanism in conjugated polymers.

DPP is a dye first developed by Ciba Company. It can be easily synthesized and has strong coloring ability. **DPP** based dyes are mostly accompanied with flanking benzene rings. However, the unplanar structure of **DPP**-benzene derivatives make the dyes not suitable for polymer FET materials. Recently, using thiophenenitrile instead of benzonitrile, **DPP**-bithiophene monomer was synthesized and successfully used in organic electronics. Subsequently, other aromatic heterocycles were used, resulting in furan [51], selenophene [52], thienothiophene [53], or thiazole [54] substituted **DPP** derivatives. After coupling of **DPP**-bithiophene with another alkylated bithiophene, Winnewisser et al. obtained an ambipolar conjugated polymer [55]. The polymer displayed balanced ambipolar with hole and electron mobility of near 0.1 cm^2 V^{-1} s^{-1} and exhibited infra-red emission property in light-emitting transistors.

A large number of high-performance **DPP** polymers have been synthesized in the last few years and many have exhibited high mobilities over 1 cm^2 V^{-1} s^{-1}. Li et al. reported **PDBT-co-TT** using thienothiophene as donor, which showed hole mobility of 0.94 cm^2 V^{-1} s^{-1} [56]. By using the same polymer, Ong et al. reported that after significantly increasing polymer molecular weight and using BGBC device structure, high hole mobilities of up to 10.5 cm^2 V^{-1} s^{-1} can be obtained [42]. Li et al. also reported polymer **PDQT** using bisthiophene as donor [57]. This polymer showed high hole mobility of 0.89 cm^2 V^{-1} s^{-1} without thermal annealing and subsequently 100 °C annealing can enhance the mobility to 0.97 cm^2 V^{-1} s^{-1}. Low annealing temperature is beneficial for device fabrication on heat-sensitive substrates. By using more electron-rich biselenophene as the donor, Choi et al. synthesized **P(DPP-*alt*-DTBSe)** and obtained a higher hole mobility of 1.5 cm^2 V^{-1} s^{-1} [58]. Liu et al. reported polymer **PDVT10** using π-extended (*E*)-2-(2-(thiophen-2-yl)vinyl)thiophene (**TVT**) as donor, which showed the maximum hole mobility of 8.2 cm^2 V^{-1} s^{-1}, significantly higher than that of **PDVT8** with shorter alkyl side chains (4.5 cm^2 V^{-1} s^{-1}) [59]. They explained that the lengths of the alkyl side chains might affect π–π stacking distance and the π–π stacking distance of **PDVT10** is smaller. However, **PDVT10** synthesized by Kwon et al. only showed mobility of 2.77 cm^2 V^{-1} s^{-1} and was then increased to 4.97 cm^2 V^{-1} s^{-1} by substituting thiophene with selenophene [60]. Instead of using electron-rich donors, Li et al. used benzothiadiazole as the donor to lower the LUMO level of **DPP** polymers and obtained polymer **PDPP-TBT** [61]. This polymer exhibited ambipolar transport behaviors with hole mobility of 0.35 cm^2 V^{-1} s^{-1} and electron mobility of 0.4 cm^2 V^{-1} s^{-1}. Using **DPP**-thienothiophene as acceptor, McCulloch et al. synthesized polymer **P1**, which showed hole mobilities of up to 1.95 cm^2 V^{-1} s^{-1} by using a TGBC device structure. This polymer also showed good PCE of 5.4 % when used as the donor of OSCs [53].

BBT and benzobisthiadiazole–bithiophene were first synthesized by Yamashita et al. [62]. These building blocks were originally used in n-type small molecule FET materials. Yuen and Wudl et al. used **BBT** for donor-acceptor polymer FETs and obtained a series of p-type and ambipolar FET materials. Polymer **PBBTQT** that using bisthiophene as donor showed high hole mobilities of up to 2.5 $cm^2\ V^{-1}\ s^{-1}$ [63], and polymer using thienothiophene as donor showed balanced ambipolar transport with hole mobility of 1.0 $cm^2\ V^{-1}\ s^{-1}$ and electron mobility of 0.7 $cm^2\ V^{-1}\ s^{-1}$ [64]. **NDI** and perylene diimide (**PDI**) are the most extensively investigated strong electron-deficient building blocks and have been widely used in small molecule n-type FETs [65]. Facchetti et al. reported n-type FET polymers based on **NDI** and **PDI** [66], in which polymer **P(NDIO2D-T2)** based on **NDI** displayed higher electron mobility and better air stability due to its regioregular polymer structure. After using TGBC device structure, the electron mobility of **P(NDIO2D-T2)** was as high as 0.85 $cm^2\ V^{-1}\ s^{-1}$ [67].

The last few years have witnessed a rapid development of polymer FET materials and several novel high-mobility building blocks have been developed. Compared with p-type polymer materials, ambipolar and n-type materials are less investigated. Particularly, the mobilities of n-type semiconductors always lag far behind those of p-type ones, which limits the applications of organic semiconductors in high speed and low power dissipation complementary circuits. On the other hand, although many high mobility polymers have been developed, the structure-property relationships in polymer FETs are seldom investigated due to the difficulty in the structural analysis of the amorphous polymer films, which further hinders the development of this field. Thus, more efforts are required in both developing new building blocks and better understanding the structure-property relationships.

1.3 Research Strategy and Overview of This Thesis

Figure 1.8 illustrates the research strategy used in this thesis: (1) design molecular structures based on knowledge, experience and hypothesis, and predict materials' properties by theoretical calculation; (2) study synthetic routes and characterize the physical properties of new compounds; (3) investigate polymer thin film microstructures and molecular packings to understand the relationships between molecular structure and intermolecular interactions; (4) fabricate devices based on the new materials and analyze device results to understand the underlying physical process; (5) summarize the structure-property relationships to guide the future design of new materials.

We started our research in conjugated polymers from the analysis of week interactions among alkyl side chains and proposed a design strategy called "molecular docking" to avoid the steric hindrance effects of alkyl side chains. Isoindigo, a dye discovered over a century ago, was used in polymer FETs for the first time. On the basis of isoindigo and the concept of "molecular docking", a

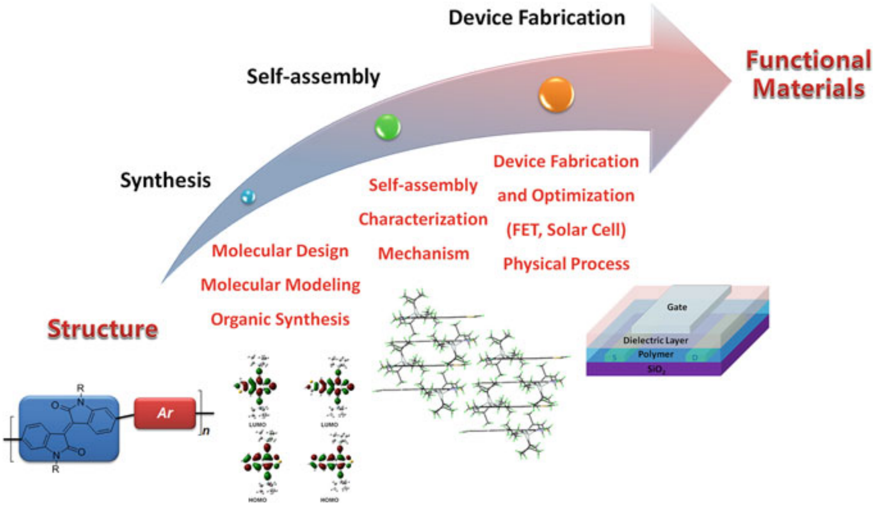

Fig. 1.8 Schematic representation of our research strategy

series of high-mobility and high-stability polymer FET materials have been developed (Fig. 1.9a). We found that isoindigo polymers with centrosymmetric donors showed systematically higher hole mobilities (>0.1 cm^2 V^{-1} s^{-1}) than those with axisymmetric donors (~0.01 cm^2 V^{-1} s^{-1}). On the basis of the above results, we propose that donor symmetry and backbone curvature may affect interchain “molecular docking” of conjugated polymers, ultimately leading to different device performance (Fig. 1.9b). In order to further increase interchain interactions, we investigate how moving the branching positions of alkyl side chains away from polymer backbone influences the mobilities. The sequential changing of these “more conventional” branched alkyl chains resulted in a remarkably high mobility of 3.62 cm^2 V^{-1} s^{-1}, which is the highest result in isoindigo-based conjugated polymers (Fig. 1.9c). These works are described in Chap. 2.

In Chap. 3, our efforts on tuning the electronic properties of conjugated polymers by introducing functional groups are described. We introduced fluorine atoms on the isoindigo core to lower polymer LUMO level (Fig. 1.9d). After introducing fluorine atoms, ambipolar transport behavior in isoindigo-based conjugated polymers was observed for the first time. Fluorination on the isoindigo unit significantly increased the electron mobility from 10^{-2} to 0.43 cm^2 V^{-1} s^{-1} while maintaining high hole mobility of up to 1.85 cm^2 V^{-1} s^{-1} for devices fabricated under ambient conditions. Furthermore, we chlorinated isoindigo-based polymers through an efficient chlorination reaction (Fig. 1.9e). Balanced charge carrier transport with hole mobilities of up to 0.81 cm^2 V^{-1} s^{-1} and electron mobilities of up to 0.66 cm^2 V^{-1} s^{-1} were obtained for devices fabricated under ambient conditions. In addition, complementary-like inverters with high gain values were also

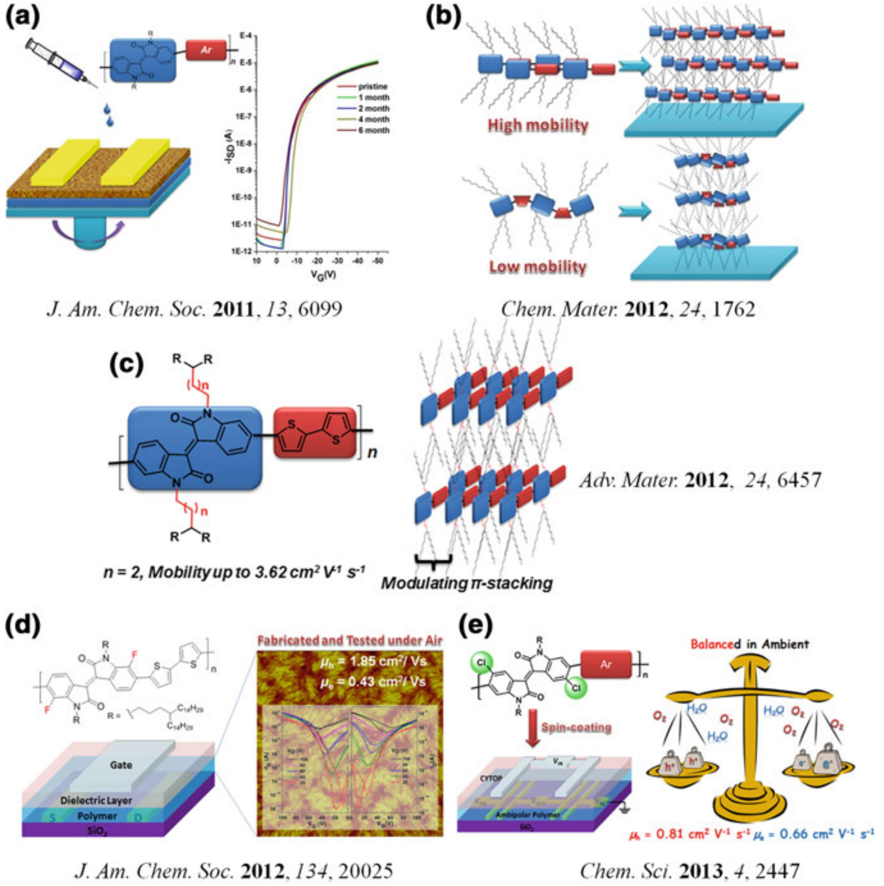

J. Am. Chem. Soc. **2011**, *13*, 6099

Chem. Mater. **2012**, *24*, 1762

Adv. Mater. **2012**, *24*, 6457

J. Am. Chem. Soc. **2012**, *134*, 20025

Chem. Sci. **2013**, *4*, 2447

Fig. 1.9 **a** First isoindigo-based polymer FETs. **b** Impact of polymer symmetry and backbone curvature. **c** Branching position effects of polymer side chains. **d** Ambipolar transport in fluorinated isoindigo-based polymers. **e** Chlorination as a useful method to modulate charge transport in conjugated polymers

demonstrated. This work represented the first example that using chlorination to tune the carrier transport in conjugated polymers.

In Chap. 4, to further modulate the electronic properties of isoindigo, we designed a novel structure **BDOPV** based on isoindigo by breaking the double bond between two lactam rings and inserting a conjugated moiety (Fig. 1.10a). Through polymerization with (*E*)-1,2-bis(tributylstannyl)ethene, an electron-deficient poly (*p*-phenylene vinylene) (**PPV**) derivative (**BDPPV**) was obtained (Fig. 1.10b). This new **PPV** derivative displayed high electron mobilities of up to 1.1 cm^2 V^{-1} s^{-1} under ambient conditions (four orders of magnitude higher than those of other **PPV**s). **BDOPV** was then used to construct a D-A polymer **BDOPV-2T** (Fig. 1.10c), which showed a high electron mobility of 1.74 cm^2 V^{-1} s^{-1}. Upon oxygen

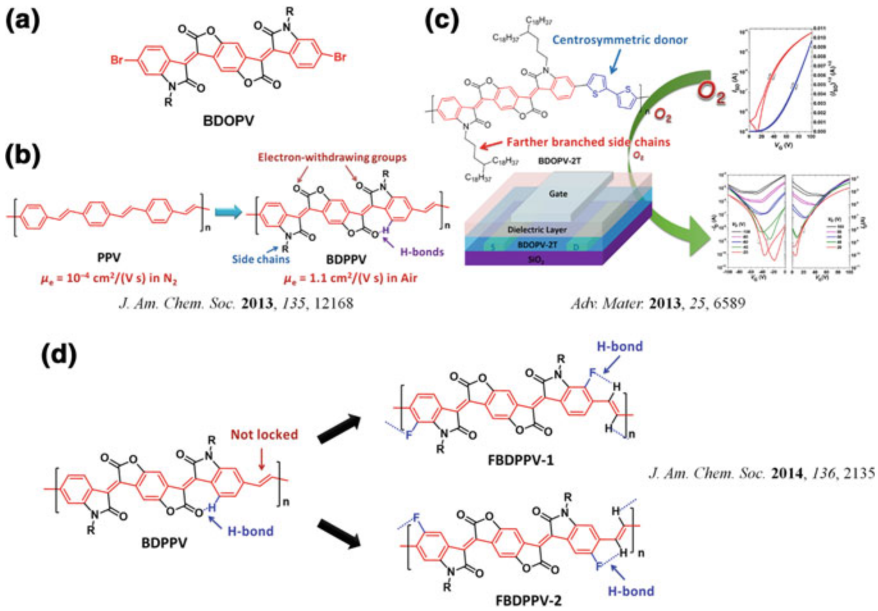

J. Am. Chem. Soc. **2013**, *135*, 12168

Adv. Mater. **2013**, *25*, 6589

J. Am. Chem. Soc. **2014**, *136*, 2135

Fig. 1.10 **a** Molecular structure of **BDOPV**. **b** An electron-deficient PPV derivative **BDPPV** was constructed. **c** A **BDOPV**-based D-A polymer **BDOPV-2T** for n-type and oxygen-doped ambipolar FETs. **d** Design strategy of fully "conformation locked" PPV-based conjugated polymers, **FBDPPV-1** and **FBDPPV-2**

exposure, **BDOPV-2T** displayed interesting ambipolar transporting behavior, which maintained high electron mobilities of up to 1.45 $cm^2\ V^{-1}\ s^{-1}$ along with significantly increased hole mobilities of up to 0.47 $cm^2\ V^{-1}\ s^{-1}$. Besides, the oxygen-doping effect and possible mechanism was also investigated based on theoretical calculation. To "lock" the double bond in **BDPPV**, we introduced one fluorine atom on each side and synthesized polymer **FBDPPV-1** and **FBDPPV-2** (Fig. 1.10d). Compared with **BDPPV**, **FBDPPV-1** showed increased electron mobility of 1.70 $cm^2\ V^{-1}\ s^{-1}$, whereas **FBDPPV-2** only showed 0.81 $cm^2\ V^{-1}\ s^{-1}$. This work demonstrated that fluorination is more than lowering the energy levels of conjugated polymers, it also influences backbone conformations, which is critical to the device performance.

References

1. Hodes G (2007) When small is different: some recent advances in concepts and applications of nanoscale phenomena. Adv Mater 19:639–655
2. Vollath D (2008) Nanomaterials: an introduction to synthesis, properties and applications, 1st edn. Wiley-VCH, Weinheim
3. Heeger AJ, Sariciftci NS, Namdas EB (2010) Semiconducting and metallic polymers. Oxford University Press, Oxford

4. Chiang CK, Fincher CR Jr, Park YW, Heeger AJ, Shirakawa H, Louis EJ, Gau SC, MacDiarmid AG (1977) Electrical conductivity in doped polyacetylene. Phys Rev Lett 39:1098–1101
5. Tang CW, VanSlyke SA (1987) Organic electroluminescent diodes. Appl Phys Lett 51:913–915
6. Tang CW (1986) Two-layer organic photovoltaic cell. Appl Phys Lett 48:183–185
7. Tsumura A, Koezuka H, Ando T (1986) Macromolecular electronic device: field-effect transistor with a polythiophene thin film. Appl Phys Lett 49:1210–1212
8. Yu G, Gao J, Hummelen JC, Wudl F, Heeger AJ (1995) Polymer photovoltaic cells: enhanced efficiencies via a network of internal donor-acceptor heterojunctions. Science 270:1789–1791
9. Carsten D, Vladimir D (2010) Polymer–fullerene bulk heterojunction solar cells. Rep Prog Phys 73:096401
10. He Z, Zhong C, Su S, Xu M, Wu H, Cao Y (2012) Enhanced power-conversion efficiency in polymer solar cells using an inverted device structure. Nat Photon 6:591–595
11. You J, Dou L, Yoshimura K, Kato T, Ohya K, Moriarty T, Emery K, Chen C-C, Gao J, Li G, Yang Y (2013) A polymer tandem solar cell with 10.6 % power conversion efficiency. Nat Commun 4:1446
12. Ebisawa F, Kurokawa T, Nara S (1983) Electrical properties of polyacetylene/polysiloxane interface. J Appl Phys 54:3255–3259
13. Minemawari H, Yamada T, Matsui H, Tsutsumi Jy, Haas S, Chiba R, Kumai R, Hasegawa T (2011) Inkjet printing of single-crystal films. Nature 475:364–367
14. Gong X, Tong M, Xia Y, Cai W, Moon JS, Cao Y, Yu G, Shieh C-L, Nilsson B, Heeger AJ (2009) High-detectivity polymer photodetectors with spectral response from 300 nm to 1450 nm. Science 325:1665–1667
15. Hide F, Díaz-García MA, Schwartz BJ, Andersson MR, Pei Q, Heeger AJ (1996) Semiconducting polymers: a new class of solid-state laser materials. Science 273:1833–1836
16. Tessler N, Denton GJ, Friend RH (1996) Lasing from conjugated-polymer microcavities. Nature 382:695–697
17. Williams-Harry M, Bhaskar A, Ramakrishna G, Goodson T, Imamura M, Mawatari A, Nakao K, Enozawa H, Nishinaga T, Iyoda M (2008) Giant thienylene-acetylene-ethylene macrocycles with large two-photon absorption cross section and semishape-persistence. J Am Chem Soc 130:3252–3253
18. Liu B, Bazan GC (2005) Methods for strand-specific DNA detection with cationic conjugated polymers suitable for incorporation into DNA chips and microarrays. Proc Natl Acad Sci USA 102:589–593
19. Pierret RF (1996) Semiconductor device fundamentals. Pearson Education, New Delhi
20. Reese C, Bao Z (2007) Organic single-crystal field-effect transistors. Mater Today 10:20–27
21. Brédas J-L, Beljonne D, Coropceanu V, Cornil J (2004) Charge-transfer and energy-transfer processes in π-conjugated oligomers and polymers: a molecular picture. Chem Rev 104:4971–5004
22. Coropceanu V, Cornil J, da Silva Filho DA, Olivier Y, Silbey R, Brédas J-L (2007) Charge transport in organic semiconductors. Chem Rev 107:926–952
23. Di C-A, Liu Y, Yu G, Zhu D (2009) Interface engineering: an effective approach toward high-performance organic field-effect transistors. Acc Chem Res 42:1573–1583
24. Grozema FC, van Duijnen PT, Berlin YA, Ratner MA, Siebbeles LDA (2002) Intramolecular charge transport along isolated chains of conjugated polymers: effect of torsional disorder and polymerization defects. J Phys Chem B 106:7791–7795
25. Prins P, Grozema FC, Schins JM, Patil S, Scherf U, Siebbeles LDA (2006) High intrachain hole mobility on molecular wires of ladder-type poly(*p*-phenylenes). Phys Rev Lett 96:146601
26. Tsao HN, Cho DM, Park I, Hansen MR, Mavrinskiy A, Yoon DY, Graf R, Pisula W, Spiess HW, Müllen K (2011) Ultrahigh mobility in polymer field-effect transistors by design. J Am Chem Soc 133:2605–2612

27. Tseng H-R, Ying L, Hsu BBY, Perez LA, Takacs CJ, Bazan GC, Heeger AJ (2012) High mobility field effect transistors based on macroscopically oriented regioregular copolymers. Nano Lett 12:6353–6357
28. Niedzialek D, Lemaur V, Dudenko D, Shu J, Hansen MR, Andreasen JW, Pisula W, Müllen K, Cornil J, Beljonne D (2013) Probing the relation between charge transport and supramolecular organization down to angstrom resolution in a benzothiadiazole-cyclopentadithiophene copolymer. Adv Mater 25:1939–1947
29. McCullough RD, Lowe RD (1992) Enhanced electrical conductivity in regioselectively synthesized poly(3-alkylthiophenes). J Chem Soc Chem Commun 1:70–72
30. Marrocchi A, Lanari D, Facchetti A, Vaccaro L (2012) Poly(3-hexylthiophene): synthetic methodologies and properties in bulk heterojunction solar cells. Energy Environ Sci 5:8457–8474
31. Sirringhaus H, Brown PJ, Friend RH, Nielsen MM, Bechgaard K, Langeveld-Voss BMW, Spiering AJH, Janssen RAJ, Meijer EW, Herwig P, de Leeuw DM (1999) Two-dimensional charge transport in self-organized, high-mobility conjugated polymers. Nature 401:685–688
32. Ong BS, Wu Y, Liu P, Gardner S (2004) High-performance semiconducting polythiophenes for organic thin-film transistors. J Am Chem Soc 126:3378–3379
33. McCulloch I, Heeney M, Bailey C, Genevicius K, MacDonald I, Shkunov M, Sparrowe D, Tierney S, Wagner R, Zhang W, Chabinyc ML, Kline RJ, McGehee MD, Toney MF (2006) Liquid-crystalline semiconducting polymers with high charge-carrier mobility. Nat Mater 5:328–333
34. Li J, Bao Q, Li CM, Zhang W, Gong C, Chan-Park MB, Qin J, Ong BS (2010) Organic thin-film transistors processed from relatively nontoxic, environmentally friendlier solvents. Chem Mater 22:5747–5753
35. Fong HH, Pozdin VA, Amassian A, Malliaras GG, Smilgies D-M, He M, Gasper S, Zhang F, Sorensen M (2008) Tetrathienoacene copolymers as high mobility, soluble organic semiconductors. J Am Chem Soc 130:13202–13203
36. He M, Li J, Sorensen ML, Zhang F, Hancock RR, Fong HH, Pozdin VA, Smilgies D-M, Malliaras GG (2009) Alkylsubstituted thienothiophene semiconducting materials: structure–property relationships. J Am Chem Soc 131:11930–11938
37. He M, Li J, Tandia A, Sorensen M, Zhang F, Fong HH, Pozdin VA, Smilgies D-M, Malliaras GG (2010) Importance of C_2 symmetry for the device performance of a newly synthesized family of fused-ring thiophenes. Chem Mater 22:2770–2779
38. Osaka I, Zhang R, Sauvé Gv, Smilgies D-M, Kowalewski T, McCullough RD (2009) High-lamellar ordering and amorphous-like π-network in short-chain thiazolothiazole–thiophene copolymers lead to high mobilities. J Am Chem Soc 131:2521–2529
39. Osaka I, Takimiya K, McCullough RD (2010) Benzobisthiazole-based semiconducting copolymers showing excellent environmental stability in high-humidity air. Adv Mater 22:4993–4997
40. Osaka I, Abe T, Shinamura S, Miyazaki E, Takimiya K (2010) High-mobility semiconducting naphthodithiophene copolymers. J Am Chem Soc 132:5000–5001
41. Heeger AJ (2010) Semiconducting polymers: the third generation. Chem Soc Rev 39:2354–2371
42. Li J, Zhao Y, Tan HS, Guo Y, Di C-A, Yu G, Liu Y, Lin M, Lim SH, Zhou Y, Su H, Ong BS (2012) A stable solution-processed polymer semiconductor with record high-mobility for printed transistors. Sci Rep 2:754
43. Yuen JD, Wudl F (2013) Strong acceptors in donor-acceptor polymers for high performance thin film transistors. Energy Environ Sci 6:392–406
44. Chen J, Cao Y (2009) Development of novel conjugated donor polymers for high-efficiency bulk-heterojunction photovoltaic devices. Acc Chem Res 42:1709–1718
45. Zhang M, Tsao HN, Pisula W, Yang C, Mishra AK, Müllen K (2007) Field-effect transistors based on a benzothiadiazole–cyclopentadithiophene copolymer. J Am Chem Soc 129:3472–3473

46. Tsao HN, Cho D, Andreasen JW, Rouhanipour A, Breiby DW, Pisula W, Müllen K (2009) The influence of morphology on high-performance polymer field-effect transistors. Adv Mater 21:209–212
47. Wang S, Kappl M, Liebewirth I, Müller M, Kirchhoff K, Pisula W, Müllen K (2012) Organic field-effect transistors based on highly ordered single polymer fibers. Adv Mater 24:417–420
48. Zhang W, Smith J, Hamilton R, Heeney M, Kirkpatrick J, Song K, Watkins SE, Anthopoulos T, McCulloch I (2009) Systematic improvement in charge carrier mobility of air stable triarylamine copolymers. J Am Chem Soc 131:10814–10815
49. Zhang W, Smith J, Watkins SE, Gysel R, McGehee M, Salleo A, Kirkpatrick J, Ashraf S, Anthopoulos T, Heeney M, McCulloch I (2010) Indacenodithiophene semiconducting polymers for high-performance, air-stable transistors. J Am Chem Soc 132:11437–11439
50. Zhang X, Bronstein H, Kronemeijer AJ, Smith J, Kim Y, Kline RJ, Richter LJ, Anthopoulos TD, Sirringhaus H, Song K, Heeney M, Zhang W, McCulloch I, DeLongchamp DM (2013) Molecular origin of high field-effect mobility in an indacenodithiophene–benzothiadiazole copolymer. Nat Commun 4:2238
51. Li Y, Sonar P, Singh SP, Zeng W, Soh MS (2011) 3,6-di(furan-2-yl)pyrrolo[3,4-*c*]pyrrole-1,4(2H,5H)-dione and bithiophene copolymer with rather disordered chain orientation showing high mobility in organic thin film transistors. J Mater Chem 21:10829–10835
52. Shahid M, McCarthy-Ward T, Labram J, Rossbauer S, Domingo EB, Watkins SE, Stingelin N, Anthopoulos TD, Heeney M (2012) Low band gap selenophene-diketopyrrolopyrrole polymers exhibiting high and balanced ambipolar performance in bottom-gate transistors. Chem Sci 3:181–185
53. Bronstein H, Chen Z, Ashraf RS, Zhang W, Du J, Durrant JR, Tuladhar PS, Song K, Watkins SE, Geerts Y, Wienk MM, Janssen RA, Anthopoulos T, Sirringhaus H, Heeney M, McCulloch I (2011) Thieno[3,2-b]thiophene-diketopyrrolopyrrole-containing polymers for high-performance organic field-effect transistors and organic photovoltaic devices. J Am Chem Soc 133:3272–3275
54. Carsten B, Szarko JM, Lu L, Son HJ, He F, Botros YY, Chen LX, Yu L (2012) Mediating solar cell performance by controlling the internal dipole change in organic photovoltaic polymers. Macromolecules 45:6390–6395
55. Bürgi L, Turbiez M, Pfeiffer R, Bienewald F, Kirner H-J, Winnewisser C (2008) High-mobility ambipolar near-infrared light-emitting polymer field-effect transistors. Adv Mater 20:2217–2224
56. Li Y, Singh SP, Sonar P (2010) A high mobility p-type DPP-thieno[3,2-b]thiophene copolymer for organic thin-film transistors. Adv Mater 22:4862–4866
57. Li Y, Sonar P, Singh SP, Soh MS, van Meurs M, Tan J (2011) Annealing-free high-mobility diketopyrrolopyrrole–quaterthiophene copolymer for solution-processed organic thin film transistors. J Am Chem Soc 133:2198–2204
58. Ha JS, Kim KH, Choi DH (2011) 2,5-Bis(2-octyldodecyl)pyrrolo[3,4-c]pyrrole-1,4-(2H,5H)-dione-based donor–acceptor alternating copolymer bearing 5,5′-di(thiophen-2-yl)-2,2′-biselenophene exhibiting 1.5 $cm^2 V^{-1} s^{-1}$ hole mobility in thin-film transistors. J Am Chem Soc 133:10364–10367
59. Chen H, Guo Y, Yu G, Zhao Y, Zhang J, Gao D, Liu H, Liu Y (2012) Highly π-extended copolymers with diketopyrrolopyrrole moieties for high-performance field-effect transistors. Adv Mater 24:4618–4622
60. Kang I, An TK, Hong J-A, Yun H-J, Kim R, Chung DS, Park CE, Kim Y-H, Kwon S-K (2013) Effect of selenophene in a DPP copolymer incorporating a vinyl group for high-performance organic field-effect transistors. Adv Mater 25:524–528
61. Sonar P, Singh SP, Li Y, Soh MS, Dodabalapur A (2010) A low-bandgap diketopyrrolopyrrole-benzothiadiazole-based copolymer for high-mobility ambipolar organic thin-film transistors. Adv Mater 22:5409–5413
62. Karikomi M, Kitamura C, Tanaka S, Yamashita Y (1995) New narrow-bandgap polymer composed of benzobis(1,2,5-thiadiazole) and thiophenes. J Am Chem Soc 117:6791–6792

63. Fan J, Yuen JD, Cui W, Seifter J, Mohebbi AR, Wang M, Zhou H, Heeger A, Wudl F (2012) High-hole-mobility field-effect transistors based on co-benzobisthiadiazole-quaterthiophene. Adv Mater 24:6164–6168
64. Fan J, Yuen JD, Wang M, Seifter J, Seo J-H, Mohebbi AR, Zakhidov D, Heeger A, Wudl F (2012) High-performance ambipolar transistors and inverters from an ultralow bandgap polymer. Adv Mater 24:2186–2190
65. Zhan X, Facchetti A, Barlow S, Marks TJ, Ratner MA, Wasielewski MR, Marder SR (2011) Rylene and related diimides for organic electronics. Adv Mater 23:268–284
66. Chen Z, Zheng Y, Yan H, Facchetti A (2009) Naphthalenedicarboximide- vs perylenedicarboximide-based copolymers. Synthesis and semiconducting properties in bottom-gate n-channel organic transistors. J Am Chem Soc 131:8–9
67. Yan H, Chen Z, Zheng Y, Newman C, Quinn JR, Dotz F, Kastler M, Facchetti A (2009) A high-mobility electron-transporting polymer for printed transistors. Nature 457:679–686

Chapter 2
Side Chain Effects and Design of Isoindigo-Based Polymers

2.1 Roles of Flexible Chains in Organic Semiconductors

Solution processability is one of the most attractive features of organic semiconductors, enabling low-cost, low-temperature, and large-area device fabrication. In order to realize solution processability in organic conjugated molecules, the introduction of solubilizing side chains is indispensable. To date, a large number of organic semiconductors have been developed to improve the device performance, where most of the efforts focused on the design and synthesis of new π-conjugated backbones [1]. However, much less efforts have been devoted to understanding the role of the side chains of organic semiconductors. Alkyl chains, oligo (ethylene glycol) chains, and fluoroalkyl chains are three commonly used side chains in organic semiconductors. As insulating parts, these side chains generally do not directly contribute to charge transport in organic semiconductors and are usually used as solubilizing groups. However, more and more studies have demonstrated the substantial impact of the flexible chains on the device performance of organic semiconductors. Some results have also indicated that even a subtle change of the flexible chains may result in a great influence on device performance. Several side chain effects, such as length [2], odd-even effect [3], substitution position [4] etc. contribute to the molecular packing of organic semiconductors in solid state, which in turn affects device performance. Therefore besides solubilizing property, other effects of side chains need to be considered in the design of organic semiconductors.

Boese et al. reported the single crystal structure of *n*-propane to *n*-nonane [5]. They found that the odd-even effect in these alkanes strongly correlated with their solid-state packing. Even-numbered *n*-alkanes have optimal intermolecular contacts at both ends, whereas the odd-numbered ones have these only at one end, and the distances are longer at the other end. This leads to a less dense packing for the odd *n*-alkanes and thereby lower melting points. This odd-even effect has been demonstrated to exert its influence on crystal packing and charge transport after being

T. Lei, *Design, Synthesis, and Structure-Property Relationship Study of Polymer Field-Effect Transistors*, Springer Theses, DOI 10.1007/978-3-662-45667-5_2

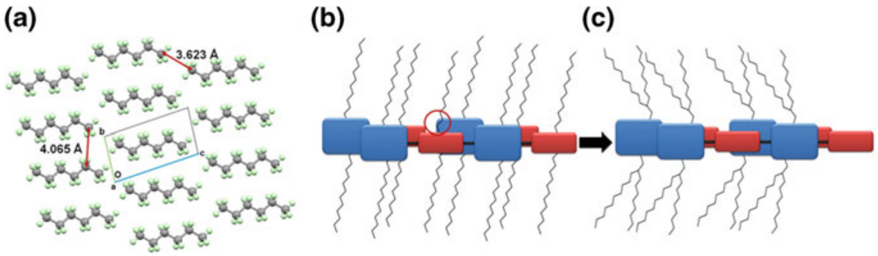

Fig. 2.1 **a** Crystal packing of *n*-hexane viewed from *a* axis [5]. **b** Polymers contain alkyl chains on both the donor and the acceptor. Steric hindrance may exist when polymers are stacked (*red circle*). **c** Proposed docking model to avoid the side-chain impediments after moving the alkyl chains from the small cores (*red cube*) to the large cores (*blue cube*)

attached onto aromatic cores [6]. Figure 2.1a shows the single crystal packing of *n*-hexane [5]. The shortest C–C distance (3.623 Å) in the crystal comes from the methyl C atoms of adjacent columns, and the shortest distance between parallel packed alkyl chains is 4.065 Å. These distances are obviously larger than the typical π–π stacking distances (3.3–3.6 Å) found in many organic semiconductors [1]. Thus, the alkyl chain packing in organic semiconductors may sometimes impede the π–π stacking of aromatic cores. For example, in those polymers with each unit substituted with one alkyl chain, steric hindrance may occur as indicted by the red circle in Fig. 2.1b. To avoid the steric hindrance caused by polymer side chains, we proposed a “molecular docking” strategy realized by moving the alkyl chains from the small units (red cube) to the large ones (blue cube) (Fig. 2.1c). This strategy may reduce the steric hindrance, thereby making the small aromatic units “dock into” the large aromatic ones. In addition, large fused aromatics can also reduce the reorganization energy of carrier hopping, which has been demonstrated in the design of high-mobility small molecules.

2.2 Design of Isoindigo-Based Polymers

Indigo is a very famous dye, widely used in dyeing and printing industry. Unlike its famous isomer indigo, isoindigo is a less investigated dye and can be isolated as a by-product from certain biological processes. It has two lactam rings and exhibits strong electron-withdrawing character. Although discovered as a dye over a century ago, isoindigo has joined the “acceptor club” of D-A polymers only recently. Reynolds et al. first used isoindigo in organic solar cells in 2010 and represented the first application of isoindigo in organic electronics [7]. Inspired by this seminal work, our group developed the first isoindigo-based polymer FETs (Scheme 2.1).

Compared with small-molecule FETs, polymer FETs are less studied and have lower mobility. Although several polythiophene-based polymer FETs were reported with mobilities over 0.5 $cm^2 V^{-1} s^{-1}$ and an on/off ratio over 10^6, it is still challenging

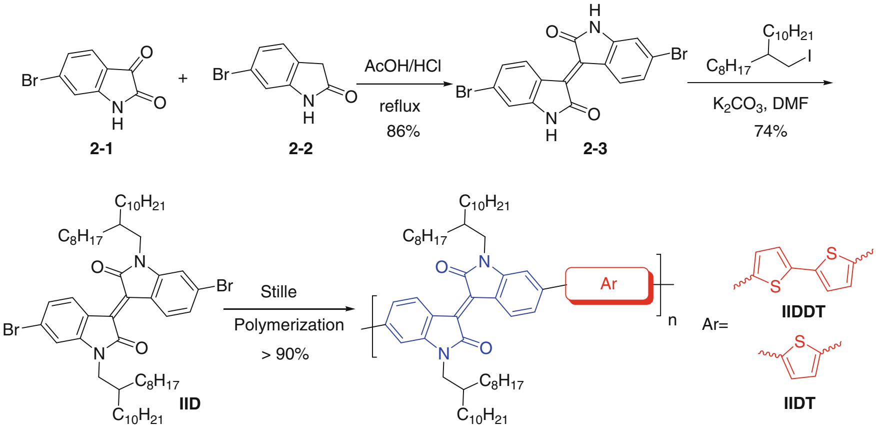

Scheme 2.1 Synthesis of the first isoindigo-based polymer FET materials

to design polymer with both high mobility and good ambient stability [8]. An effective approach to improve the stability is to introduce electron deficient aromatic rings into the backbone of polythiophene to lower the HOMO level [9]. Isoindigo is an electron-deficient building block and polymers based on it have low HOMO levels (−5.4 to −5.8 eV). Thus, isoindigo may provide polymer FETs with good ambient stability.

The synthesis was started from two commercial available compounds, 6-bromoisatin (**2-1**) and 6-bromooxindole (**2-2**) (Scheme 2.1). A direct condensation of **2-1** and **2-2** in acetic acid afforded isoindigo **2-3** in 86 % yield. Subsequently, **2-3** was alkylated with 1-iodo-2-octyldodecane, giving monomer **IID** in 74 % yield. A Stille-coupling polymerization between 4 and bis(trimethylstannyl)thiophene or 5,5′-bis(trimethylstannyl)-2,2′-bithiophene gave two polymers, **IIDT** and **IIDDT**, in high yields. Because of the introduction of long alkyl chains, both polymers were readily soluble in common solvents such as $CHCl_3$, toluene, and THF. Both polymers were obtained as dark metallic solids after purification. The molecular weights of both polymers were initially measured by room-temperature gel permeation chromatography (GPC). **IIDT** showed an M_n of 19.8 kg/mol, while **IIDDT** showed a very high M_n of up to 87.9 kg/mol. However, when using 1,2,4-trichlorobenzene (TCB) as eluent and measured at higher temperature of 150 °C, the M_n of **IIDDT** decreased to 33.7 kDa and that of **IIDT** kept at about 19.6 kDa. This result indicates that **IIDDT** has much stronger interchain interactions than **IIDT**. Both polymers showed decomposition temperature over 350 °C under nitrogen atmosphere, and no phase transition was observed before decomposition.

Figure 2.2a and b display the absorption spectra of **IIDDT** and **IIDT** in $CHCl_3$ (1×10^{-5}), in thin film, and in annealed film. The absorption peaks of **IIDDT** and **IIDT** in films did not show obvious red-shift relative to those in the solution. After annealing the films at 150 °C, **IIDDT** only showed a slightly increased absorption

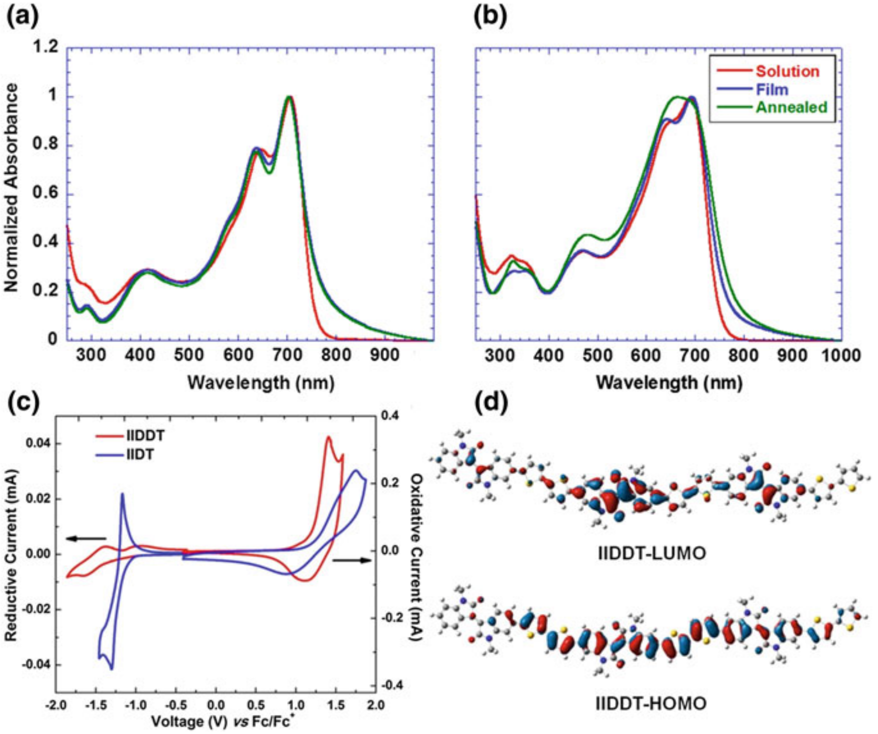

Fig. 2.2 Normalized UV-*vis* absorption spectra of **a IIDDT** and **b IIDT** in $CHCl_3$ (1×10^{-5} M), in thin film, and in annealed film (at 150 °C for 20 min). **c** Cyclic voltammogram of **IIDDT** and **IIDT** in thin film drop-casting on a glassy carbon and tested in Bu_4NPF_6/CH_3CN solution (scan rate: 50 mV s^{-1}). The oxidative currents are almost an order of magnitude higher. **d** Calculated molecular orbitals of the **IIDDT** trimer (B3LYP/6-31G (d))

intensity of the 0–0 vibrational peak; in contrast, the absorption feature of the **IIDT** annealed film showed a large change with its 0–1 peak largely increased and the absorption onset slightly red-shift. These results suggest that the packing conformation of the **IIDT** were largely changed and the polymers might become planar after annealing.

The cyclic voltammetry measurements of both polymers in thin films showed that **IIDDT** owned HOMO/LUMO level of −5.7/−3.7 eV, and **IIDT** had HOMO/LUMO level of −5.8/−3.8 eV. Both polymers showed much stronger oxidative peaks than their reductive peaks, and the oxidative peak of **IIDDT** seems more reversible than that of **IIDT** (Fig. 2.2c). This result is consistent with the device performance that both the polymers are typical p-type semiconductors and **IIDDT** exhibited a better performance. Compared with traditional thiophene or fused thiophene based polymers, both polymers showed much deeper HOMO levels, which is attributed to the strong election-withdrawing ability of the isoindigo core. Computational results indicate that the HOMO of the polymers are well delocalized along the polymer chain, whereas the LUMO are mostly localized on the isoindigo core (Fig. 2.2d). Therefore, these polymers are typical donor-acceptor conjugated polymers, and the absorption bands from 520 to 800 nm are typical charge transfer absorption from the thiophene unit to the isoindigo core.

Bottom-gate/top-contact (BG/TC) devices were fabricated by spin-coating the polymer solutions (4 mg/mL in chloroform or in trichloroethylene (TCE)) onto octadecyltrichlorosilane (OTS)-treated SiO_2 (300 nm)/n^{++}-Si substrate. The OTS self-assembled monolayer (SAM) was modified according to the method reported by Bao et al. [10] which showed a high crystalline ultra-smooth surface and improved device performances for vacuum deposited OFETs. Chloroform and TCE did not show any significant difference in device performances, but TCE provided films with higher quality because of its high boiling point. For **IIDT**, directly spin-coated films did not exhibit observable field effect characteristics. However, after annealed at 150 °C, **IIDT** showed a hole mobility of 0.01–0.02 $cm^2 V^{-1} s^{-1}$. As discussed above, the annealing process increased molecular packing, which resulted in higher mobility. After spin-coating the solution of **IIDDT**, the pristine films exhibited a hole mobility around 0.1–0.2 $cm^2 V^{-1} s^{-1}$. After annealing at 150 °C for 20 min, **IIDDT** exhibited a hole mobility of up to 0.79 $cm^2 V^{-1} s^{-1}$ and an average mobility of 0.42 $cm^2 V^{-1} s^{-1}$, which is one order of magnitude higher than that of **IIDT** (Table 2.1). This large improvement can be attributed to better molecular packing, C_2-symmetry and high molecular weight of **IIDDT**. The polymer also exhibited good transfer curves with a small hysteresis. The output curves showed almost no contact resistance. Therefore the low-lying HOMO level did not interfere with the charge injection from the Au electrode. Both polymers were long-time stable at least for 4 months under ambient conditions, and the devices of **IIDDT** were also stable at high humidity (R_H = 60 %) for at least 1 month, largely attributed to its low-lying HOMO level (Fig. 2.3).

With the above results in hand, we employed grazing incidence X-ray diffraction (GIXD) and atomic force microscopy (AFM) to investigated molecular packings and morphologies of the polymer films. In the 2D-GIXD, **IIDDT** showed a strong diffraction peaks at 2θ of 3.58° corresponding to a d-spacing of 19.88 Å ($\lambda = 1.240$ Å). Another three diffraction peeks can be attributed to 200, 300, and 400 diffractions, indicating that **IIDDT** had an edge-on lamellar packing in film. In contrast, **IIDT** showed only one weak diffraction at 3.25°, indicating the films are relatively

Table 2.1 Polymer molecular weights and FETT performances

Polymers	M_n/M_w	PDI	Mobility (μ/$cm^2 V^{-1} s^{-1}$)	$I_{on/off}$
IIDT	19,800/39,100	2.0	N/A[a]	N/A
			0.019 (0.015)[b]	~10^6
IIDDT	87,900/185,800	2.1	0.1–0.2[a]	~10^6
			0.79 (0.42)[b]	~10^7

[a] Pristine film spin-coating from TCE solution

[b] Maximum values of the hole mobility after annealed at 150 °C for 20 min. Average mobilities are shown in parentheses (more than 20 devices were tested)

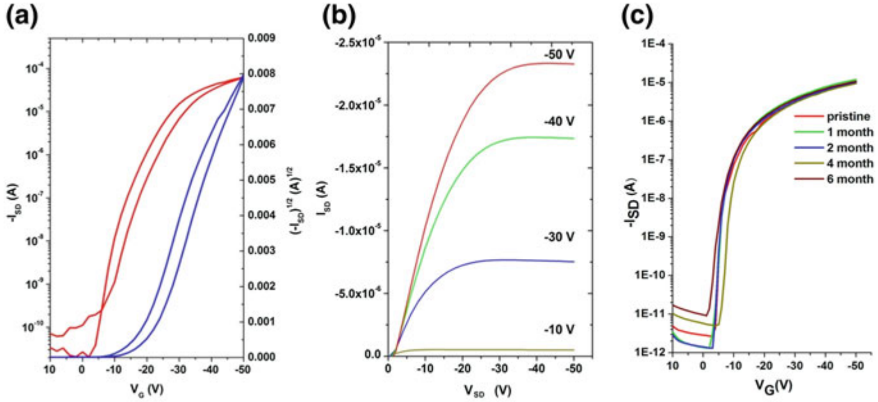

Fig. 2.3 **a** Transfer and **b** output characteristics of an **IIDDT** device at $V_{DS} = -50$ V ($L = 60$ μm, $W = 3.0$ mm) after 150 °C annealing. **c** Changes in transfer characteristics of an **IIDDT** device. The device was stored in dark at 25 °C under humidity around 10 %

amorphous. In the AFM images, **IIDDT** showed crystalline fibrillar intercalating networks. Such crystalline networks were likely the result of the strong intermolecular π–π interactions, which were also observed in other high performance OFET materials. In contrast, the films of **IIDT** were more amorphous without obviously crystallized zones. Therefore, the difference of **IIDDT** and **IIDT** in crystallinity may explain the largely different device performances.

2.3 Impact of Polymer Symmetry and Backbone Curvature

Compared with small molecule, conjugated polymer films are difficult to be analyzed due to their amorphous states. Encouraged by the aforementioned results, we synthesized eight other isoindigo-based polymers based on "molecular docking" strategy to investigate the structure–property relationship in polymer FETs (Fig. 2.4) [11]. In the molecular modeling field, "docking" is a method to predict the structure of intermolecular complex formed between two or more constituent molecules [12]. Molecular docking has been broadly used to understand the biological processes determined by non-covalent interactions, especially for rational design of drugs [13].

Because isoindigo homopolymer is a typical n-type semiconductor, [14] in order to obtain *p*-type isoindigo-based polymers, electron-rich groups should be introduced to increase the HOMO level of the desired polymers. The donor-acceptor interactions of electron-deficient isoindigo units and electron-rich units may enhance the interchain π–π stacking interactions. Selenophene-(**2-4**) and thiophene-containing (**2-5** to **2-11**) units are used to construct the copolymers (Scheme 2.2). Units **2-4**–**2-7** and unit **2-10** are centrosymmetric, and units **2-8**, **2-9** and **2-11** are

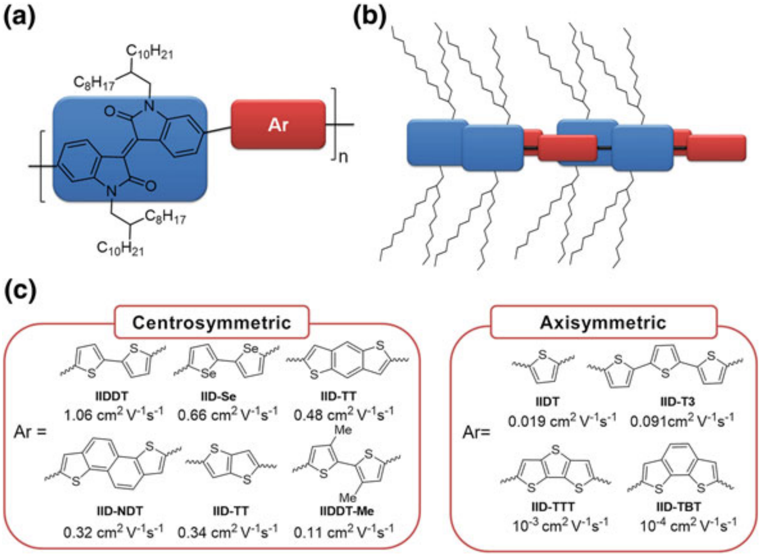

Fig. 2.4 **a** Chemical structures of isoindigo-based conjugated polymers. **b** Proposed docking model to avoid the side-chain impediments after moving the alkyl chains from small (*red cube*) to the large cores (*blue cube*). **c** Centrosymmetric and axisymmetric donors of the polymers

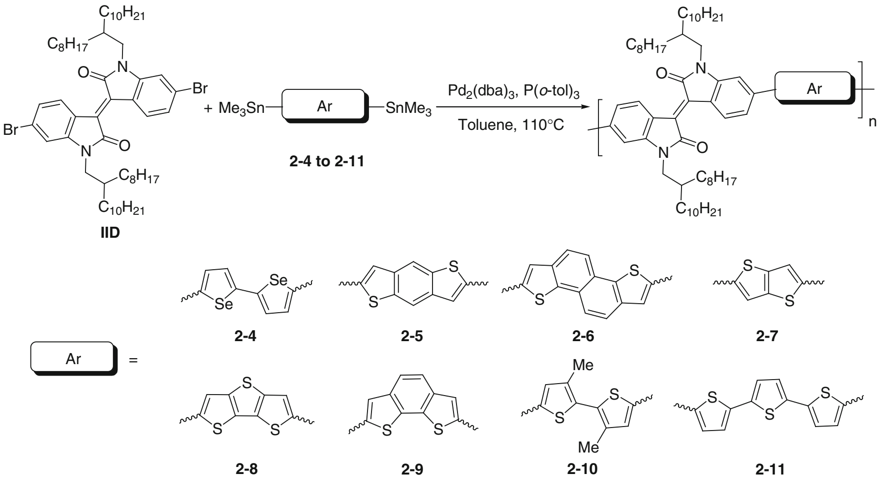

Scheme 2.2 Synthesis of isoindigo-based copolymers

axisymmetric. To prove our molecular docking strategy, we also synthesized 3,3′-dimethyl-2,2′-bithiophene (10) to compare with 2,2′-bithiophene. We envision that the methyl groups may hinder π–π stacking and interchain docking. Compounds **2-4**, **2-5**, **2-6**, **2-7**, **2-8**, and **2-9** were synthesized according to literature [15–19].

The synthesis of monomer **IID** needs only two steps with high yield from commercially available 6-bromoisatin (**2-1**) and 6-bromooxindole (**2-2**). All monomers can be prepared in 10-g scale. The copolymers were obtained through Stille-coupling polymerization using $Pd_2(dba)_3$ and $P(o\text{-tol})_3$ as catalysts. After the polymerization, a strongly complexing agent *N*,*N*-diethylphenylazothioformamide was added to remove any residual catalyst. All polymers were purified by Soxhlet extraction (sequentially by methanol, hexane, and $CHCl_3$), and afforded dark or dark blue solids. After introducing the branched alkyl chains, all polymers (except **IID-T3**) showed good solubility in common solvents, such as $CHCl_3$, toluene, and THF. **IID-T3** only dissolved in chloro-containing solvents such as $CHCl_3$, TCE, and dichlorobenzene (DCB). Molecular weights of all polymers were evaluated by GPC using 1,2,4-tricholorobenzene as eluent at 150 °C. Large PDI remained at this high temperature, presumably due to the strong aggregation of the polymers. All polymers showed good thermal stability with decomposition temperatures over 350 °C. No phase transition was observed by differential scanning calorimetry (DSC) before decomposition.

The absorption spectra of all the polymers in solution, thin film and annealed film are shown in Fig. 2.5. All the polymers showed typically dual band absorption both in solution and in film: band I (from 500 to 800 nm) and band II (from 300 to 500 nm). Band II is attributed to the absorption of the donor part, which varied among different polymers because of different donor electronic structures. In contrast, these polymers showed similar absorption features in band I region with three obvious vibrational peaks 0–0, 0–1, 0–2, indicating the absorption band originated from the isoindigo core, a shape-persistent molecular structure. Moreover, band I is also a typical charge-transfer absorption from the donor part to the isoindigo core, which is consistent with computational results that the HOMOs are well delocalized along the polymer chains, and the LUMOs are mostly localized on the isoindigo core. Except polymer **IIDDT-Me**, the absorption peaks of other polymers in film show no obvious red-shift relative to those in solution, which suggested that the polymers adopted similar geometry in solution and in film. Scrutiny of spectra reveals that the 0–0 vibrational transition increased while 0–1 decreased in film, suggesting polymers became more planar or formed some aggregates in film. After annealing the film at 150 °C for 30 min, a further increase of the 0–0 transition was also observed, indicating the packing and planarity of polymers became much better. **IIDDT-Me** had two methyl groups that caused a great rotational angle and broke the conjugation, which led to an obvious blue-shift in solution. When the polymer went into solid state, the rotational angles were suppressed because of interchain π–π stacking. This change caused a huge red-shift of the absorption maximum of **IIDDT-Me**, and this polymer showed a similar optical bandgap as other polymers in film state (Table 2.2).

The cyclic voltammetries (CV) of all the polymers in thin films were measured to evaluate their electronic energy level (Fig. 2.6). Most of the polymers showed much stronger oxidative peaks than their reductive ones, almost one order of magnitude higher, which indicated that the polymers were more easily oxidized. All the polymers showed similar reductive potentials with LUMO levels around

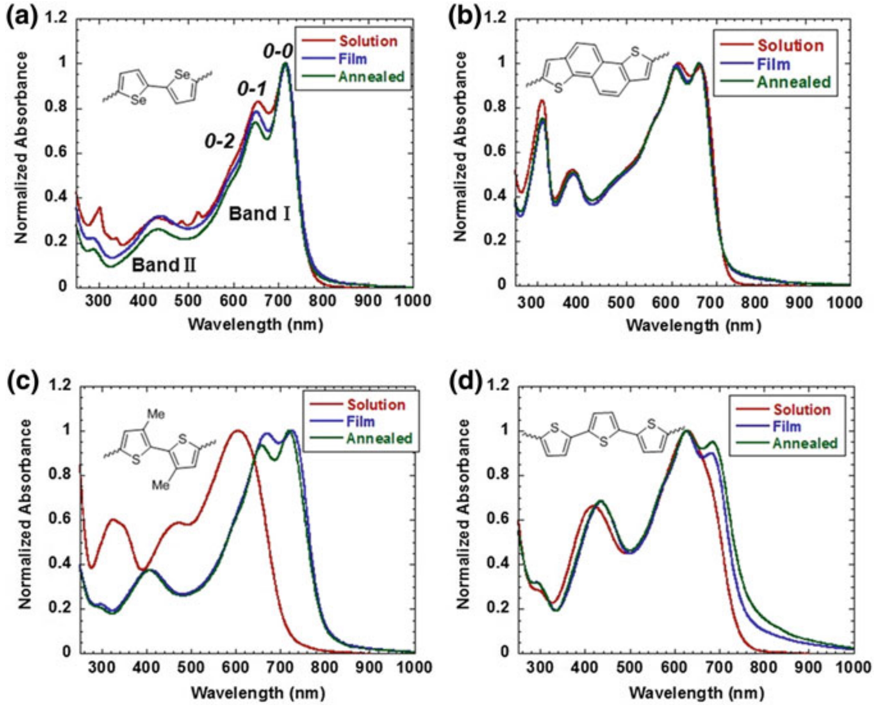

Fig. 2.5 Normalized UV-*vis* absorption spectra of **a IID-Se**; **b IID-NDT**; **c IIDDT-Me**; and **d IID-T3** in $CHCl_3$ (1×10^{-5} M), in thin film (spin-coated from TCE solution, 1 mg/mL), and in annealed film (at 150 °C for 30 min)

−3.70 eV. HOMO levels of the polymers varied according to the electron-donating properties of the donor part. For example, **IID-Se** and **IID-TT** gave HOMO/LUMO levels of −5.65/−3.79 and −5.70/−3.73 eV, respectively. After the introduction of relatively electron-deficient donors, benzodithiophene (BDT) and naphtho[1,2-b:5,6-b′]dithiophene (NDT), polymer **IID-BDT** and **IID-NDT** showed lowered HOMO levels of −5.84 and −5.90 eV. These results are consistent with the computational results that the LUMO levels of all the polymers are mostly localized on the isoindigo core and the HOMO levels are distributed along the polymer chains. Thus the HOMO levels of the polymer are more easily affected by the electronic structure of the donor moiety, while the LUMO stays unchanged. Interestingly, **IID-TTT** showed two oxidative peaks and a HOMO level of −5.44 eV, indicating the strong electron-donating property of dithieno[3,2-b:2′,3′-d]thiophene. **IID-BDT**, **IID-NDT** and **IID-TBT** showed obvious blue-shift of the absorption spectra compared to other polymers. Using DFT calculation, we obtained the theoretical HOMO/LUMO levels of polymers by extrapolating the calculated energy levels of the oligomers.

Table 2.2 Optical and electrochemical properties of all the isoindigo-based polymers

Polymers	M_n (kDa)/ PDI[a]	λ_{max}^{0-0} sol (nm)[b]	λ_{max}^{0-1} sol (nm)[b]	λ_{max}^{0-0} film (nm)[c]	λ_{max}^{0-1} film (nm)[c]	E_g^{opt} (eV)[d]	E_{HOMO} (eV)[e]	E_{LUMO} (eV)[e]	E_g^{cv} (eV)[f]
IIDDT	33.7/5.4	706	647	701	637	1.59	−5.65	−3.78	1.87
IID-Se	26.7/3.5	716	655	715	649	1.56	−5.56	−3.79	1.77
IID-BDT	27.3/4.7	674	646	676	620	1.66	−5.84	−3.77	2.07
IID-NDT	24.8/3.5	666	616	662	610	1.69	−5.90	−3.75	2.15
IID-TT	25.5/3.5	723	666	720	656	1.55	−5.70	−3.73	1.97
IIDDT-Me	20.1/3.9	604	N/A	725	670	1.54	−5.54	−3.78 [g]	1.76
IIDT	19.6/3.1	691	644	697	645	1.58	−5.80	−3.81	1.99
IID-T3	38.8/3.4	N/A	628	682	628	1.58	−5.48	−3.70 [g]	1.78
IID-TTT	26.6/3.7	719	662	720	656	1.55	−5.44	−3.72	1.73
IID-TBT	11.2/2.5	658	613	668	615	1.65	−5.55	−3.70	1.85

[a] GPC versus polystyrene standards, TCB as eluent, at 150 °C

[b] Solution absorption spectra (10^{-5} M in chloroform)

[c] Thin film absorption spectra from pristine film spin-cast from 5 mg/mL TCE solution

[d] Optical energy gap estimated from the onset of the film absorption

[e] Cyclic voltammetry determined using Fc/Fc$^+$ (E_{HOMO} = –4.80 eV) as external reference

[f] $E_g^{CV} = E_{LUMO} - E_{HOMO}$

[g] The first reduction peak is weak

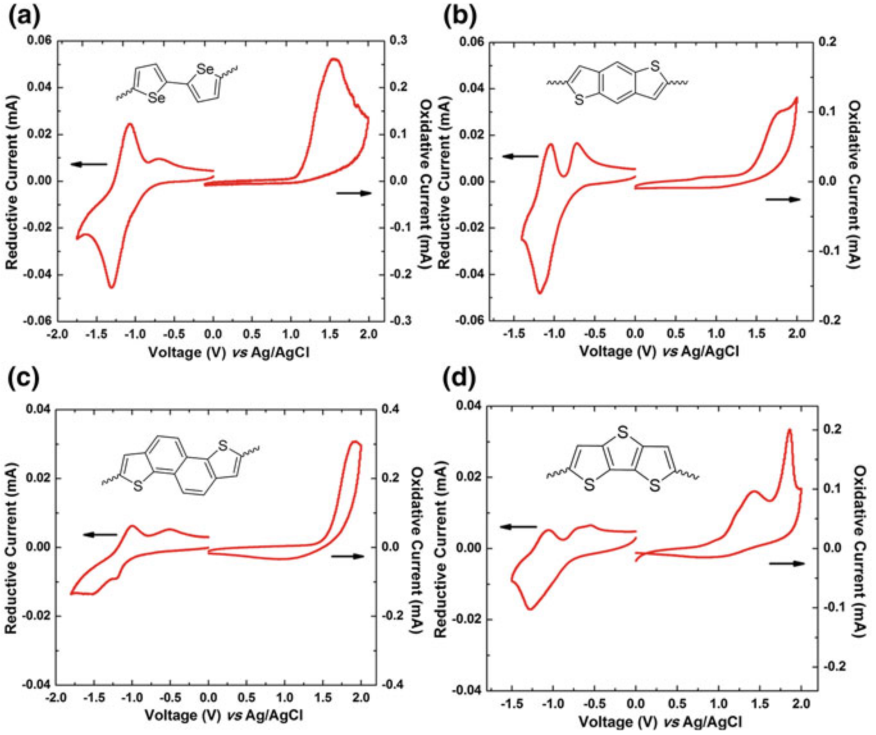

Fig. 2.6 Cyclic voltammogram of **a IID-Se**, **b IID-NDT**, **c IIDDT-Me**, and **d IID-T3** in thin film drop-casting on a glassy carbon electrode and tested in n-Bu_4NPF_6/CH_3CN solution (scan rate: 50 mV s^{-1})

BG/TC device structure was used for device fabrication by spin-coating the polymer solutions (4 mg/mL) onto octadecyltrimethoxysilane (OTS) treated SiO_2 (300 nm) on heavily doped Si substrate. Previously, we used TCE as the solvent to fabricate the thin film transistors. After optimizing conditions, we found that using TCB provided better device performance. For example, using TCE as the solvent, **IIDDT** only gave an average hole-mobility of 0.42 $cm^2\ V^{-1}\ s^{-1}$, while using TCB a higher mobility of 1.06 $cm^2\ V^{-1}\ s^{-1}$ and average mobility of 0.66 $cm^2\ V^{-1}\ s^{-1}$ were obtained (Fig. 2.5a). This result is among the highest results reported to date. Using TCB as solvent to improve FETs device performance was also reported in the fabrication of P3HT, high boiling point TCB provided P3HT with better intrachain packing and more condensed uniform film [20, 21]. Because the OTS treated SiO_2 surface is very hydrophobic and TCB has a relatively higher contact angle than TCE, spin-coating on the surface can only be achieved by using the TCB solution containing polymers **IIDDT**, **IID-Se** or **IID-NDT**, which may be attributed to their higher molecular weight and viscosity. For other polymers, spin-coating from their TCB solutions did not provide continuous films. We also found that solvent-annealing in TCE atmosphere in Petri dish could also improve the device performance after spin-coating from TCE solutions. Thus solvent-annealing using TCE in Petri dish were also performed for all the polymers after spin-coating. Very excitingly, all the polymers with centrosymmetric donors showed excellent hole-transporting properties with mobility over 0.1 cm^2 V^{-1} s^{-1} (Fig. 2.7 and Table 2.3). Moreover, these polymers also exhibited good transfer curves with small hysteresis. These systematically excellent results rarely appear in literature, which suggests that the isoindigo core is an excellent building block for high-performance polymer FETs. Recently, selenophene-containing polymers were reported to show a better carrier-transporting performance in FETs; however, in our system, after replacing thiophene with selenophene, **IID-Se** only showed a comparable result with **IIDDT** with the highest hole mobility of up to 0.66 cm^2 V^{-1} s^{-1} and average mobility of

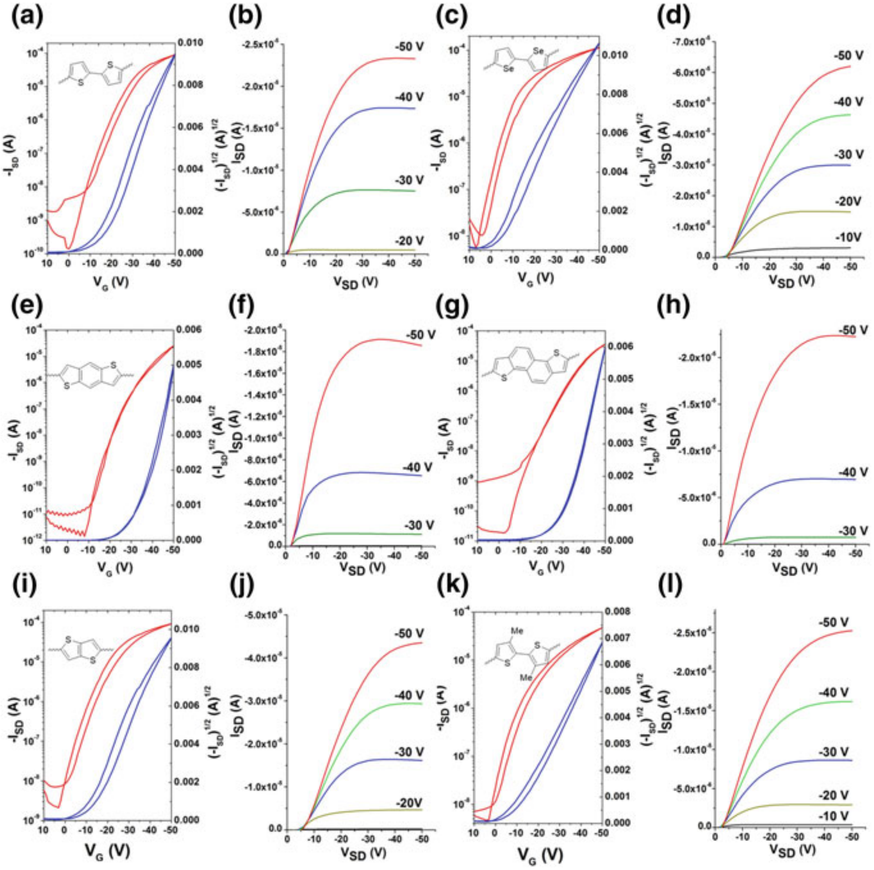

Fig. 2.7 Transfer and output characteristics of **IIDDT** (**a** and **b**), **IID-Se** (**c** and **d**), **IID-BDT** (**e** and **f**), **IID-NDT** (**g** and **h**), **IID-TT** (**i** and **j**), and **IIDDT-Me** (**k** and **l**) device (spin-cast from TCB or TCE solutions, 4 mg/mL) at V_{DS} = −50 V (L = 60 μm, W = 3.0 mm) after thermal annealing

Table 2.3 FET device performance of isoindigo-based polymers measured under ambient condition (R_H = 50–60 %)

Polymers	$T_{annealing}$ (°C)	Mobility μ (cm^2 V^{-1} s^{-1})[a]	V_T (V)	I_{on}/I_{off}
IIDDT	150	1.06 (0.66)	−18	10^6–10^7
IID-Se	160	0.66 (0.46)	−10	10^5–10^6
IID-BDT	150	0.48 (0.37)	−28	10^6–10^7
IID-NDT	200	0.32 (0.25)	−30	10^6–10^7
IID-TT	150	0.34 (0.31)	−6	10^5–10^6
IIDDT-Me	150	0.11 (0.091)	−5	10^5–10^6
IIDT	150	0.019 (0.015)	−20	10^5
IID-T3	150	0.061 (0.048)	−4	10^5
IID-TTT	200	1.03×10^{-3}	−4	10^4
IID-TBT	150	1.35×10^{-4}	−16	10^3

[a] Maximum values of hole mobility and average mobilities are shown in parentheses (more than 10 devices were tested for each polymer)

0.46 cm^2 V^{-1} s^{-1}. We also designed polymer **IIDDT-Me** to understand our molecular docking strategy. Although **IIDDT** and **IIDDT-Me** have identical conjugated structure and very similar photophysical and electrochemical properties, **IIDDT-Me** only gave the highest hole mobility of 0.11 cm^2 V^{-1} s^{-1} and average mobility of 0.091 cm^2 V^{-1} s^{-1}, which is the lowest among polymers containing centrosymmetric donor and almost one order of magnitude lower than that of **IIDDT**. This result pointed out that introducing methyl groups may hinder the interchain π–π stacking and thereby reduce the mobility.

Systematically comparing the transfer characteristics, a good correlation between the oxidative potential of the polymers and the threshold voltage of their devices exists in this system. **IID-Se** and **IID-TT** had higher HOMO levels than **IIDDT**, and they gave a more positive threshold voltage of −10 and −6 V, respectively. Similarly, **IID-BDT** and **IID-NDT** had relatively lower HOMO levels and they all provided a more negative threshold voltage of −28 and −30 V, respectively. This correlation is related to the hole-injection barrier from the gold electrode to the organic semiconducting layer. Because gold electrode has a work function of −5.1 eV, further lowering the HOMO level of the polymers increased the barrier, and hence the threshold voltage became more negative. However, even though **IID-BDT** and **IID-NDT** exhibited threshold voltage up to –30 V, high mobility of 0.48 cm^2 V^{-1} s^{-1} for **IID-BDT** and 0.32 cm^2 V^{-1} s^{-1} for **IID-NDT** were achieved. Interestingly, **IID-BDT** and **IID-NDT** showed very small hysteresis in the transfer characteristics, indicating less traps in the polymer films [9]. Moreover, the output curves of all the devices showed almost no contact resistance in this system. In sharp contrast, all the polymers with non-centrosymmetric donors showed much lower hole mobilities. **IIDT** and **IID-T3** only displayed the highest hole-mobilities of 0.019 and 0.061 cm^2 V^{-1} s^{-1}, respectively. **IID-TTT** and **IID-TBT** showed hole-mobility in the range of 10^{-3}–10^{-4} cm^2 V^{-1} s^{-1}.

It is worth noting that **IIDDT** exhibited good stability for at least 6 months under ambient condition. After the storage, only a slight increase of the off-current was observed for the device. Other centrosymmetric polymers, such as **IID-Se**, **IID-TT**, and **IIDDT-Me** were also tested under this condition, and they all showed good long-time stability for at least 2 months. This systematically good stability of the devices further supported the low-HOMO design strategy for ambient-stable polymer FETs [9].

Tapping-mode AFM was employed to investigate the surface morphology of the polymer films. Figure 2.8 displays the height images of the polymer films prepared under the same condition as their device fabrications. The root-mean-square (RMS) analyses of the height images were employed to reflect the roughness of the films. Film morphologies did not show obvious difference before and after thermal annealing at 150 °C for 30 min. However, all the polymers with centrosymmetric units, even **IIDDT-Me**, showed obviously crystallized zones or fibrillar intercalating networks in the films. Such crystalline networks were likely the result of good intermolecular packing, which were also observed in other high performance polymer FET materials. In contrast, the polymers without centrosymmetric units showed almost smooth and totally amorphous films. Because of the formation of the fibrillar networks, polymers with centrosymmetric donor showed higher surface

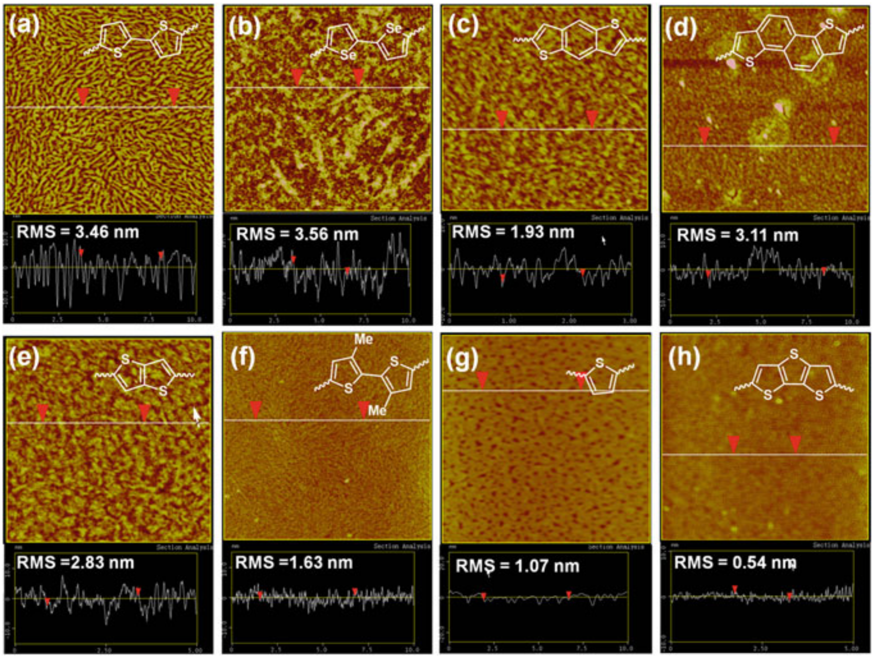

Fig. 2.8 Tapping-mode AFM height images of **a IIDDT**, **b IID-Se**, **c IID-BDT**, **d IID-NDT**, **e IID-TT**, **f IIDDT-Me**, **g IIDT**, and **h IID-TTT** films spin-cast on OTS treated SiO_2/Si substrate and annealed at 150 °C for 30 min

roughness than polymers without centrosymmetric donor. For instance, **IIDDT** and **IID-TT** presented higher surface roughness of 3.46 and 2.83 nm, respectively, while **IIDT** and **IID-TTT** only exhibited surface roughness of 1.07 and 0.54 nm.

To understand the device performances from a molecular level, we employed GIXD to investigate the polymer packing in thin film. Figure 2.9 shows the two-dimensional GIXD (2D-GIXD) patterns of the polymer films prepared by spin-casting the TCE solution of the polymers onto OTS-treated SiO_2/Si substrate. **IIDDT** and **IID-Se** films showed four out-of-plane diffraction peaks as spin-casted from TCE solution. The peaks are assigned to 100, 200, 300, and 400 diffractions. After thermal annealing the films at 150 °C for 30 min, the intensity of the diffraction peaks further increased, and the diffraction points became more centered. **IID-BDT** and **IID-NDT** only showed three diffraction peaks before annealing, but after annealing the fourth order diffraction peaks appeared. These results indicate that although these polymers are relatively amorphous compared with P3HT films, they also had ordered lamellar packing perpendicular to the substrate. According to the out-of-plane GIXD, the first strong diffraction peaks of **IIDDT**, **IID-Se**, **IID-BDT** and **IID-NDT** were at 2θ of 3.58°, 3.60°, 3.59°, and 3.65°, corresponding to a *d*-spacing of 19.85, 19.74, 19.79, 19.46 Å respectively. These results are in agreement with molecular models that the polymer films had an edge-on lamellar packing in film. However, for **IIDDT-Me**, only three diffraction peaks were observed after thermal annealing and the 100 diffraction became much broader compared to **IIDDT**, indicating a relatively disordered lamellar packing in the film. We speculate that the methyl groups in **IIDDT-Me** hindered the interpolymer π–π stacking, which might deteriorate out-of-plane lamellar packing. In sharp contrast, all the polymers containing non-centrosymmetric donor did not show good lamellar packing. **IID-T3** only displayed one diffraction peak, and the peak of **IIDT** became much weaker (Fig. 2.9k, l). Polymers **IID-TTT** and **IID-TBT** showed no obvious diffraction peak in film. Interestingly, the first diffraction peak of **IIDT** was at 2θ of 3.25°, corresponding to a *d*-spacing of 21.86 Å, significantly larger than those of the centrosymmetric polymers.

To further demonstrate our proposed packing model of the polymers, we performed ab initio calculations using DFT to understand the polymer packings. Specifically, ωB97X-D functional, which includes empirical dispersion, was used in order to correctly describe the weak intermolecular interaction [22]. The long alkyl chains were replaced by isobutyl groups for simplicity. We used oligomers (n = 2) of **IIDDT** to explore the π–π stacking of two polymer chains and several local minimum structures were found from different starting structures. Direct overlap of the isoindigo cores exhibited much higher energy because of the strong repulsion caused by the alkyl chains. The most stable intermolecular stacking is shown in Fig. 2.10a and the association energy of the dimer is 55.1 kcal/mol. The bithiophene units partially overlapped with the isoindigo cores with π–π stacking distances in the range of 3.4–3.5 Å. This result agreed with the absorption spectra that the polymer formed some J-aggregates in film. Figure 2.10b shows the electrostatic potential of the dimer. The HOMO of the dimers was delocalized on both oligomers which indicated a strong interaction of their frontier orbitals. However,

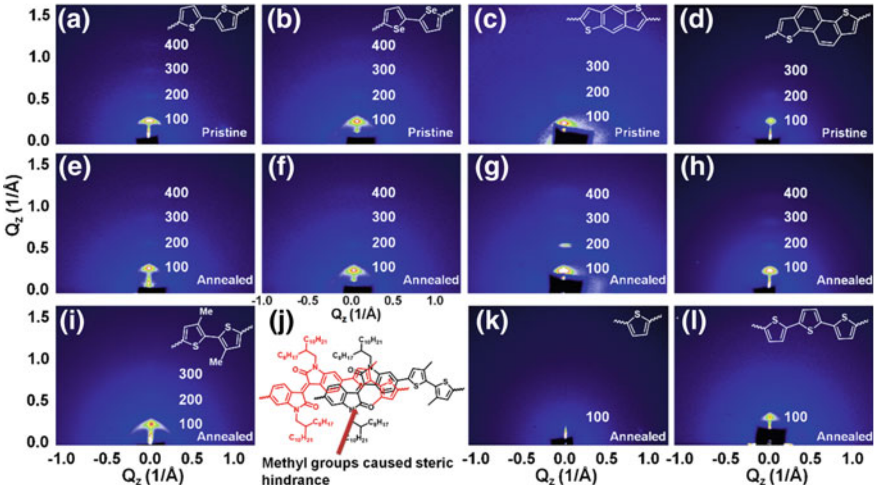

Fig. 2.9 2D-GIXD patterns of **a**, **e** **IIDDT**, **b**, **f** **IID-Se**, **c**, **g** **IID-BDT**, **d**, **h** **IID-NDT**, **i** **IIDDT-Me**, **k** **IIDT** and **l** **IID-TTT** pristine or annealed films. **j** Schematic representation of the steric hindrance that caused by the methyl groups of **IIDDT-Me**

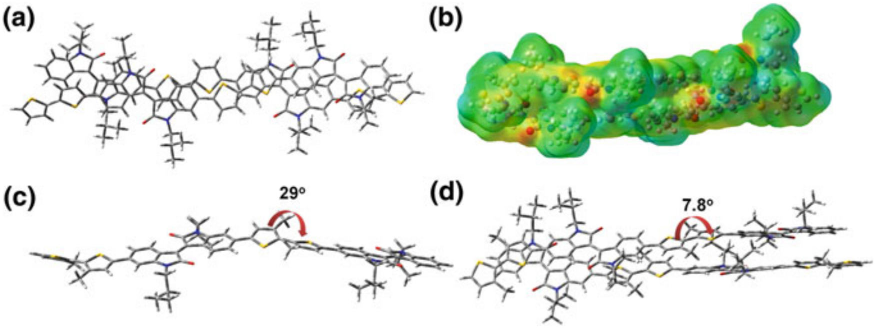

Fig. 2.10 **a** Calculated dimer structures of the **IIDDT** oligomers (n = 2). **b** Side view of the electrostatic potential of the dimer. **c** Calculated structure of the **IIDDT-Me** oligomers (n = 2). The bithiophene rotational angle in **IIDDT-Me** is 29°. **d** Calculated dimer structure of the **IIDDT-Me** oligomers (n = 2). The bithiophene rotational angle decreased to 7.8°. Structural optimization and energy calculation were all performed at ωB97X-D /6-31G(d) level

after incorporating methyl groups, oligomers of **IIDDT-Me** showed larger π–π stacking distance, and the association energy was 49.9 kcal/mol, which is smaller than that of **IIDDT**. Interestingly, the π–π stacking also suppressed the rotational angles of **IIDDT-Me** from 29° to 7.8°, which is also consistent with the absorption spectra (Fig. 2.10c, d). Polymers without centrosymmetric donor, such as **IIDT**, cannot form good π–π stacking and the association energy of the **IIDT** dimer was only 43.5 kcal/mol. It could be predicted that the difference of the association energy among these three polymers will be much larger. Therefore, these computational results prove our molecular packing models and support the “molecular docking” strategy that the small donor moieties may dock into the large isoindigo cores to form a better interchain π–π stacking.

In a typical polymer film, three possible carrier transporting pathways are marked with arrows in Fig. 2.11a: (1) intrachain carrier transport, which is very fast and efficient; (2) interchain carrier transport at well-ordered sites, which may adopt a hopping mechanism like ordered small molecules; (3) interchain carrier transport at loosely contacted sites, which is very slow. Therefore, the carrier transport is obviously limited by the loosely contact sites, and improve the carrier mobility at pathway (3) is crucial for high–performance polymeric FETs. One effective way to reduce the zones of pathway (3) is to increase the interpolymer chain interactions and thereby to increase the polymer packing orders.

Traditional polymers designed for polymer FETs, such as P3HT, always contain one or two alkyl chains on each unit (Fig. 2.11b). Because typical alkanes (C_nH_{2n+2}) ($n = 6$–9) have inter alkyl chain distances of 3.6–3.8 Å in single crystal, larger than a typical π–π distance of 3.4 Å, we assumed that steric hindrance may exist in the system when polymer stacked with each other. Using the aforementioned “molecular docking” strategy, this kind of steric hindrance can be avoided (Fig. 2.11c). The strategy contains two critical points of view: (1) reducing the steric hindrance of alkyl chains by making the small units “dock into” the large aromatic cores, similar to the “bricklayer” packing of TIPS-pentacene [23]; (2) large aromatic core can also reduce reorganization energy when charge transporting [24].

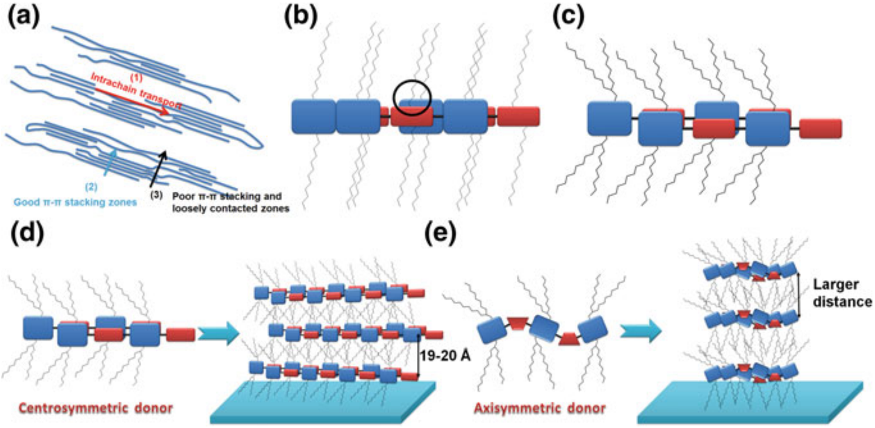

Fig. 2.11 **a** Cartoon representation of conjugated polymer film, and its three possible charge transport pathways; **b** Traditional polymers contain one or two alkyl chains on each unit. Steric hindrance may exist when polymers stacked with each other (*black circle*); **c** Molecular docking strategy to avoid steric hindrance and improve the inter-polymer π–π interaction. Cartoon representation of the copolymers with different symmetries and their film packings; **d** polymers with centrosymmetric donors and **e** polymers axisymmetric donors

As described above, the device performances of the polymers apparently correlated with their film morphologies and polymer packings. Polymers with centrosymmetric units exhibited better crystallinity and lamellar packing in thin films. To understand this correlation, we illustrated a cartoon representation of molecular packing in film (Fig. 2.11d, e). Those polymers with centrosymmetric units exhibited good interchain π–π stacking. The "small core" can readily dock into the cavity formed by the "large core" and the branched alkyl chains. The donor-acceptor interaction of the isoindigo core and the donor part can also help such docking. More importantly, because of the centrosymmetric units, the polymer backbones are almost linear and parallel to the substrate. The decent π–π stacking and the linear backbone of polymers led to good lamellar phase in the polymer films, as demonstrated by GIXD experiment (Fig. 2.11d). However, when the donor units lost centrosymmetry, the polymer backbones become like waves, docking an asymmetric "small core" into centrosymmetric "large core" becomes inappropriate, and the wave-like backbones also disturb good lamellar packing in polymer film, as shown in Fig. 2.11e. Moreover, for **IIDDT-Me**, after introducing methyl groups, the backbone of the polymer is still linear. Thus the polymer still exhibited good lamellar packing and the highest mobility of 0.11 $\mathrm{cm^2\ V^{-1}\ s^{-1}}$. Thus, we assume that the poor π–π stacking caused by methyl groups led to the relatively low mobility in **IIDDT-Me**. **IID-T3**, which contains a more linear backbone, exhibited hole-mobility up to 0.061 $\mathrm{cm^2\ V^{-1}\ s^{-1}}$, much better than other polymers with non-centrosymmetric donor. This result further demonstrates that backbone curvature is also an important factor. Accordingly, centrosymmetry and linear backbone curvature are critical for polymer docking and the formation of lamellar phase. Several groups also noticed the important effect of symmetry [25] and backbone curvature [26] on polymer FETs, which thereby supports our discussions.

It is meaningful to raise the question whether this design strategy is applicable to other systems except for isoindigo. Diketopyrrolopyrrole (DPP) and naphthalenedicarboximide (NDI) are also good examples for understanding the "molecular docking" strategy. Scheme 2.3 presents several recently developed polymers. Most of the polymers exhibited mobilities approaching or surpassing 1 $\mathrm{cm^2\ V^{-1}\ s^{-1}}$, which were systematically higher than traditional polymers. In these polymers, polymers with centrosymmetric units, such as **PDBP-co-TT**, [27] **PDQT**, [28] **P(DPP-*alt*-DTBSe)** [29] and n-type **P(NDI2OD-T2)**, [30] showed excellent mobilities. In contrast, **PDP3T** [31] and **PDPP-TBT** [32] exhibited relatively low mobilities because of their non-centrosymmetric building blocks and wave-like polymer backbones. Although **P1** [33] contains non-centrosymmetric thiophene units, it has an almost linear backbone and still exhibits good mobility, which is similar to **IID-T3**. Winnewisser et al. synthesized **BBTDPP1** [34], which has an identical backbone to **PDQT**. However, after introducing dodecyl chains, the highest hole mobility was only 0.1 $\mathrm{cm^2\ V^{-1}\ s^{-1}}$, almost one order of magnitude lower than **PDQT**. This example is comparable with **IIDDT-Me**, which supported our "molecular docking" strategy that the alkyl chains on "small core" will hinder the polymer π–π stacking and lead to reduced device performance.

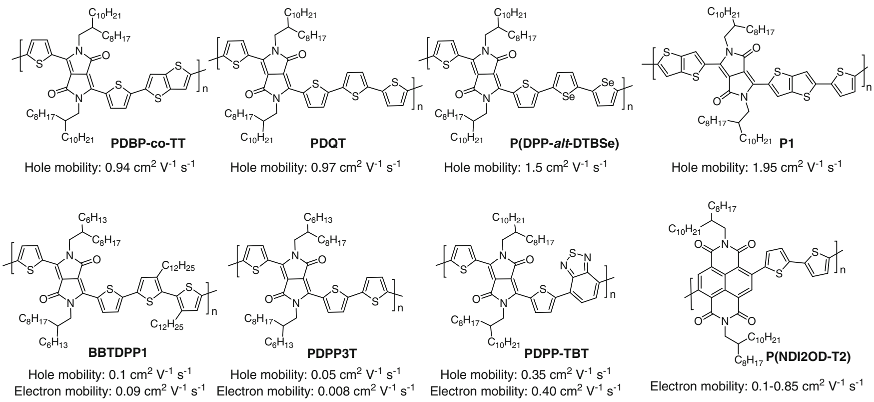

Scheme 2.3 Diketopyrrolopyrrole and naphthalenedicarboximide-based conjugated polymers and their FET performances

2.4 Influence of Side Chain Branching Positions

Compared with linear alkyl chains, branched alkyl chains, such as 2-ethylhexyl, 2-octyldodecyl, and 2-decyltetradecyl groups, generally provide better solubility. Interestingly, the distance of the branching point of these branched chains to the conjugated backbone is only one methylene group, presumably because they are readily available. As discussed above, alkyl chains may impede interchain π–π interactions. Similarly, when the branching points are close to polymer backbones, steric hindrance may also occur due to the large van der Waals radii in the branching position. To increase the structural diversity of solubilizing groups, Bao designed an unconventional siloxane-terminated hexyl chain, which exhibited closer backbone packing and increased hole mobility up to 2.48 $cm^2\ V^{-1}\ s^{-1}$ [35]. However, the trimethylsilyl group can’t survive under certain reaction conditions, hence limiting the application of this group. Thus, we designed three novel branched alkyl chains (3-decyltridecyl, 4-decyltetradecyl, and 5-decylpentadecyl) to modify the polymer (Scheme 2.4). We investigated how moving the branching point of these “more conventional” alkyl chains farther from the backbone influence the mobilities [36]. The sequential changing of these “more conventional” branched alkyl chains result in a remarkably high mobility of 3.62 $cm^2\ V^{-1}\ s^{-1}$. Thus we demonstrate that a subtle change of conventional alkyl chains can lead to a significant improvement of device performance.

Scheme 2.4 illustrates the synthetic route of these polymers. The alkyl side chains with various branching positions can be readily synthesized and introduced to isoindigo core with high yield. Interestingly, the R_f values of **IID-C3** and **IID-C4** on TLC (0.52 for **IID-C3** and 0.53 for **IID-C4**) are significantly smaller than those of **IID** and **IID-C2** (0.61 for both) (Fig. 2.12). It is likely that the polar carbonyl groups in the isoindigo core are somewhat shielded by the alkyl side chains, and moving the branched point away exposes these polar groups, thus leading to stronger interactions

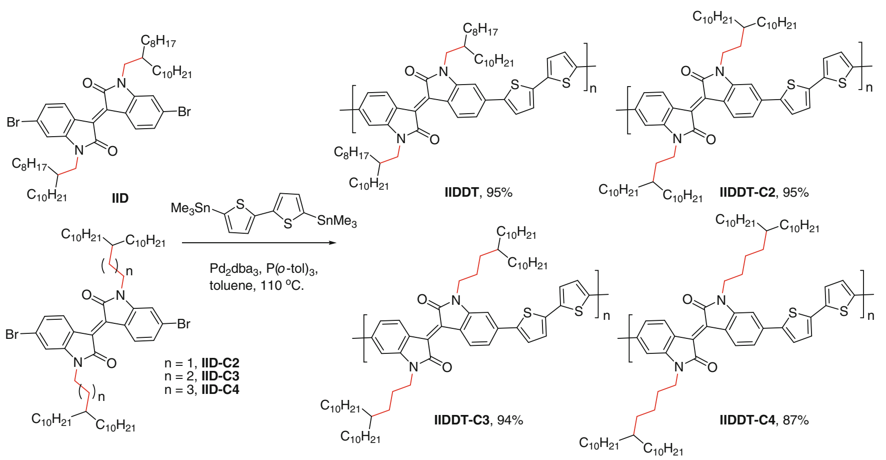

Scheme 2.4 Synthesis of isoindigo polymers with alkyl side chains branched at various positions

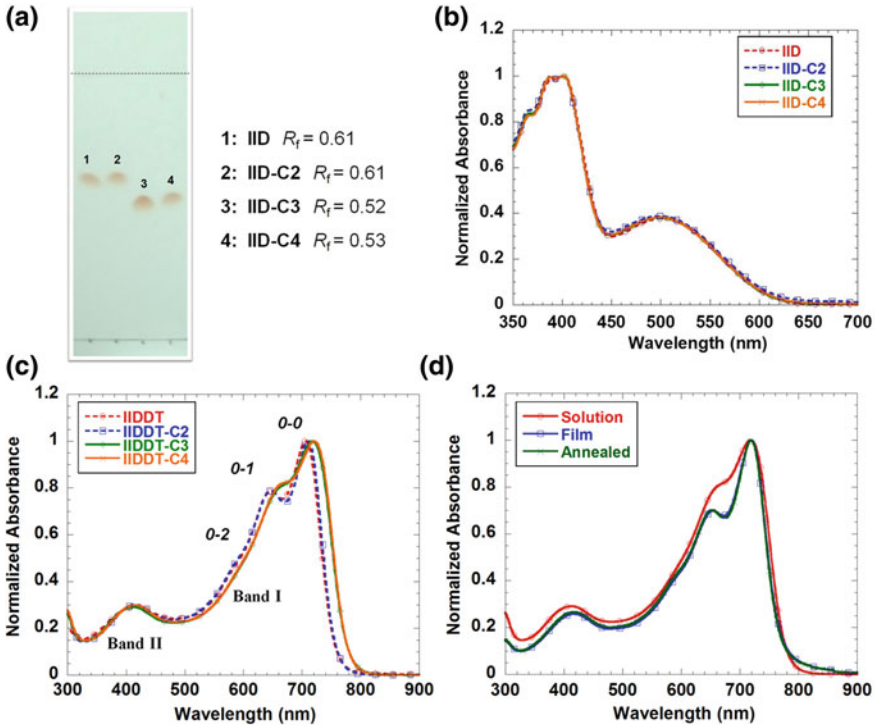

Fig. 2.12 **a** Thin layer chromatography (TLC) experiment of four monomers **IID**, **IID-C2**, **IID-C3**, and **IID-C4** (eluent: PE:DCM = 1:1). Although they have identical backbone and similar alkyl chains, **IID-C3** and **IID-C4** showed stronger interaction with silica gel. **b** Normalized UV-*vis* absorption spectra of monomers in chloroform (1×10^{-5} M). All monomers showed almost identical absorption spectra. Normalized absorption spectra of **c** four polymers in $CHCl_3$ (1×10^{-5} M) and **b** **IIDDT-C3** in $CHCl_3$, in thin film, and in annealed film (at 150 °C for 30 min)

of the monomer with the silica gel. Similar to the preparation of polymer **IIDDT**, Stille-coupling polymerization between dibromide **IID-C2**, **IID-C3**, or **IID-C4** and 5,5′-bis(trimethylstannyl)-2,2′-bithiophene was used to afford **IIDDT-C2**, **IIDDT-C3**, and **IIDDT-C4** in high yields. All polymers were obtained as dark metallic solids after standard purification including precipitation into methanol and subsequent Soxhlet extraction with acetone, hexane, and chloroform. Molecular weights of all polymers were evaluated by GPC with 1,2,4-tricholorobenzene (TCB) as eluent at 150 °C (Table 2.4). **IIDDT-C3** and **IIDDT-C4** appeared to have larger molecular weight (M_n) and polydispersity index (PDI) because of shoulder peaks in the large molecular weight region. These shoulder peaks are presumably attributed to inter-polymer aggregations. All the polymers showed good thermal stability with decomposition temperatures over 370 °C. No phase transition was observed for all polymers by DSC in the range of −10 to 300 °C.

Absorption spectra of all polymers and monomers were measured both in solution and in thin film. All monomers showed almost identical absorption spectra (Fig. 2.12b), suggesting that the alkyl chains do not affect the photophysical properties of the aromatic core. All polymers showed typically dual band absorption (Fig. 2.12c). Compared with **IIDDT** and **IIDDT-C2**, **IIDDT-C3** and **IIDDT-C4** showed obviously red-shifted absorption in solution. The red-shift may be attributed to interpolymer π–π stacking, which makes the polymer backbone of **IIDDT-C3** and **IIDDT-C4** more planar. This result is in agreement with the GPC result that **IIDDT-C3** and **IIDDT-C4** exhibited some aggregation even at 150 °C. Absorption peaks of all the polymers in thin film showed interesting blue-shift (especially 0–1 vibrational peaks) in comparison with those in solution, which may correlate with their solid state packing. Scrutiny of spectra revealed that the 0–0 vibrational transition increases whereas 0–1 decreases in film, suggesting that polymers become more planar in film with enhanced π–π stacking. Annealing the films led to a further slightly increase of the 0–0 vibrational absorption, indicating that the packing and planarity of polymers are improved.

Table 2.4 Molecular weight, optical and electrochemical properties of polymers

Polymers	M_n (kDa)/PDI	T_d (°C)	λ_{max}^{sol} (nm)[a]	λ_{max}^{film} (nm)	E_g^{opt} (eV)[b]	E_{HOMO} (eV)[c]	E_{LUMO} (eV)[c]	E_g^{CV} (eV)[d]	E_{HOMO}^{PES} (eV)
IIDDT	20.4/2.0	390	706, 647	701, 637	1.60	−5.70	−3.70	2.00	−5.54
IIDDT-C2	18.4/2.0	384	711, 647	707, 641	1.60	−5.60	−3.70	1.90	−5.57
IIDDT-C3	39.2/3.2	392	718, 673	719, 653	1.58	−5.52	−3.74	1.78	−5.33
IIDDT-C4	37.3/2.3	374	719, 675	716, 647	1.58	−5.50	−3.74	1.76	−5.26

[a] 10^{-5} M in chloroform

[b] Estimated from the onset of thin-film absorption

[c] Cyclic voltammetry determined with Fc/Fc$^+$ ($E_{HOMO} = -4.80$ eV) as external reference

[d] $E_g^{CV} = E_{LUMO} - E_{HOMO}$

Cyclic voltammetry was used to evaluate electronic energy levels of the polymers. All the polymers showed much stronger oxidative peaks than their reductive ones, almost one order of magnitude higher, indicating that these polymers are easier to be oxidized than to be reduced (Fig. 2.13). Moving the branching point away from the polymer backbones led to noticeable increase of the HOMO levels from −5.70 eV (**IIDDT**) to −5.50 eV (**IIDDT-C4**). However, the LUMO levels showed only slight decrease from −3.70 eV (**IIDDT**) to −3.74 eV (**IIDDT-C4**). This result may be again due to more planar backbone and better π–π stacking in **IIDDT-C3** and **IIDDT-C4**. The computational study also displayed that LUMO of the polymers are localized on isoindigo core whereas HOMO are distributed along the polymer chain. Thus, HOMO levels of the polymers are more easily affected by their conformational change. Photoelectron spectroscopy (PES) was also used to measure the HOMO energy levels of the polymers. A similar variation trends was found, thus further confirming the CV results.

It is known that charge carrier mobility in OFETs strongly depends on the frontier orbital overlap integrals. The overlap integrals are sensitive to π–π stacking distance and molecular packing conformation [37]. To probe how moving alkyl chain branched point away influences the charge transport of the polymers, we fabricated bottom-gate/top-contact field-effect devices. A thin layer of polymers was deposited on OTS-treated SiO_2 (300 nm)/n^{++}-Si substrate by spin-coating a polymer solution (4 mg/mL in 1,1,2,2-tetrachloroethane) at 1,000 rpm for 40 s. In our previous report, **IIDDT** films showed an average hole mobility of 0.66 $cm^2\ V^{-1}\ s^{-1}$ and a maximum mobility of 1.06 $cm^2\ V^{-1}\ s^{-1}$ [14]. In contrast, **IIDDT-C3** films exhibited a mobility up to 3.62 $cm^2\ V^{-1}\ s^{-1}$ and an average mobility of 2.98 $cm^2\ V^{-1}\ s^{-1}$ after annealing at 175 °C for 30 min (Fig. 2.14a). **IIDDT-C4** films also displayed increased mobility: the highest mobility was up to 1.76 $cm^2\ V^{-1}\ s^{-1}$ and the average mobility was 1.44 $cm^2\ V^{-1}\ s^{-1}$. Unexpectedly, **IIDDT-C2** films showed decreased device performance compared with **IIDDT** films. The highest mobility of **IIDDT-C2** films was only 0.40 $cm^2\ V^{-1}\ s^{-1}$ (Table 2.5). Recently, Müllen et al. reported that molecular

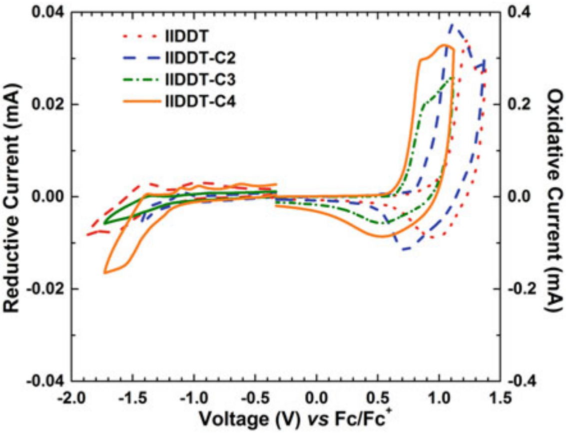

Fig. 2.13 Cyclic voltammogram of polymers in thin film drop-casted on a glassy carbon electrode and tested in *n*-Bu_4NPF_6/CH_3CN solution (scan rate: 50 mV s^{-1})

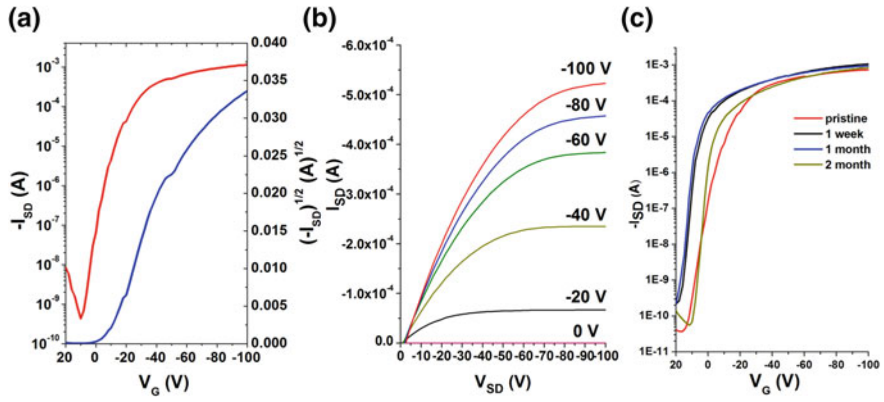

Fig. 2.14 **a** Transfer and **b** output characteristics of an **IIDDT-C3** device (spin-casted from TCE solutions, 4 mg/mL) after thermal annealing. $V_{SD} = -100$ V ($L = 60$ μm, $W = 3.0$ mm). The hole mobility in the saturation regime was calculated from the slopes obtained by linear fitting of $(I_{SD})^{1/2}$ versus V_G in the V_G range from −21 to −30 V. **c** Changes in transfer characteristics of a **IIDDT-C3** device under 50–60 % humidity

weight played an important role in improving hole mobilities [38]. We were aware of the relatively low M_n of **IIDDT** and **IIDDT-C2**. Hence we synthesized polymer **IIDDT-C3** with a M_n of 20 kDa, comparable to those of **IIDDT** and **IIDDT-C2**. The low molecular weight **IIDDT-C3** also showed the highest hole mobility of over 3 cm^2 V^{-1} s^{-1}, thus further confirming the significant effect of moving branching point away. Nonetheless, increased M_n of **IIDDT-C3** and **IIDDT-C4** may still contribute to their high hole mobilities. In addition, **IIDDT-C3** and **IIDDT-C4** also displayed good stability under ambient conditions (R_H = 50–60 %) for at least 2 months (Fig. 2.14c).

The high hole mobilities of **IIDDT-C3** and **IIDDT-C4** are likely due to the more exposed isoindigo core and stronger π–π interactions of the polymer backbones. To gain further understanding, GIXD and AFM were used to investigate polymer packings and film morphologies. As shown in Fig. 2.15, **IIDDT-C3** displays a strong out-of-plane diffraction at 2θ of 2.88º, corresponding to a d-spacing of

Table 2.5 FET device performances and GIXD results of polymers

Polymers	$T_{annealing}$ (°C)	μ (cm^2 V^{-1} s^{-1})^a	V_T (V)	I_{on}/I_{off}	d (Å)^b	
					L	π
IIDDT	150	1.06 (0.66)	−18	>10^6	20.3	3.75
IIDDT-C2	200	0.40 (0.28)	−10	>10^5	23.7	3.61
IIDDT-C3	175	3.62 (2.98)	−2	>10^6	24.7	3.57
IIDDT-C4	175	1.76 (1.44)	−5	>10^6	26.1	3.57

[a] Measured under ambient condition (R_H = 50–60 %). Maximum values of hole mobilities, and average mobilities are shown in parentheses (more than 10 devices were tested)

[b] Lamellar (L) and π–π stacking (π) distances determined by GIXD experiments

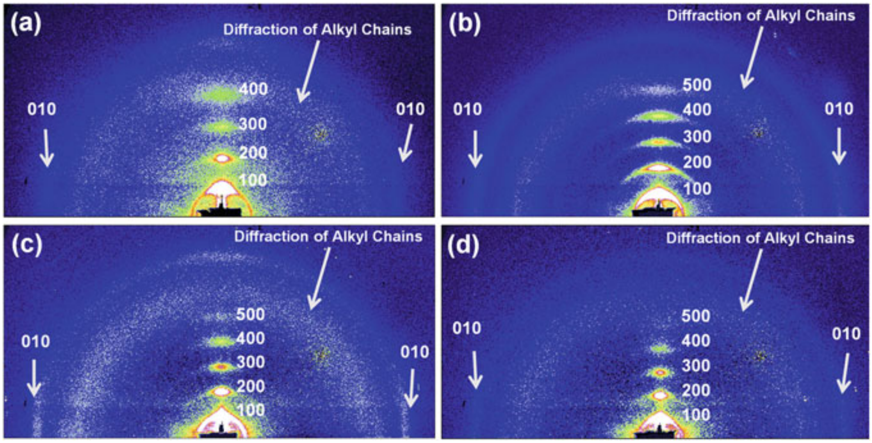

Fig. 2.15 2D-GIXD patterns of **a IIDDT**, **b IIDDT-C2**, **c IIDDT-C3** and **d IIDDT-C4** film after thermal annealing (at 150 °C for 30 min). All polymers display lamellar packings

24.7 Å (λ = 1.2398 Å). Other four diffractions are attributed to 200, 300, 400, and 500 diffractions, indicating that **IIDDT-C3** has a long-range ordered edge-on lamellar packing. **IIDDT-C2** and **IIDDT-C4** also show similar out-of-plane lamellar packing with a *d*-spacing of 23.7 and 26.1 Å, respectively. Their *d*-spacings correlate well with their alkyl chain lengths, suggesting the alkyl side chains all adopt a similar extended conformation in films. Compared with **IIDDT-C3**, **IIDDT** shows obviously broader diffractions and only four lamellar diffraction peaks. Thus polymer packings in **IIDDT-C3** film are more ordered. In the in-plane diffractions, the π–π stacking diffractions of polymers (010) are observed. After moving the branching point away from backbones, the polymers show gradually decreased π–π stacking distances (3.75 Å for **IIDDT**, 3.61 Å for **IIDDT-C2**, and 3.57 Å for both **IIDDT-C3** and **IIDDT-C4**). **IIDDT-C3** also displays more intense 010 diffractions, suggesting stronger π–π stacking interactions. Besides, diffraction halos of alkyl chains are also observed in the range of 4–5 Å, larger than π–π stacking distances. Therefore, largely improved mobilities are likely due to decreased π–π stacking distances. AFM images of the polymer films show crystalline fibrillar intercalating networks. The crystalline networks are likely the result of strong intermolecular π–π interactions, similar to other high performance OFET materials.

In Bao's work, the polymer with a hole mobility of 2.48 cm^2 V^{-1} s^{-1} has a π–π stacking distance of 3.58 Å, and the reference polymer has a mobility of 0.57 cm^2 V^{-1} s^{-1} and a distance of 3.76 Å [35]. In Liu's work, the DPP-based polymer with 2-decyltetradecyl group gives a record-breaking high mobility of 8.2 cm^2 V^{-1} s^{-1} with a π–π stacking distance of 3.66 Å, and the reference polymer with 2-octyldodecyl group has a mobility of 4.5 cm^2 V^{-1} s^{-1} and a distance of 3.72 Å [39]. Our results further confirmed this hypothesis that **IIDDT-C3** shows the highest mobility (3.62 cm^2 V^{-1} s^{-1}) and the shortest distance (3.57 Å). On the other hand, although π–π stacking distances of **IIDDT** and **IIDDT-C4** decreased with the moving branching positions, their mobilities did not always increase correspondingly. For instance, π–π stacking distance of **IIDDT-C2** (3.61 Å) is considerably shorter than that of **IIDDT** (3.75 Å), but the mobility of **IIDDT-C2** is lower than (0.40 $cm^2 V^{-1} s^{-1}$) that of **IIDDT** (1.06 $cm^2 V^{-1} s^{-1}$). **IIDDT-C3** and **IIDDT-C4** both have the shortest distance (3.57 Å), but their mobilities differ (3.62 $cm^2 V^{-1} s^{-1}$ for high M_n **IIDDT-C3**, 3.00 $cm^2 V^{-1} s^{-1}$ for low M_n **IIDDT-C3**, and 1.76 $cm^2 V^{-1} s^{-1}$ for **IIDDT-C4**). Besides, we have also been aware that in Liu's work, it is the length of alkyl chains rather than the branching position plays a dramatic role. Thus we prepared **IIDDT** with 2-decyltetradecyl group and found a mobility of 0.96 $cm^2 V^{-1} s^{-1}$ and a π–π stacking distance of 3.75 Å, almost identical to those of **IIDDT** (1.06 $cm^2 V^{-1} s^{-1}$ and 3.75 Å). Recently, Beljonne and coworkers demonstrated that charge transport correlates with the supramolecular organization of polymers; in addition, the π–π stacking distance and the packing conformation greatly affect the interpolymer chain carrier transport [40]. We propose that the polymer packing conformation of the polymers, such as degrees of translation and rotation, also plays a critical role in carrier mobility, which resulted in the inconsistency between device performances and π–π stacking distances.

2.5 Conclusions

In this chapter, we have analyzed the single crystal structure of alkanes and found that the alkyl chains may hinder the π–π stacking in conjugated polymers. In order to reduce the steric hindrance, we have proposed "molecular docking" strategy to design high-performance polymer FET materials. According to this concept, we have developed the first isoindigo-based polymer FETs for the first time and demonstrated that isoindigo can endow polymers with both high mobility and excellent ambient stability. The devices of **IIDDT** showed excellent stability for 6 months under ambient conditions, largely due to its low-lying HOMO level.

To further prove this strategy, we designed and synthesized 10 polymers to compare their physical properties and device performances. The key concept of molecular docking is that the small conjugated units can dock into the cavity formed by large aromatic cores and alkyl chains. This docking leads to increased interchain π–π stacking of the polymer. According to the strategy, six polymers with centrosymmetric units show hole mobilities of over 0.1 $cm^2 V^{-1} s^{-1}$, in which five polymers show hole mobilities of over 0.3 $cm^2 V^{-1} s^{-1}$. We also found that polymer symmetry and backbone curvature also affect interchain "molecular docking" of isoindigo-based polymers in film, ultimately leading to different device performances (Fig. 2.16).

We further assumed that the branching positions of alkyl side chains may close to the polymer backbones, so that the large van der Waals radii of the branching point may also hinder the π–π stacking in the conjugated polymers. Therefore, we synthesised novel alkyl side chains with different branching positions and introduced them to polymer FETs for the first time. We investigated how the branching

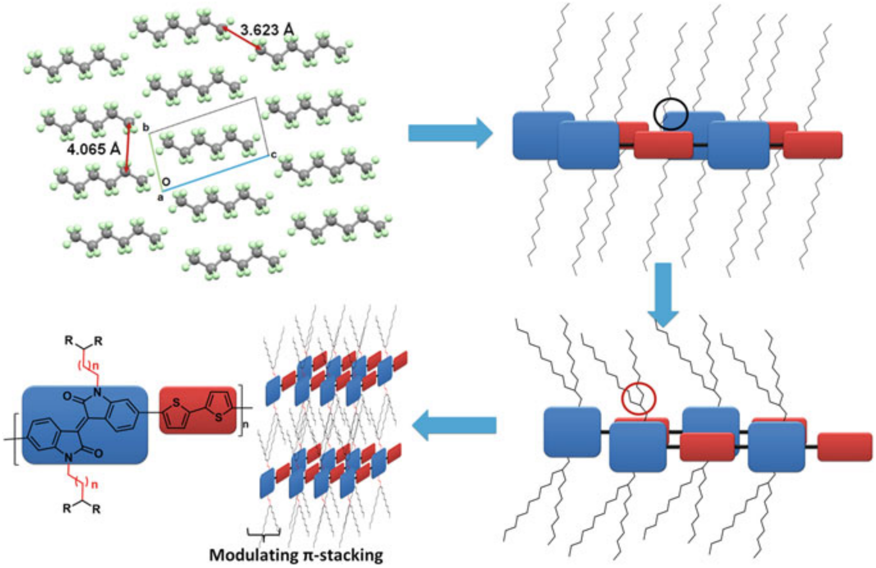

Fig. 2.16 Design strategy of this chapter

positions influenced polymer's mobility and further increased the hole mobility of isoindigo-based polymers to 3.62 $cm^2 V^{-1} s^{-1}$. We also found the inconsistency between device performances and π–π stacking distances, which is probably caused by the different polymer packing conformations. This work reveals that side chain engineering is a powerful strategy to modulate the device performance of conjugated polymers.

2.6 Experimental Details and Characterization

2.6.1 Device Fabrication and Characterization

Bottom-gate top-contact (BGTC) OTFT devices were fabricated using n^{++}-Si/SiO_2 (300 nm) substrates where n^{++}-Si and SiO_2 were used as the gate electrode and gate dielectric, respectively. The substrates were subjected to cleaning using ultrasonication in acetone, cleaning agent, deionized water (twice), and *iso*-propanol. The cleaned substrates were dried under vacuum at 80 °C. The substrates were then treated with plasma for 15 min and transfer into a glove box. The substrates were modified with OTS to form a SAM monolayer. Thin films of the polymer were deposited on the treated substrates by spin coating using a polymer solution (4 mg/mL), optionally followed by thermal annealing at different temperatures under nitrogen. After polymer thin film deposition, 30 nm thick gold electrodes were deposited as source and drain using a shadow mask. The OTFT devices had a channel length (*L*) of 60 μm and a channel width (*W*) of 3 mm or *L* of 60 μm and *W* of 0.44 mm.

The evaluations of the OTFTs were carried out using a Keithley 4200 SCS parameter analyzer on a probe stage under ambient conditions. The carrier mobility, μ, was calculated from the data in the saturated regime according to the equation $I_{DS} = (W/2L)C_i\mu(V_G - V_T)^2$, where I_{DS} is the drain current in the saturated regime. W and L are, the semiconductor channel width and length, respectively. C_i ($C_i = 11$ nF) is the capacitance per unit area of the gate dielectric layer. V_G and V_T are the gate voltage and threshold voltage. $V_G - V_T$ was determined from its relationship with the square root of I_{DS} at the saturated regime.

2.6.2 Synthetic Procedures and Characterization

6,6′-dibromoisoindigo [7], 1-iodo-2-octyldodecane, [41] and monomer **3-4** [29], **3-5** [15], **3-6** [16], **3-7** [17], **3-8** [18], and **3-9** [19] were synthesized according to the literature. The alkyl iodide compounds with farther branching positions were purchased from Lyn (Beijing) Science & Technology Co., Ltd. (http://www.lyntech.cn/).

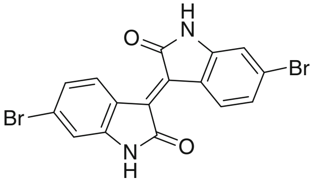

6,6′-dibromoisoindigo: To a suspension of 6-bromooxindole (2.13 g, 0.942 mmol) and 6-bromoisatin (2.00 g, 0.942 mmol) in AcOH (60 mL) was added conc. HCl (37 %) solution (0.5 mL). The mixture was refluxed for 24 h. The mixture was allowed to cool and filtered. The solid material was washed with water, ethanol, and ether. After drying under vacuum, brown 6,6′-dibromoisoindigo (3.4 g, 86 %) was obtained.

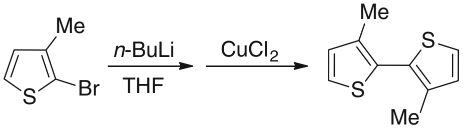

2-12

3,3′-dimethyl-2,2′-bithiophene (**2-12**) [42]: 2-Bromo-3-methylthiophene (2.5 g, 12.70 mmol) was dissolved in anhydrous THF (20 mL). The solution was cooled to −78 °C and *n*-BuLi (5.59 mL, 2.5 M solution) was added dropwise. The mixture was stirred at −78 °C for 10 min, and then $CuCl_2$ (1.88 g, 14.00 mmol) was added in portions carefully. The mixture was then allowed to stir at −78 °C for 1 h and then at room temperature for 5 h. The mixture was quenched with 20 mL of water. The aqueous layer was extracted with CH_2Cl_2, the combined extracts were washed with distilled water, dried over anhydrous Na_2SO_4. After removal of the solvents under reduced pressure, the residue was purified via chromatography with silica (petroleum ether as eluent) to afford colorless oil (680 mg, yield: 55 %). ^1H NMR ($CDCl_3$, 300 MHz, ppm): δ 7.26–7.28 (d, $J = 5.4$ Hz, 2H), 6.92–6.94 (d, $J = 5.4$ Hz, 2H), 2.17 (s, 6H).

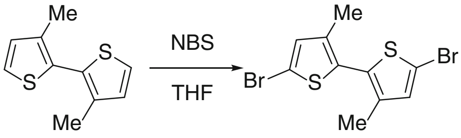

2-13

5,5′-Dibromo-3,3′-dimethyl-2,2′-bithiophene (**2-13**) [42]: To a solution of 3,3′-dimethyl-2,2′-bithiophene (680 mg, 3.51 mmol) in THF (30 mL) was added *N*-bromosuccinimide (1.25 g, 7.01 mmol). After stirred overnight, the reaction was quenched with water. The aqueous layer was extracted with CH_2Cl_2, the combined extracts were washed with distilled water, dried over anhydrous Na_2SO_4. After removal of the solvents under reduced pressure, the residue was purified via chromatography with silica (petroleum ether as eluent) to give yellow oil **12** (800 mg, yield: 58 %). ^1H NMR ($CDCl_3$, 300 MHz, ppm): δ 6.88 (s, 2H), 2.12 (s, 6H).

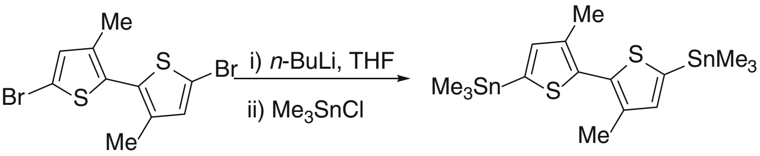

2-14

5,5′-Bis(trimethylsilyl)-3,3′-dimethyl-2,2′-bithiophene (**2-14**) [43]: To a solution of 5,5′-dibromo-3,3′-dimethyl-2,2′-bithiophene (500 mg) in anhydrous THF (30 mL) was added dropwies *n*-BuLi (1.23 mL, 2.5 M solution) at −78 °C. After the addition, the mixture was stirred at −78 °C for 1 h. A solution of trimethyltin chloride (712 mg, 3.57 mmol) in 5 mL of anhydrous THF was added dropwise. After stirred overnight at room temperature, the mixture was quenched with water.

The aqueous layers were extracted with ether, the combined extracts were washed with distilled water, dried over anhydrous Na_2SO_4. After removal of the solvents at reduced pressure, the residue was evaporated in vacuum to obtain a green solid. (620 mg, yield: 93 %). ^{1}H NMR ($CDCl_3$, 300 MHz, ppm): δ 7.00 (s, 2H), 2.21 (s, 6H), 0.37 (s, 18H).

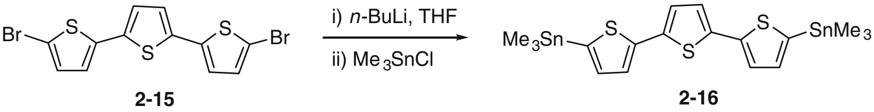

2,5″-Bis(trimethylsilyl)-5,2′,5′,2″-terthiophene (**2-15**) [44]: To a solution of 2,5″-Dibromo-5,2′,5′,2″-terthiophene (1 g, 2.46 mmol) was dissolved in anhydrous THF (50 mL). The mixture was cooled to −78 °C and *n*-BuLi (2.27 mL, 2.5 M solution) was added dropwise. After the addition, the mixture was stirred at same temperature for 1 h. A solution of trimethyltin chloride (1.18 g, 5.91 mmol) in THF (5 mL) was added dropwise. After stirred overnight, the mixture was quenched with water. The aqueous layers were extracted with ether, the combined extracts were washed with distilled water, dried over anhydrous Na_2SO_4. After removal of the solvents at reduced pressure, the residue was evaporated in vacuum. Recrystallization of the crude product in ethanol afforded a yellow solid. (875 mg, yield 62 %). ^{1}H NMR ($CDCl_3$, 300 MHz, ppm) δ: 7.27–7.28 (d, J = 3.6 Hz, 2H), 7.09–7.10 (d, J = 3.6 Hz, 2H), 7.07 (s, 2H), 0.39 (s, 18H).

General procedures for alkylation of 6,6′-dibromoisoindigo:

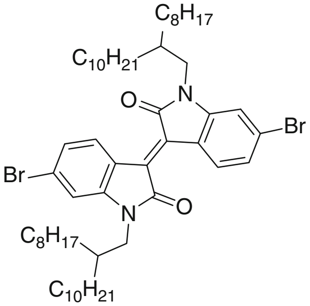

IID: To a solution of 6,6′-dibromoisoindigo (510 mg, 1.21 mmol), potassium carbonate (500 mg, 3.63 mmol) in dimethylformamide (DMF) (40 mL), 1-iodo-2-octyldodecane (1.19 g, 2.91 mmol) was added under nitrogen. The mixture was stirred for 24 h at 100 °C and then the solvent was removed under reduced pressure. The residues were purified by silica gel chromatography with eluting (PE: DCM = 5:1) to give 6,6′-dibromo-*N*,*N*′-(2-octyldodecanyl)-isoindigo as a deep-red solid. (882 mg, 74 %). ^{1}H NMR ($CDCl_3$, 300 MHz, ppm): δ 9.05–9.02 (d,

$J = 8.7$ Hz, 2H), 7.16–7.13 (dd, $J_1 = 8.7$ Hz, $J_2 = 1.5$ Hz, 2H), 6.86 (d, $J = 1.5$ Hz, 2H), 3.59–3.57 (m, 4H), 1.85 (m, 2H), 1.30–1.20 (m, 48H), 0.93–0.84 (m, 12H). ^{13}C NMR (CDCl$_3$, 100 MHz, ppm): δ 168.09, 146.20, 132.55, 131.03, 126.65, 125.09, 120.38, 111.52, 44.69, 36.09, 31.92, 31.87, 31.50, 29.98, 29.62, 29.60, 29.35, 29.29, 26.36, 22.69, 14.12. ESI-HRMS: Calcd. for $[M + H]^+$: 981.5270. Found: 981.5277. Elemental Anal.: Calcd. for $C_{56}H_{88}Br_2N_2O_2$: C, 68.55; H, 9.04; N, 2.86. Found: C, 68.48; H, 9.01; N, 2.88.

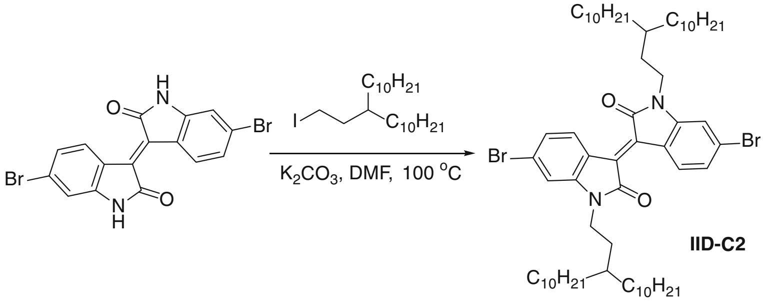

IID-C2

IID-C2: The synthetic procedure is similar as described for **IID**. Yield: 88 %. ^{1}H NMR (CDCl$_3$, 400 MHz, ppm) δ 9.09–9.07 (d, $J = 8.6$ Hz, 2H), 7.17–7.15 (dd, $J_1 = 8.6$ Hz, $J_2 = 1.6$ Hz, 2H), 6.89–6.88 (d, $J = 1.6$ Hz, 2H), 3.74–3.70 (t, $J = 7.4$ Hz 4H), 1.71–1.56 (q, $J = 6.3$ Hz, 4H), 1.42–1.26 (m, 74H), 0.90–0.86 (t, $J = 6.8$ Hz, 4H). ^{13}C NMR (CDCl$_3$, 100 MHz, ppm): δ 167.49, 145.68, 132.55, 131.22, 126.66, 125.05, 120.44, 111.18,55 38.39, 35.61, 33.44, 31.93, 30.96, 30.04, 29.70, 29.69, 29.66, 29.36, 26.62, 22.70, 14.12. Elemental Anal.: Calcd. for $C_{62}H_{100}Br_2N_2O_2$: C, 69.90; H, 9.46; N, 2.63. Found: C, 69.78; H, 9.46; N, 2.62. ESI-HRMS: Calcd. for $[M + H]^+$: 1063.62243. Found: 1063.6248.

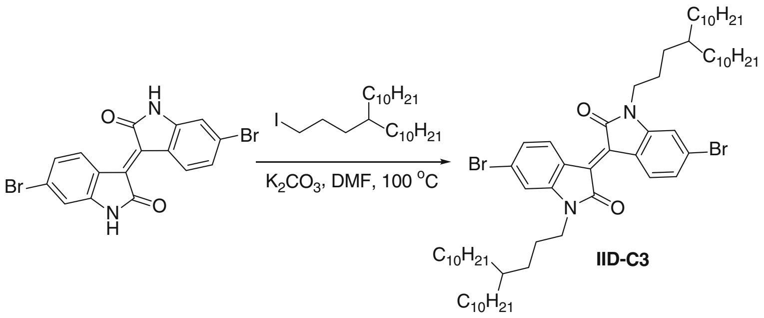

IID-C3

IID-C3: The synthetic procedure is similar as described for **IID**. Yield: 71 %. ^{1}H NMR (CDCl$_3$, 400 MHz, ppm): δ 9.10–9.08 (d, $J = 8.6$ Hz, 2H), 7.18–7.16 (dd, $J_1 = 8.6$ Hz, $J_2 = 1.6$ Hz, 2H), 6.93–6.92 (d, $J = 1.6$ Hz, 2H), 3.73–3.69

(t, J = 7.4 Hz, 4H), 1.68–1.64 (m, 4H), 1.34–1.22 (m, 78H), 0.89–0.86 (t, J = 6.6 Hz, 12H). ^{13}C NMR (CDCl$_3$, 100 MHz, ppm): δ 167.68, 145.76, 132.60, 131.21, 126.72, 125.10, 120.41, 111.28, 40.61, 37.10, 33.52, 31.93, 30.81, 30.09, 29.69, 29.65, 29.36, 26.67, 24.47, 22.69, 14.12. Elemental Anal.: Calcd. for $C_{64}H_{104}Br_2N_2O_2$: C, 70.31; H, 9.59; N, 2.56. Found: C, 70.50; H, 9.62; N, 2.53. ESI-HRMS: Calcd. for $[M + H]^+$: 1091.65373. Found: 1093.6549.

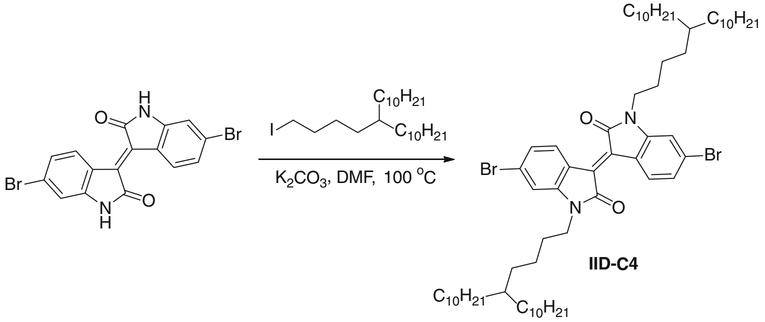

IID-C4: The synthetic procedure is similar as described for **IID**. Yield: 83 %. ^{1}H NMR (CDCl$_3$, 400 MHz, ppm) δ 9.10–9.07 (d, J = 8.6 Hz, 2H), 7.17–7.14 (dd, J_1 = 8.6 Hz, J_2 = 1.6 Hz, 2H), 6.92–6.91 (d, J = 1.6 Hz, 2H), 3.74–3.70 (t, J = 7.4 Hz, 4H), 1.67–1.62 (m, 4H), 1.36–1.22 (m, 82H), 0.89–0.86 (t, J = 6.8 Hz, 12H). ^{13}C NMR (CDCl$_3$, 100 MHz, ppm): δ 167.67, 145.76, 132.59, 131.23, 126.71, 125.10, 120.41, 111.26, 40.27, 37.39, 33.61, 33.36, 31.93, 30.13, 29.72, 29.66, 29.37, 27.78, 26.71, 24.22, 22.70, 14.12. Elemental Anal.: Calcd. for $C_{66}H_{108}Br_2N_2O_2$: C, 70.69; H, 9.71; N, 2.50. Found: C, 70.79; H, 9.55; N, 2.49. ESI-HRMS: Calcd. for $[M + Na]^+$: 1141.66670. Found: 1141.6684.

General procedures for Stille polymerization and polymer purification:

IIDT: 6,6′-Dibromo-*N*,*N*′-(2-octyldodecanyl)-isoindigo (329 mg, 0.335 mmol), 2,5-bis(trimethylstannyl)thiophene (137.5 mg, 0.335 mmol), $Pd_2(dba)_3$ (3.0 mg, 1 mol%.), P(*o*-tol)$_3$ (8.2 mg, 8 mol%) and 20 mL of toluene were added to a Schlenk tube. The tube was charged with nitrogen through a *freeze-pump-thaw* cycle for three times. The mixture was stirred for 48 h at 110 °C. A strongly complexing ligand *N*,*N*-diethylphenylazothioformamide (20 mg) was then added and stirred with the polymer for 3 h to remove any residual catalyst before being precipitated into methanol (100 mL). The precipitate was filtered through a nylon filter and purified via Soxhlet extraction for 8 h with methanol, 12 h with hexanes and finally was collected with chloroform. The chloroform solution was then concentrated by evaporation and precipitated into methanol (200 mL) and filtered off as a dark solid (290 mg, yield 96 %). Elemental Anal. Calcd: for $(C_{60}H_{90}N_2O_2S)_n$: C, 79.77; H, 10.04; N, 3.10. Found: C, 75.49; H, 9.48; N, 2.83.

IIDDT: The synthetic procedure is similar as described for **IIDT**. Yield: 95 %. Elemental Anal. Calcd. for $(C_{64}H_{94}N_2O_2S_2)_n$: C, 77.84; H, 9.59; N, 2.84. Found: C, 76.99; H, 9.13; N, 2.78.

IID-Se: The synthetic procedure is similar as described for **IIDT**. Yield: 89 %. Elemental Anal.: Calcd. for $(C_{64}H_{92}N_2O_2Se_2)_n$: C, 71.22; H, 8.59; N, 2.60; Found: C, 68.16; H, 8.10; N, 2.35.

IID-BDT: The synthetic procedure is similar as described for **IIDT**. Yield: 90 %. Elemental Anal.: Calcd. for $(C_{66}H_{92}N_2O_2S_2)_n$: C, 75.82; H, 9.19; N, 2.77; Found: C, 77.18; H, 9.02; N, 2.69.

IID-NDT: The synthetic procedure is similar as described for **IIDT**. Yield: 75 %. Elemental Anal.: Calcd. for $(C_{70}H_{94}N_2O_2S_2)_n$: C, 79.34; H, 8.94; N, 2.64; Found: C, 78.07; H, 8.87; N, 2.57.

IID-TT: The synthetic procedure is similar as described for **IIDT**. Yield: 93 %. Elemental Anal.: Calcd. for $(C_{62}H_{90}N_2O_2S_2)_n$: C, 74.22; H, 9.00; N, 2.75; Found: C, 76.28; H, 9.30; N, 2.79.

IID-Me: The synthetic procedure is similar as described for **IIDT**. Yield: 79 %. Elemental Anal.: Calcd. for $(C_{66}H_{96}N_2O_2S_2)_n$: C, 78.21; H, 9.55; N, 2.76; Found: C, 76.78; H, 9.43; N, 2.68.

IID-T3: The synthetic procedure is similar as described for **IIDT**. Yield: 80 %. Elemental Anal.: Calcd. for $(C_{68}H_{94}N_2O_2S_3)_n$: C, 76.50; H, 8.87; N, 2.62; Found: C, 75.64; H, 8.86; N, 2.55.

IID-TTT: The synthetic procedure is similar as described for **IIDT**. Yield: 72 %. Elemental Anal.: Calcd. for $(C_{64}H_{90}N_2O_2S_3)_n$: C, 75.69; H, 8.93; N, 2.76; Found: C, 74.52; H, 8.88; N, 2.72.

IIDDT-C2: The synthetic procedure is similar as described for **IIDT**. Yield: 94 %. Elemental Anal. Calcd: for $(C_{70}H_{104}N_2O_2S_2)_n$: C, 78.52; H, 9.88; N, 2.62. Found: C, 77.78; H, 9.47; N, 2.55.

IIDDT-C3: The synthetic procedure is similar as described for **IIDT**. Yield: 94 %. Elemental Anal. Calcd. for $(C_{72}H_{108}N_2O_2S_2)_n$: C, 77.78; H, 9.92; N, 2.55. Found: C, 77.85; H, 9.75; N, 2.48.

IIDDT-C4: The synthetic procedure is similar as described for **IIDT**. Yield: 87 %. Elemental Anal. Calcd. for $(C_{74}H_{112}N_2O_2S_2)_n$: C, 78.95; H, 10.03; N, 2.49. Found: C, 78.25; H, 9.91; N, 2.46.

References

1. Wang C, Dong H, Hu W, Liu Y, Zhu D (2012) Semiconducting π-conjugated systems in field-effect transistors: a material odyssey of organic electronics. Chem Rev 112:2208–2267
2. Wang X-Y, Lin H-R, Lei T, Yang D-C, Zhuang F-D, Wang J-Y, Yuan S-C, Pei J (2013) Azaborine compounds for organic field-effect transistors: efficient synthesis, remarkable stability, and bn dipole interactions. Angew Chem Int Ed 52:3117–3120
3. Ding L, Ying H-Z, Zhou Y, Lei T, Pei J (2010) Polycyclic imide derivatives: synthesis and effective tuning of lowest unoccupied molecular orbital levels through molecular engineering. Org Lett 12:5522–5525

4. Biniek L, Fall S, Chochos CL, Anokhin DV, Ivanov DA, Leclerc N, Lévêque P, Heiser T (2010) Impact of the alkyl side chains on the optoelectronic properties of a series of photovoltaic low-band-gap copolymers. Macromolecules 43:9779–9786
5. Boese R, Weiss H-C, Bläser D (1999) The melting point alternation in the short-chain n-alkanes: single-crystal X-ray analyses of propane at 30 K and of *n*-butane to *n*-nonane at 90 K. Angew Chem Int Ed 38:988–992
6. Ding L, Li H-B, Lei T, Ying H-Z, Wang R-B, Zhou Y, Su Z-M, Pei J (2012) Alkylene-chain effect on microwire growth and crystal packing of π-moieties. Chem Mater 24:1944–1949
7. Mei J, Graham KR, Stalder R, Reynolds JR (2010) Synthesis of isoindigo-based oligothiophenes for molecular bulk heterojunction solar cells. Org Lett 12:660–663
8. McCulloch I, Heeney M, Bailey C, Genevicius K, MacDonald I, Shkunov M, Sparrowe D, Tierney S, Wagner R, Zhang W, Chabinyc ML, Kline RJ, McGehee MD, Toney MF (2006) Liquid-crystalline semiconducting polymers with high charge-carrier mobility. Nat Mater 5:328–333
9. Osaka I, Takimiya K, McCullough RD (2010) Benzobisthiazole-based semiconducting copolymers showing excellent environmental stability in high-humidity air. Adv Mater 22:4993–4997
10. Ito Y, Virkar AA, Mannsfeld S, Oh JH, Toney M, Locklin J, Bao Z (2009) Crystalline ultrasmooth self-assembled monolayers of alkylsilanes for organic field-effect transistors. J Am Chem Soc 131:9396–9404
11. Lei T, Cao Y, Zhou X, Peng Y, Bian J, Pei J (2012) Systematic investigation of isoindigo-based polymeric field-effect transistors: design strategy and impact of polymer symmetry and backbone curvature. Chem Mater 24:1762–1770
12. Höltje HD, Folkers G (2008) Molecular modeling: basic principles and applications. Wiley-VCH, New York
13. Kitchen DB, Decornez H, Furr JR, Bajorath J (2004) Docking and scoring in virtual screening for drug discovery: methods and applications. Nat Rev Drug Discov 3:935–949
14. Stalder R, Mei J, Subbiah J, Grand C, Estrada LA, So F, Reynolds JR (2011) N-type conjugated polyisoindigos. Macromolecules 44:6303–6310
15. Rieger R, Beckmann D, Mavrinskiy A, Kastler M, Müllen K (2010) Backbone curvature in polythiophenes. Chem Mater 22:5314–5318
16. Osaka I, Abe T, Shinamura S, Miyazaki E, Takimiya K (2010) High-mobility semiconducting naphthodithiophene copolymers. J Am Chem Soc 132:5000–5001
17. Sato M, Asami A, Maruyama G, Kosuge M, Nakayama J, Kumakura S, Fujihara T, Unoura K (2002) Synthesis and redox property of the binuclear Pt (II) complexes bridged by thieno[3,2-b]thiophenes. J Organomet Chem 654:56–65
18. Li J, Bao Q, Li CM, Zhang W, Gong C, Chan-Park MB, Qin J, Ong BS (2010) Organic thin-film transistors processed from relatively nontoxic, environmentally friendlier solvents. Chem Mater 22:5747–5753
19. Rieger R, Beckmann D, Pisula W, Steffen W, Kastler M, Müllen K (2010) Rational optimization of benzo[2,1-b;3,4-b′]dithiophene-containing polymers for organic field-effect transistors. Adv Mater 22:83–86
20. Majewski LA, Kingsley JW, Balocco C, Song AM (2006) Influence of processing conditions on the stability of poly (3-hexylthiophene)-based field-effect transistors. Appl Phys Lett 88:222108
21. Chang J-F, Clark J, Zhao N, Sirringhaus H, Breiby DW, Andreasen JW, Nielsen MM, Giles M, Heeney M, McCulloch I (2006) Molecular-weight dependence of interchain polaron delocalization and exciton bandwidth in high-mobility conjugated polymers. Phys Rev B 74:115318
22. Chai J-D, Head-Gordon M (2008) Long-range corrected hybrid density functionals with damped atom-atom dispersion corrections. Phys Chem Chem Phys 10:6615–6620
23. Anthony JE (2008) The larger acenes: versatile organic semiconductors. Angew Chem Int Ed 47:452–483

24. Takimiya K, Shinamura S, Osaka I, Miyazaki E (2011) Thienoacene-based organic semiconductors. Adv Mater 23:4347–4370
25. He M, Li J, Tandia A, Sorensen M, Zhang F, Fong HH, Pozdin VA, Smilgies D-M, Malliaras GG (2010) Importance of C_2 symmetry for the device performance of a newly synthesized family of fused-ring thiophenes. Chem Mater 22:2770–2779
26. Osaka I, Abe T, Shinamura S, Takimiya K (2011) Impact of isomeric structures on transistor performances in naphthodithiophene semiconducting polymers. J Am Chem Soc 133: 6852–6860
27. Li Y, Singh SP, Sonar P (2010) A high mobility p-type DPP-thieno[3,2-b]thiophene copolymer for organic thin-film transistors. Adv Mater 22:4862–4866
28. Li Y, Sonar P, Singh SP, Soh MS, van Meurs M, Tan J (2011) Annealing-free high-mobility diketopyrrolopyrrole–quaterthiophene copolymer for solution-processed organic thin film transistors. J Am Chem Soc 133:2198–2204
29. Ha JS, Kim KH, Choi DH (2011) 2,5-Bis(2-octyldodecyl)pyrrolo[3,4-c]pyrrole-1,4-(2H,5H)-dione-based donor–acceptor alternating copolymer bearing 5,5′-di(thiophen-2-yl)-2,2′-biselenophene exhibiting 1.5 $\mathrm{cm^2\ V^{-1}\ s^{-1}}$ hole mobility in thin-film transistors. J Am Chem Soc 133:10364–10367
30. Yan H, Chen Z, Zheng Y, Newman C, Quinn JR, Dotz F, Kastler M, Facchetti A (2009) A high-mobility electron-transporting polymer for printed transistors. Nature 457:679–686
31. Bijleveld JC, Zoombelt AP, Mathijssen SGJ, Wienk MM, Turbiez M, de Leeuw DM, Janssen RAJ (2009) Poly(diketopyrrolopyrrole–terthiophene) for ambipolar logic and photovoltaics. J Am Chem Soc 131:16616–16617
32. Sonar P, Singh SP, Li Y, Soh MS, Dodabalapur A (2010) A low-bandgap diketopyrrolopyrrole-benzothiadiazole-based copolymer for high-mobility ambipolar organic thin-film transistors. Adv Mater 22:5409–5413
33. Bronstein H, Chen Z, Ashraf RS, Zhang W, Du J, Durrant JR, Shakya Tuladhar P, Song K, Watkins SE, Geerts Y, Wienk MM, Janssen RAJ, Anthopoulos T, Sirringhaus H, Heeney M, McCulloch I (2011) Thieno[3,2-b]thiophene–diketopyrrolopyrrole-containing polymers for high-performance organic field-effect transistors and organic photovoltaic devices. J Am Chem Soc 133:3272–3275
34. Bürgi L, Turbiez M, Pfeiffer R, Bienewald F, Kirner H-J, Winnewisser C (2008) High-mobility ambipolar near-infrared light-emitting polymer field-effect transistors. Adv Mater 20:2217–2224
35. Mei J, Kim DH, Ayzner AL, Toney MF, Bao Z (2011) Siloxane-terminated solubilizing side chains: bringing conjugated polymer backbones closer and boosting hole mobilities in thin-film transistors. J Am Chem Soc 133:20130–20133
36. Lei T, Dou J-H, Pei J (2012) Influence of alkyl chain branching positions on the hole mobilities of polymer thin-film transistors. Adv Mater 24:6457–6461
37. Coropceanu V, Cornil J, da Silva Filho DA, Olivier Y, Silbey R, Brédas J-L (2007) Charge transport in organic semiconductors. Chem Rev 107:926–952
38. Tsao HN, Cho DM, Park I, Hansen MR, Mavrinskiy A, Yoon DY, Graf R, Pisula W, Spiess HW, Müllen K (2011) Ultrahigh mobility in polymer field-effect transistors by design. J Am Chem Soc 133:2605–2612
39. Chen H, Guo Y, Yu G, Zhao Y, Zhang J, Gao D, Liu H, Liu Y (2012) Highly π-extended copolymers with diketopyrrolopyrrole moieties for high-performance field-effect transistors. Adv Mater 24:4618–4622
40. Niedzialek D, Lemaur V, Dudenko D, Shu J, Hansen MR, Andreasen JW, Pisula W, Müllen K, Cornil J, Beljonne D (2013) Probing the relation between charge transport and supramolecular organization down to ångström resolution in a benzothiadiazole-cyclopentadithiophene copolymer. Adv Mater 25:1939–1947
41. Letizia JA, Salata MR, Tribout CM, Facchetti A, Ratner MA, Marks TJ (2008) N-channel polymers by design: optimizing the interplay of solubilizing substituents, crystal packing, and field-effect transistor characteristics in polymeric bithiophene-imide semiconductors. J Am Chem Soc 130:9679–9694

42. van Pham C, Burkhardt A, Shabana R, Cunningham DD, Mark HB, Zimmer H (1989) A convenient synthesis of 2,5-thienylene oligomers: some of their spectroscopic and electrochemical properties. Phosphorus Sulfur Silicon Relat Elem 46:153–168
43. Sotgiu G, Zambianchi M, Barbarella G, Botta C (2002) Synthesis and optical properties of soluble sexithiophenes with one central head-to-head junction. Tetrahedron 58:2245–2251
44. Li Y, Li Z, Wang C, Li H, Lu H, Xu B, Tian W (2010) Novel low-bandgap oligothiophene-based donor-acceptor alternating conjugated copolymers: synthesis, properties, and photovoltaic applications. J Polym Sci Part A: Polym Chem 48:2765–2776

Chapter 3
Ambipolar Polymer Field-Effect Transistors Based on Functionalized Isoindigo

3.1 Recent Development on Ambipolar FETs

Ambipolar polymer field-effect transistors (FETs), capable of both hole and electron transport, exhibit simpler processing requirements in complementary-like circuits and potential application in organic light-emitting transistors [1]. With the fast development of the third generation polymer—donor–acceptor (D-A) polymer, a series of electron-deficient building block, such as benzothiadiazole (BT), naphthalene diimide (NDI), benzobisthiadiazole (BBT), diketopyrrolopyrrole (DPP), and isoindigo (II), have been developed for polymer FETs. Polymers based on these building blocks have shown hole mobilities surpassing 1 $\mathrm{cm^2\ V^{-1}\ s^{-1}}$ [2], and some polymers based on DPP exhibited both hole and electron mobilities of over 1 $\mathrm{cm^2\ V^{-1}\ s^{-1}}$ [3, 4]. However, high electron mobilities based on these polymers were achieved under nitrogen. Further investigation on ambipolar polymers which operate in ambient is very important for their practical applications, as well as fundamental understanding of the carrier transport in conjugated polymers.

On the other hand, an ideal ambipolar FET needs balanced carrier transport and similar performance under both *p*- and *n*-channel operation modes [5, 6]. Nonetheless, only a few of these polymers can be operated in ambient conditions [7], and fewer showed balanced carrier transport [5, 8]. To our knowledge, none offer both balanced carrier transport and transport under ambient conditions—criteria for an ideal ambipolar material that can significantly simplify circuit design and minimize patterning and fabrication process.

3.2 Fluorinated Isoindigo-Based Polymer FETs

In Chap. 2, we have successfully applied isoindigo unit to polymer FETs for the first time [9], and obtained a high hole mobility of 3.62 $\mathrm{cm^2\ V^{-1}\ s^{-1}}$ after engineering the side chain branching positions [10]. Isoindigo molecule have also been used as

T. Lei, *Design, Synthesis, and Structure-Property Relationship Study of Polymer Field-Effect Transistors*, Springer Theses, DOI 10.1007/978-3-662-45667-5_3

the donor material in polymer solar cells, and high power conversion efficiency of over 8 % was achieved [11, 12]. The highly electron-deficient isoindigo unit endows these copolymers with intriguing properties, such as broad absorption and high open circuit voltage in OPVs, as well as high hole mobility and good ambient stability in FETs. Nevertheless, isoindigo-based polymers have extremely low electron mobility (the highest one is only 3.7×10^{-7} cm^2 V^{-1} s^{-1}) [13], albeit their low-lying LUMO levels (−3.6 to −3.8 eV) [14]. Thus limiting their application in *n*-type FETs [15] or as acceptors in OPVs [16, 17].

Several studies indicated that fluorination of the backbone of polymers can effectively improve the performance of OPVs, because fluorine is electron-withdrawing and small, hence capable of modulating the electronic properties of polymers without deleterious steric effects [18, 19]. Thus, we introduced fluorine atoms onto the isoindigo units of the polymer to further lower its LUMO level. To our delight, the electron mobility of the fluorinated isoindigo-based polymer was significantly increased to 0.43 cm^2 V^{-1} s^{-1}, while maintaining high hole mobility of up to 1.85 cm^2 V^{-1} s^{-1}. This represents the first ambipolar transport behavior for isoindigo-based polymers, and these mobilities are among the highest for an ambipolar FET fabricated under ambient conditions [20].

In Chap. 2, we have demonstrated that modulating branched alkyl chains in isoindigo-based polymers significantly increased the hole mobility [10]. The 4-tetradecyloctadecyl group was chosen as the side chain of the fluorinated polymer to guarantee both good solubility and close π–π stacking. Scheme 3.1 shows the synthetic route to polymers **PFII2T** and **PII2T**. Commercially available 3-bromo-2-fluoroaniline was condensed with chloral hydrate and hydroxylamine hydrochloride to afford compound **3-1**, catalyzed by sulfuric acid. In presence of conc. sulfuric acid, crude compound **3-1** underwent cyclization to provide 6-bromo-7-fluoroisatin (**3-2**) in 61 % yield. A two-step Wolff-Kishner-Huang reduction was used to reduce the carbonyl group to methylene, giving compound **3-3**. Direct condensation of **3-2** and **3-3** in acetic acid afforded 6,6′-dibromo-7,7′-difluoroisoindigo (**3-4**) in 72 % yield. Initial attempts to alkylate **3-4** with 15-(3-iodopropyl) nonacosane using K_2CO_3 failed, presumably due to the steric hindrance caused by fluorines. A stronger base KOH was then used, and the reaction proceeded smoothly at room temperature to give compound **3-5** in 88 % yield. A Stille coupling polymerization between **3-5** and 5,5′-bis-(trimethylstannyl)-2,2′-bithiophene gave polymer **PFII2T** in high yield. **PII2T** was prepared as a reference polymer to study the effect of fluorination. Both polymers were purified by adding a coordinating ligand to remove residual palladium catalyst, then Soxhlet extraction was used to remove oligomers and other impurities. Molecular weights of both polymers were evaluated by high temperature gel permeation chromatography (GPC) with 1,2,4-tricholorobenzene (TCB) as eluent at 140 °C. Both polymers showed comparable M_n (**PFII2T**, 75.7 kDa; **PII2T**, 72.8 kDa). Nonetheless, the PDI of **PFII2T** (2.58) is larger than that of **PII2T** (1.95). Both polymers showed excellent thermal stability with decomposition temperature over 410 °C. No phase transition was observed for both polymers by differential scanning calorimetry in the range of room temperature to 330 °C.

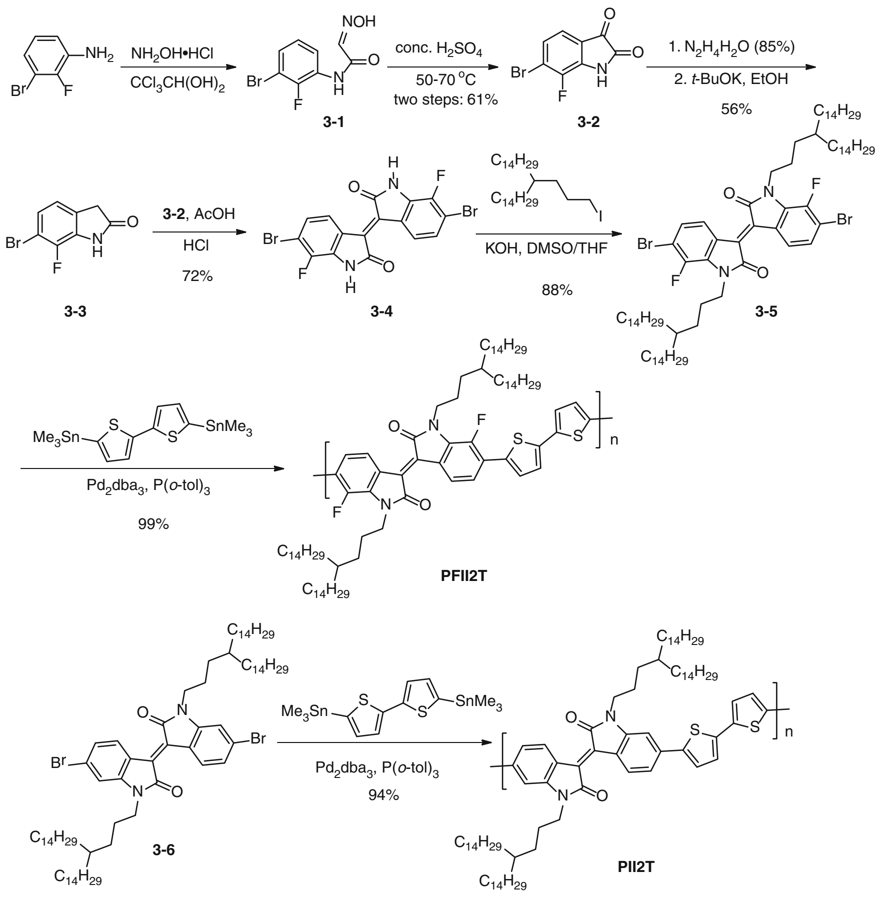

Scheme 3.1 Synthesis of fluorinated isoindigo-based polymer **PFII2T** and the reference polymer **PII2T**

Figure 3.1a illustrates the absorption spectra of both polymers in dilute solution and in thin film. Both polymers show typically dual absorption bands. After introducing fluorine atoms, the charge transfer absorption band (Band I) of **PFII2T** red-shifts obviously, whereas the Band II blue-shifts slightly and the absorption intensity is decreased. Compared with those in solution, absorption spectra of both polymers in thin film shows a slight red-shift and increased 0–0 vibrational absorption, indicating that the polymer backbones become more planar in the solid state. The bandgap of **PFII2T** in thin film estimated from the absorption onset is 1.50, 0.07 eV smaller than that of **PII2T**. Interestingly, computational analysis of the fragment structure reveals that the introduction of fluorine atoms does not increase the dihedral angle of polymer backbones (Fig. 3.1c). Instead, because of fluorine/hydrogen interaction, the phenyl-thienyl rotational angle of the fluorinated

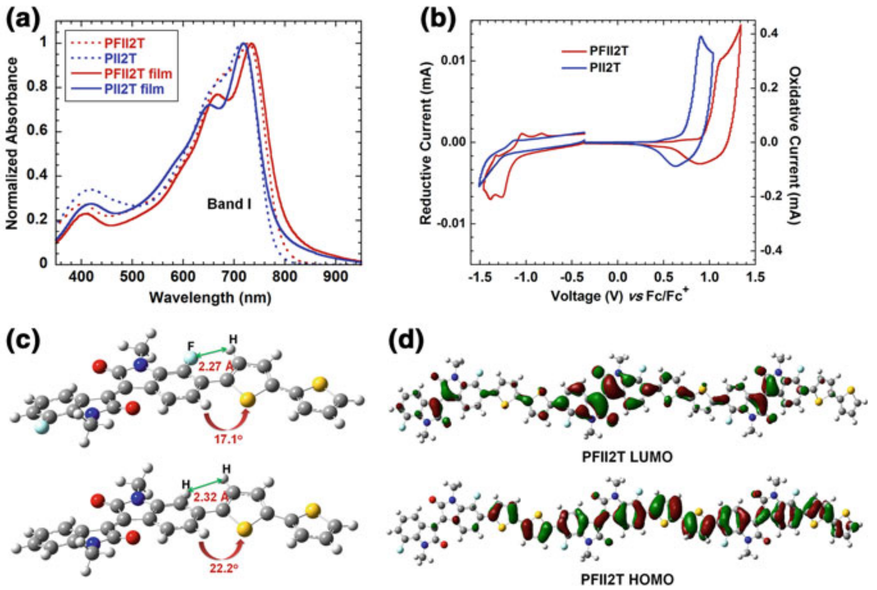

Fig. 3.1 **a** Normalized UV-vis absorption spectra of both polymers in $CHCl_3$ (1×10^{-5} M) and in thin film. **b** Cyclic voltammograms of both polymers in thin film drop-casted on a glassy carbon electrode. **c** Molecular models of **PFII2T** fragment (*above*) and **PII2T** fragment (*bottom*). Alkyl chains were replaced by methyl groups for simplicity (optimized at B3LYP/6-31G(d) level). **PFII2T** displays smaller dihedral angle (17.1°) and shorter F–H distance (2.27 Å). **d** Calculated molecular orbitals of the trimer of **PFII2T** (B3LYP/6-31G(d))

monomer is decreased from 22.2° to 17.1°, and the calculated F–H distance (2.27 Å) is significantly shorter than the sum of the fluorine and hydrogen van der Waals radii (2.56 Å) [21]. This result indicates that the introduction of fluorine atoms provides the polymer with a planar backbone, which is consistent with the absorption features.

Electrochemical properties of both polymers are explored by cyclic voltammetry (CV) measurement. Both polymers show much stronger oxidative peaks than their reductive ones (Fig. 3.1b). After introducing fluorine atoms, the reduction current of **PFII2T** increased and the doping processes appeared to be more reversible than those of **PII2T**. Compared with those of **PII2T**, both HOMO and LUMO levels of **PFII2T** are obviously decreased. The LUMO level of **PFII2T** measured by CV reaches −3.88, 0.18 eV lower than that of **PII2T**. In our previous report, changing the donor part of isoindigo-based polymers hardly affects the LUMO levels of polymers [14], because their LUMO levels are mostly localized on isoindigo cores. Herein, fluorination of isoindigo core effectively lowers the LUMO level. The HOMO level is also lowered after the fluorination, because the HOMOs of polymers are well delocalized along the backbone. The CV results are consistent with the photoelectron spectroscopy (PES) measurement. The optical bandgaps and PES results give HOMO/LUMO levels of −5.46/−3.96 eV for **PFII2T** and −5.31/

Table 3.1 Thermal, optical, and electrochemical properties of both polymers

Polymers	T_d (°C)	λ_{max}^{sol} (nm)[a]	λ_{max}^{film} (nm)	E_g^{opt} (eV)[b]	E_{HOMO}^{CV} (eV)[c]	E_{LUMO}^{CV} (eV)[c]	E_{HOMO}^{PES} (eV)[d]	E_{LUMO}^{PES} (eV)[e]
PFII2T	411	728, 682	734, 667	1.50	−5.60	−3.88	−5.46	−3.96
PII2T	416	714, 667	718, 652	1.57	−5.42	−3.70	−5.31	−3.74

[a] 10^{-5} M in chloroform

[b] Estimated from the onset of thin-film absorption

[c] Cyclic voltammetry determined with Fc/Fc^+ ($E_{HOMO} = -4.80$ eV) as external reference

[d] Determined by UV-PES

[e] $E_{LUMO}^{PES} = E_{HOMO}^{PES} - E_g^{opt}$

−3.74 eV for **PII2T**. Photophysical and electrochemical properties of both polymers are in Table 3.1. Notice that the low-lying LUMO level of **PFII2T** is lower than that of several ambient-stable ambipolar polymers and comparable to some air-stable n-type polymers based on perylenedicarboximide (PDI) and naphthalenedicarboximide (NDI) [7, 22]. Hence, ambient stable charge transport in **PFII2T** is expected.

To test the ambipolar transport capability of the isoindigo polymers, a top-gate/bottom-contact (TG/BC) device structure was used to fabricate polymer FETs. This device configuration is preferred for ambient-stable ambipolar or n-type organic materials, because of its better injection characteristics and the encapsulation effect of the top dielectric layer [15]. The semiconducting layer was deposited by spin-coating polymer solutions (6 mg/mL in DCB) on untreated Au (source-drain)/SiO_2/Si substrate. After thermal annealing the film at optimized temperature (180 °C) for 10 min, a CYTOP solution was spin-coated on top of the polymer film as the dielectric layer, and an aluminum layer was thermally evaporated as the gate electrode. We fabricated the devices both in glovebox and in ambient conditions (R_H = 50–60 %) to compare their device performance. All the devices were tested under ambient conditions on a probe station. FET devices based on **PFII2T** fabricated in glovebox and in ambient clearly showed ambipolar transport characteristics. For devices fabricated in glovebox, hole mobilities of up to 1.25 $cm^2\ V^{-1}\ s^{-1}$ and electron mobilities of up to 0.51 $cm^2\ V^{-1}\ s^{-1}$ were obtained (Table 3.2), which is comparable to several high performance DPP-based polymer FETs [8, 23].

In addition, all devices fabricated in ambient also exhibited ambipolar behaviors. The highest hole mobility was further improved to 1.85 $cm^2\ V^{-1}\ s^{-1}$ with a little decrease in electron mobility. The highest electron mobility is 0.43 $cm^2\ V^{-1}\ s^{-1}$, and the average mobility is 0.38 $cm^2\ V^{-1}\ s^{-1}$ (Fig. 3.2a). These mobilities are the highest reported to date for an ambipolar FETs fabricated under ambient conditions [7]. The reference non-fluorinated polymer **PII2T** showed comparable hole mobilities but much lower electron mobilities. Electron mobilities of up to 0.07 $cm^2\ V^{-1}\ s^{-1}$ are observed for devices fabricated in glovebox but decreased sharply to 10^{-3}–10^{-2} $cm^2\ V^{-1}\ s^{-1}$ for devices fabricated under ambient conditions. Hence, fluorination can substantially increase the ambient stability of the devices.

Table 3.2 Summary of molecular wight, OFET device performance, and GIXD results of both polymers

Polymers	μ_{hole} (cm^2/Vs)[a]	V_T (V)	log (I_{on}/I_{off})[d]	μ_{electron} (cm^2/Vs)[a]	V_T (V)	log (I_{on}/I_{off})[e]	d (Å)[f]	
							L	π
PFII2T	1.25 (1.13)[b]	−40	5–6	0.51 (0.49)[b]	+32	5–6	29.0	3.55
	1.85 (1.41)[c]	−38	6–7	0.43 (0.38)[c]	+30	5–6		
PII2T	0.76 (0.66)[b]	−35	6–7	0.07 (0.06)[b]	+25	5–6	28.8	3.56
	1.27 (1.04)[c]	−14	5–6	0.01 (0.004)[c]	+36	3–4		

[a] Measured under ambient conditions (R_H = 50–60 %). Maximum values of hole or electron mobilities and the average values are in parentheses (over 50 devices)

[b] Devices fabricated in glove box

[c] Device fabricated in ambient conditions

[d] Evaluated at $V_D = -20$ V

[e] Evaluated at $V_D = +20$V

[f] Lamellar (L) and π–π stacking (π) distances determined by GIXD experiments

The thin film microstructures and morphologies of both polymers were investigated by GIXD and AFM. In the 2D-GIXD, both polymers appear to have dual textures in thin films (Fig. 3.2c, d). Films of both polymers display strong lamellar textures with five out-of-plane (Q_z) peaks as denoted by (h00) Bragg diffraction. The (010) diffraction corresponding to the π–π stacking distances is observed in both out-of-plane (Q_z) and in-plane (Q_{xy}) diffractions. These results indicate that the polymers have both edge-on and face-on packings in thin films [24]. The measured lamellar and π–stacking distances are almost the same for both polymers because of their similar backbones and identical alkyl chains. However, the ratios of the observed edge-on to face-on packing in film are significantly different for the two polymers. Fluorinated polymer **PFII2T** displays much stronger (h00) diffraction and weaker out-of-plane (010) diffraction. In addition, the in-plane (200) diffraction is only observed for **PII2T**. These results suggest that **PFII2T** tends to form the edge-on packing, whereas **PII2T** tends to form the face-on packing. Scherrer analysis of the (010) diffraction shows that the crystalline coherence length of **PFII2T** is 62.8 Å, considerably larger than that of **PII2T** (43.4 Å). The AFM images of both polymer films show fibrillar intercalating networks. Crystalline zones similar to other high-performance polymer FET materials are formed, presumably due to strong intermolecular π-π interactions. In particular, compared with the **PII2T** film, the **PFII2T** film has stronger crystalline tendency with larger root-mean-square (RMS) deviation in the AFM height images, which agrees with the Scherrer analysis. These findings indicate that the introduction of fluorine atoms affects not only energy levels, but also interchain interactions of polymers, creating different polymer packing in films. Since dense molecular packing can result in a barrier to oxygen and water, thereby stabilizing electron transport [25], we assume that the strong crystallinity and ordered packing in **PFII2T** may also contribute to its improved ambient stability.

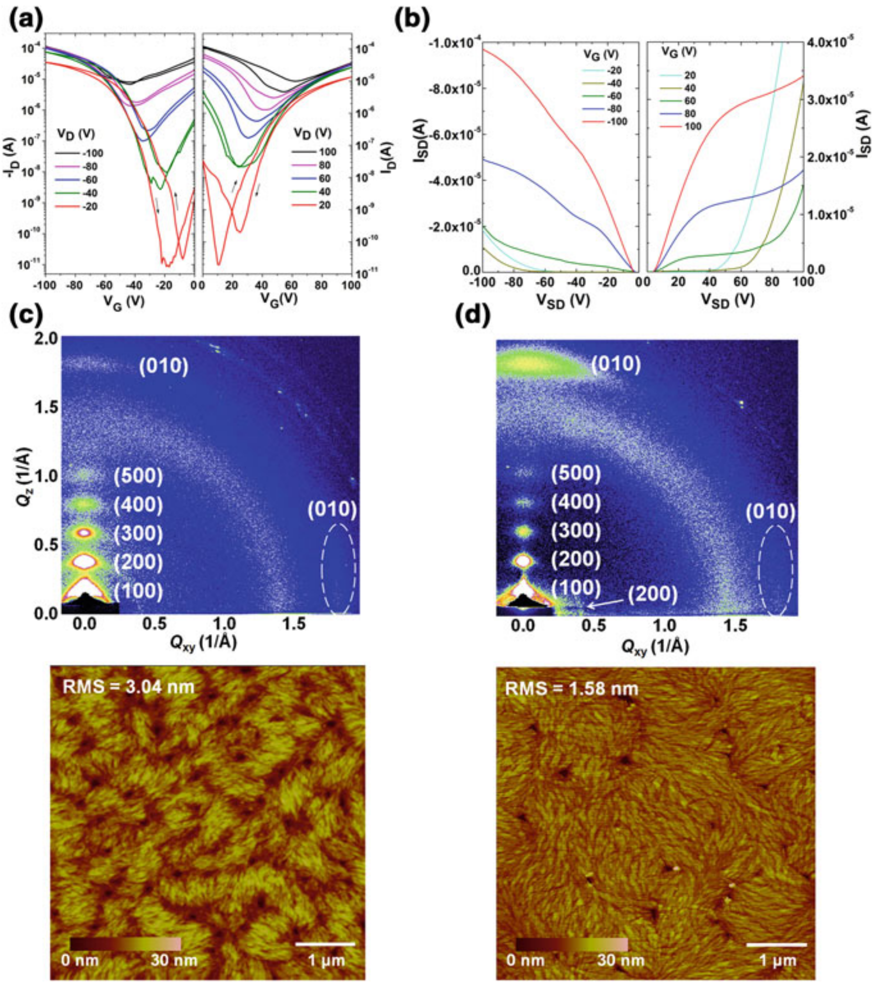

Fig. 3.2 **a** Transfer and **b** output characteristics of a **PFII2T** device fabricated under ambient conditions. OFET devices (L = 50 μm, W = 1,000 μm) were fabricated with CYTOP around 500 nm thick (capacitance C_i = 3.7 nF cm^{-2}). 2D-GIXD patterns and AFM height images of **c** **PFII2T** and **d** **PII2T** films. Films were spin-coated from the DCB solutions of the polymers (6 mg/mL) and annealed at 180 °C

3.3 Chlorinated Isoindigo for Balanced and Ambient-Stable Ambipolar Polymer FETs

Fluorine is strongly electron-withdrawing and small in size. As a popular approach for material modification, fluorination of organic small molecules or polymers can lower their LUMO levels without harmful steric hindrance effects, thus improving device stability or performance [26]. By contrast, although the chlorinated precursors are more readily available and chlorinated molecules have shown comparable or better performances than their fluorinated counterparts [27], chlorination of small molecules are investigated less [27, 28]. Moreover, chlorination of conjugated polymers has never been reported, presumably due to the larger atom size of chlorine and thereby steric hindrance effects.

In this section, we chlorinate isoindigo-based polymers through an efficient chlorination reaction (Scheme 3.2) [29]. Balanced charge carrier transport with hole mobilities of up to 0.81 cm^2 V^{-1} s^{-1} and electron mobilities of up to 0.66 cm^2 V^{-1} s^{-1} were obtained for devices fabricated under ambient conditions using these polymers. In addition, we also used these polymers to construct inverters, which showed very high gains. This work represents the first chlorination of semiconducting polymers, and the chlorinated isoindigo polymers are the first ambipolar polymers that can offer both balanced and ambient-stable carrier transport.

We chose the same alkyl side chains (4-tetradecyloctadecyl groups) as the fluorinated isoindigo polymer to guarantee both good solubility and better π–π stacking interactions. Besides 2,2′-bithiophene, 2,2′-biselenophene was also chosen as the donor unit because recent studies showed that replacing thiophene with selenophene increases mobility in polymer FETs [30, 31]. As illustrated in Scheme 3.2, the synthesis of chlorinated isoindigo polymers started from the alkylation of commercially available 6,6′-dibromoisoindigo with K_2CO_3, giving compound **3-6** in 95 % yield. Direct chlorination of the isoindigo core with *N*-chlorosuccinimide (NCS) provided 5,5′-dichloro-6,6′-dibromoisoindigo (**3-7**) in

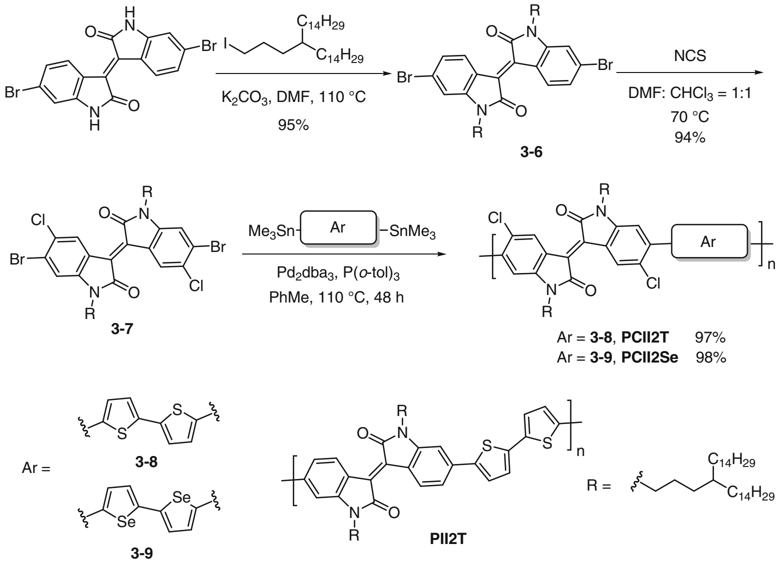

Scheme 3.2 Synthesis of chlorinated isoindigo polymers **PCII2T** and **PCII2Se**, and the chemical structure of reference polymer **PII2T**

high yield (94 %) with high regioselectivity. **3-7** was then subjected to a Stille coupling polymerization with 5,5′-bis(trimethylstannyl)-2,2′-bithiophene to give chlorinated polymer **PCII2T** in 97 % yield, and with 5,5′-bis(trimethylstannyl)-2,2′-biselenophene to give chlorinated polymer **PCII2Se** in 98 % yield. All polymers were purified by adding a coordinating ligand to remove residual palladium catalyst [32], and Soxhlet extraction was then performed to remove oligomers and other impurities. Molecular weights of all polymers were evaluated by high temperature gel permeation chromatography (GPC) using 1,2,4-trichlorobenzene (TCB) as eluent at 140 °C. Both chlorinated polymers showed similarly high molecular weight with M_n around 60 kDa and PDI around 2.1 (**PCII2T**: M_n/PDI = 60.3/2.11; **PCII2Se**: M_n/PDI = 58.6/2.13). Notice that the fluorinated isoindigo polymer needs 6 steps with only 21 % total yield, whereas the chlorinated polymer **PCII2T** needs only 3 steps with 87 % total yield. All polymers displayed high thermal stability with decomposition temperatures over 390 °C, and no phase transition was observed for any polymers in the range of 25–330 °C.

Figure 3.3a shows a comparison of the absorption spectra of chlorinated polymer **PCII2T** and the reference **PII2T** in solution and in thin film. Both polymers show similar dual band absorption spectra. **PCII2T** displays a smaller bandgap (1.53 eV) than **PII2T** (1.57 eV) but broadened Band I and blue-shifted Band II absorptions. **PCII2T** only reveals the 0–1 vibrational absorption peak in solution, and the 0–0 vibrational absorption rises as a shoulder peak in film. In contrast, **PII2T** exhibits a stronger 0–0 vibrational peak both in solution and in film. The increase of the 0–0 peak indicates that the polymer backbones may become more planar in film.

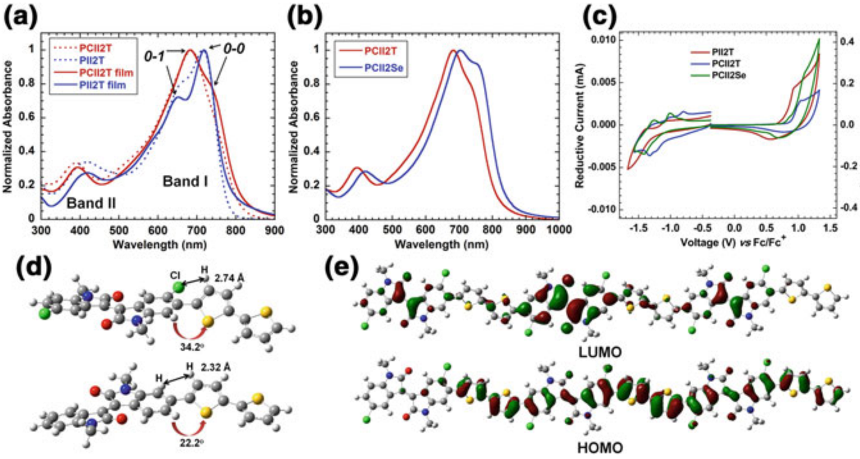

Fig. 3.3 **a** Normalized absorption spectra of **PCII2T** and **PII2T** in $CHCl_3$ (1×10^{-5} M, *dotted line*) and in film (*solid line*). **b** Normalized absorption spectra of **PCII2T** and **PCII2Se** in film. **c** Cyclic voltammograms of polymers in thin film drop-casted on a glassy carbon electrode. **d** Comparison of the phenyl-thienyl dihedral angles of **PCII2T** and **PII2T**. **PCII2T** displays larger dihedral angle (34.2°) than **PII2T** (22.2°) after introducing the chlorine atoms. **e** Calculated molecular orbitals of the trimer of **PCII2T** (B3LYP/6-31G(d))

Computational analysis of the polymer fragment reveals that the introduction of chlorine atoms increases the dihedral angle of the phenyl–thienyl connection from 22.2° to 34.2°, significantly larger than those of fluorinated polymers (17.1°) [20]. The Cl–H distance (2.74 Å) is shorter than the sum of their van der Waals radii (2.95 Å), indicating the existence of Cl–H interactions. Thus the decreased 0–0 peak in **PCII2T** may be attributed to the larger dihedral angle caused by the steric hindrance of chlorine atoms. Changing the donors to biselenophene units further lowers the polymer bandgap to 1.51 eV, due to the stronger electron-donating properties of 2,2′-biselenophene (Fig. 3.3b).

The electrochemical behaviors of the polymers were evaluated by CV. All polymers show one order of magnitude stronger oxidative peaks than their reductive ones (Fig. 3.3c). The HOMO/LUMO levels of **PCII2T** (−5.64/−3.86 eV) are lower than those of **PII2T** (−5.42/−3.70 eV), and close to those of the fluorinated isoindigo polymers (−5.60/−3.88 eV), indicating that chlorination has similar electronic effect to fluorination. When electron-rich biselenophene is used as donor, the HOMO/LUMO levels of **PCII2Se** increase to −5.57/−3.84 eV. This result is in agreement with our findings in Chap. 2 that changing the donor units can hardly affect the LUMO levels of isoindigo polymers, because their LUMOs are mostly localized on isoindigo cores (Fig. 3.3e). However, the HOMOs are well delocalized along the polymer backbone, thus direct modification of the isoindigo cores with electron-deficient chlorine atoms can lower both LUMO and HOMO levels. The CV results are supported by the energy levels calculated from PES and the optical bandgap, as summarized in Table 3.3.

Polymer FETs with TG/BC configuration were fabricated by spin-coating the polymer solution in 1,2-dichlorobenzene (DCB) (6 mg/mL) onto solvent-cleaned gold electrode (source-drain)/SiO_2/Si substrate. After thermal annealing the polymer film at optimized temperature (180 °C) for 10 min, a fluoropolymer (Cytop^{TM}) solution was spin-coated on top of the polymer film as the dielectric layer, and an aluminum layer was thermally evaporated as the gate electrode. Devices were fabricated both in glovebox and in ambient (R_H = 50–60 %) to compare their device performances. The reference polymer **PII2T** showed high hole mobility up to 0.76 cm^2 V^{-1} s^{-1} and low electron mobility of 0.07 cm^2 V^{-1} s^{-1} in glovebox. Upon

Table 3.3 Thermal, optical, and electrochemical properties of **PII2T** and the chlorinated polymers

Polymers	T_d (°C)	λ_{max}^{sol} (nm)[a]	λ_{max}^{film} (nm)	E_g^{opt} (eV)[b]	E_{HOMO}^{CV} (eV)[c]	E_{LUMO}^{CV} (eV)[c]	E_{HOMO}^{PES} (eV)[d]	E_{LUMO}^{PES} (eV)[e]
PII2T	416	714, 667	718, 652	1.57	−5.42	−3.70	−5.31	−3.74
PCII2T	405	682	745, 682	1.53	−5.64	−3.86	−5.36	−3.83
PCII2Se	397	710	758, 703	1.51	−5.57	−3.84	−5.35	−3.84

[a] 10^{-5} M in chloroform

[b] Estimated from the onset of thin-film absorption

[c] Cyclic voltammetry determined with Fc/Fc$^+$ (E_{HOMO} = −4.80 eV) as external reference

[d] Determined by PES

[e] $E_{LUMO}^{PES} = E_{HOMO}^{PES} - E_g^{opt}$

Table 3.4 Summary of OFET device performances, and GIXD results of all the polymers

Polymers	μ_{hole} ($\mathrm{cm^2\ V^{-1}\ s^{-1}}$)[a]	V_T (V)	log(I_{on}/I_{off})[d]	μ_{electron} ($\mathrm{cm^2\ V^{-1}\ s^{-1}}$)[a]	V_T (V)	log(I_{on}/I_{off})[e]	d (Å)[f]	
							L	π
PII2T	0.76 (0.66)[b]	−35	4–5	0.07 (0.06)[b]	+25	2–3	28.8	3.56
	1.27 (1.04)[c]	−14	5–6	0.01 (0.004)[c]	+36	1–2		
PCII2T	0.50 (0.38)[b]	−70	4–5	0.62 (0.47)[b]	+29	4–5	28.8	3.57
	0.54(0.51)[c]	−26	4–5	0.48 (0.42)[c]	+36	4–5		
PCII2Se	1.05 (0.85)[b]	−68	5–6	0.72 (0.62)[b]	+27	5–6	29.0	3.56
	0.81 (0.74)[c]	−38	5–6	0.66 (0.58)[c]	+47	5–6		

[a] Measured under ambient condition (R_H = 50–60 %). Maximum mobilities and average are in parentheses (over 20 devices)

[b] Devices fabricated in glovebox

[c] Device fabricated in ambient conditions

[d] Evaluated at $V_D = -20$ V

[e] Evaluated at $V_D = +20$V

[f] Lamellar (*L*) and π–π stacking (π) distances determined by GIXD experiments

exposure to air, the hole mobility further increased to 1.27 $\mathrm{cm^2\ V^{-1}\ s^{-1}}$, but the electron mobility decreased drastically to 10^{-3}–10^{-2} $\mathrm{cm^2\ V^{-1}\ s^{-1}}$ (Table 3.4). In contrast, the chlorinated polymer **PCII2T** showed balanced hole and electron transport. For devices fabricated in glovebox, hole mobility up to 0.50 $\mathrm{cm^2\ V^{-1}\ s^{-1}}$ and electron mobility up to 0.62 $\mathrm{cm^2\ V^{-1}\ s^{-1}}$ were observed; for those fabricated under ambient conditions, the hole mobility slightly increased to 0.54 $\mathrm{cm^2\ V^{-1}\ s^{-1}}$ and the electron mobility slightly decreased to 0.48 $\mathrm{cm^2\ V^{-1}\ s^{-1}}$. Hence, the introduction of the chlorine atoms obviously improved the electron transport and ambient stability of the isoindigo polymers. In contrast, although fluorinated isoindigo-based polymers showed remarkably high hole mobility (1.85 $\mathrm{cm^2\ V^{-1}\ s^{-1}}$), the carrier transport was not balanced because the electron mobility (0.43 $\mathrm{cm^2\ V^{-1}\ s^{-1}}$) was relatively low.

With **PCII2Se**, devices fabricated in glovebox and in ambient showed increased hole and electron mobilities while maintaining balanced transport upon substituting sulfur atoms to selenium atoms in the polymer. High hole and electron mobilities up to 1.05 and 0.72 $\mathrm{cm^2\ V^{-1}\ s^{-1}}$ were obtained for devices fabricated in glovebox, and in ambient the hole mobility (0.81 $\mathrm{cm^2\ V^{-1}\ s^{-1}}$) and electron mobility (0.66 $\mathrm{cm^2\ V^{-1}\ s^{-1}}$) only decreased slightly (Fig. 3.4). Our chlorinated isoindigo polymers are the first ambipolar polymers that can be operated in ambient and transport carriers in balance, and their mobilities are among the highest ones in ambipolar polymer FETs.

Inverter is the most fundamental logic gate [33], thus ambient fabrication of inverter is significant for large-area and low-cost applications of polymers in digital circuits. Hence, we used chlorinated isoindigo polymers to fabricate complementary-like inverters on a common substrate without patterning the organic semiconductor (Fig. 3.4c). The inverter consisted of two connected TG/BC ambipolar transistors with a common gate as input (V_{IN}) and a common drain as output (V_{OUT})

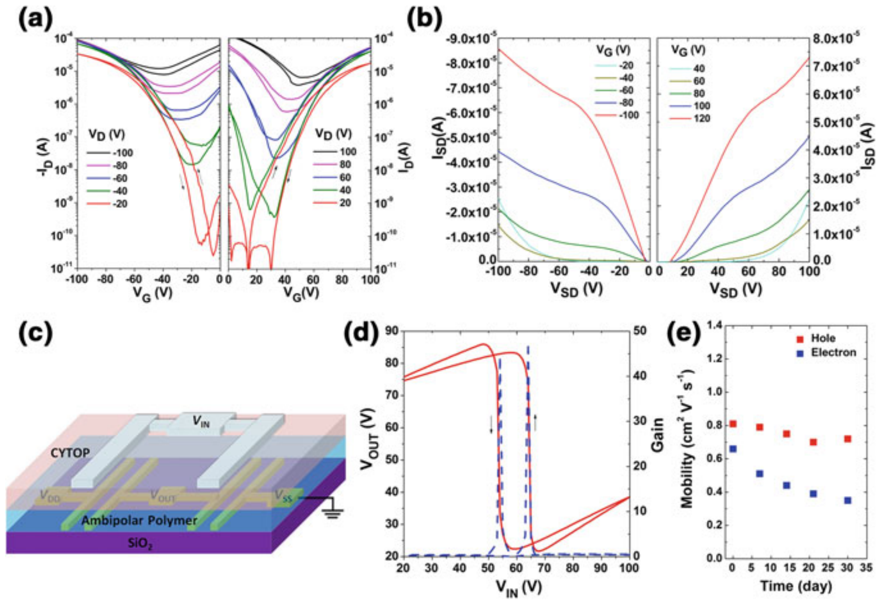

Fig. 3.4 **a** Transfer and **b** output characteristics of **PCII2Se** devices fabricated and tested in ambient ($L = 50\ \mu m$, $W = 1$ mm, $C = 3.7$ nF cm^{-2}). **c** Schematic diagram of an inverter device consisted of two connected TG/BC ambipolar transistors. **d** The VTC characteristic and gain of a complementary-like inverter fabricated with **PCII2Se** under ambient condition ($V_{DD} = 100$ V, $L = 50\ \mu m$, $W = 4$ mm). **e** Time-dependent decay of device performance of **PCII2Se** under ambient condition

were fabricated both in glovebox and in ambient. Obvious inverting functionality was observed for both chlorinated polymers when the input voltage and the supply voltage (V_{DD}) were both positively or negatively biased. The static voltage transfer characteristic (VTC) and gain of the inverter fabricated with **PCII2Se** in ambient are shown in Fig. 3.4d. Both chlorinated polymers showed high gain values in the range of 40–50. For inverters fabricated in ambient, **PCII2T** showed high gains up to 46, and **PCII2Se** showed higher gain up to 48. Notice that the hysteresis of the ambient-fabricated devices become obviously smaller than those of devices fabricated in nitrogen, presumably due to the more balanced threshold voltages in both p- and n-channel modes after exposing to air (Fig. 3.5).

Time-dependent decay of both polymer devices was also performed by storing the devices under ambient condition. For both polymers, we have observed very good stability of hole transport and a slow roll-off of electron mobility over 30 days (Fig. 3.4e). The decay of the electron mobility may be caused by the further diffusion of the oxygen and water into the semiconductors. Although devices are not long-time stable in ambient, the polymers can be fabricated and tested under ambient conditions, and the stability is also outstanding in ambipolar polymers because very few ambipolar polymers can be fabricated and tested under ambient and fewer are reported with stability data.

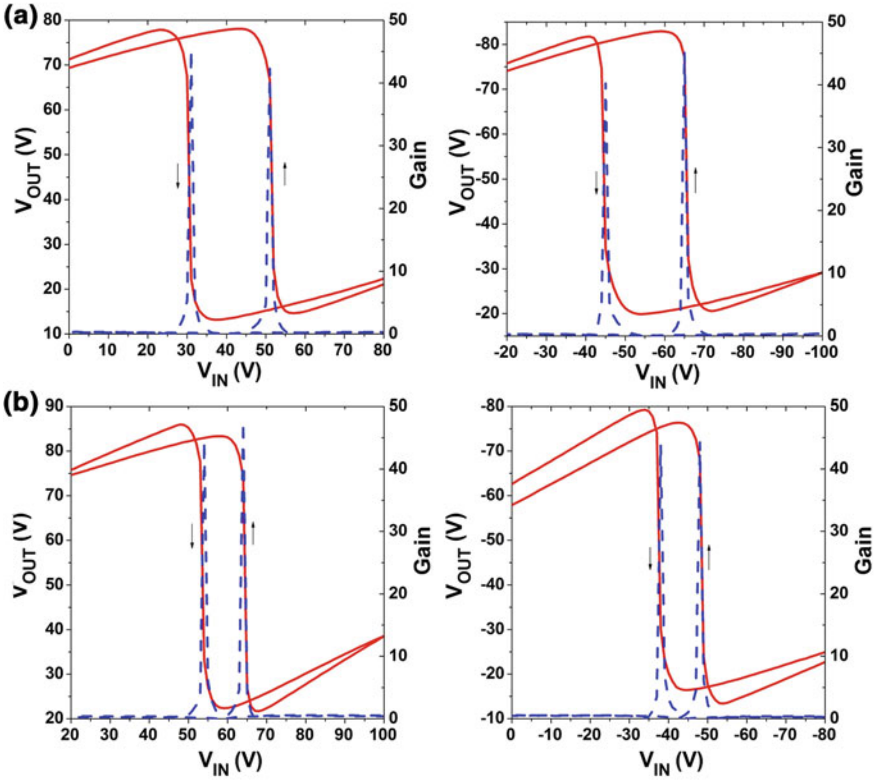

Fig. 3.5 The VTC and gains of **PCII2Se** inverter devices fabricated **a** in glovebox and **b** under ambient conditions. The threshold voltage differences of forward and reverse scans are smaller for devices fabricated under ambient conditions, presumably due to the more balanced threshold voltages in the p- and n-channel modes

In GIXD, all the polymers displayed strong out-of-plane (*h*00) diffractions, indicating that typical lamellar packing was formed in polymer film. (010) Peaks that are attributed to the π–π stacking distances were observed for all polymers. **PII2T** showed much stronger out-of-plane (010) peak and weaker (*h*00) peak, whereas **PCII2T** showed stronger in-plane (010) peak. For **PCII2Se**, only in-plane (010) peak was observed. These observations suggest that the thin film packings for three polymers are distinct. **PII2T** preferred to form a face-on packing in film. However, after introducing chlorine atoms, both edge-on and face-on packings were found in **PCII2T**, and no face-on packing was observed in **PCII2Se** when further changing the donor unit to biselenophene (Fig. 3.6g–i). Although the packings in thin film are different, all polymers exhibited almost the same lamellar packing and π–π stacking distances, due to their similar polymer backbones and identical side chains. AFM height images of the polymers displayed fiber-like intercalating networks with obviously crystallized zones, similar to other high-performance polymer FET materials. Root-mean-square (RMS) analysis of the

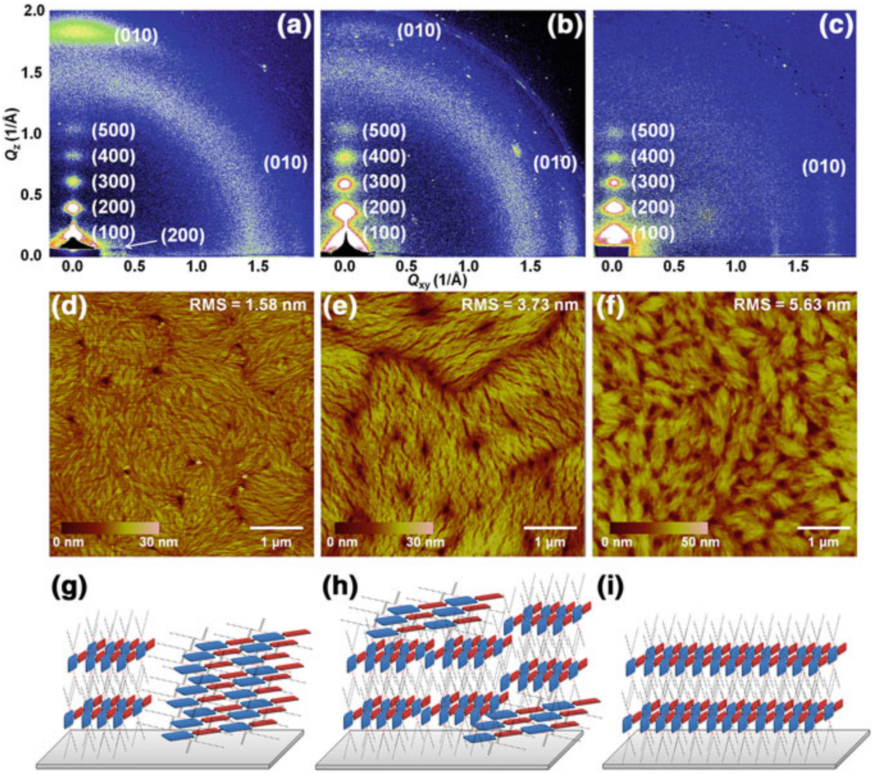

Fig. 3.6 2D-GIXD patterns, AFM height images and cartoon illustration of the proposed packing models of **a**, **d**, and **g** **PII2T**, **b**, **e**, and **h** **PCII2T** and **c**, **f**, and **i** **PCII2Se** films. Films were prepared by spin-coating from the DCB solutions of the polymers (6 mg/mL) and annealed at 180 °C

height images showed that **PCII2Se** displayed the largest roughness, presumably due to its stronger crystallinity. Therefore, the introduction of chlorine atoms and the replacement of thiophene by selenophene not only modulate the polymer energy levels, but also affect the interchain interactions, thereby leading to different polymer packings in the solid state.

3.4 Conclusions

Isoindigo-based polymers usually exhibited low electron mobilities. An effective approach to increase and stabilize electron transport is to lower polymer LUMO levels. In Chap. 2, we have shown that changing the donor part can hardly affect the LUMO levels of isoindigo-based polymers, because their LUMOs are mostly localized on isoindigo. Thus, we focused on engineering the isoindigo core, and both fluorine and chlorine were introduced.

Computational analyses showed that the introduction of fluorine atoms did not increase the dihedral angle of polymer backbones. Instead, because of F–H interaction, the dihedral angles decreased. For chlorine, the Cl–H interaction also exists but the dihedral angles increase due to the large size of chlorine atoms. Although two modification approaches give different results, both core engineering of isoindigo by introducing electron-withdrawing groups effectively lowers the LUMO levels of the polymers. Ambipolar FETs based on fluorinated polymer **PFII2T** can be fabricated and tested in ambient by solution process, and the electron mobilities increased from 10^{-2} to 0.43 cm^2 V^{-1} s^{-1} with high hole mobilities of up to 1.85 cm^2 V^{-1} s^{-1}. With chlorinated isoindigo polymers, FETs fabricated in ambient showed hole mobilities up to 0.81 cm^2 V^{-1} s^{-1} and dramatically increased electron mobilities from 10^{-2} to 0.66 cm^2 V^{-1} s^{-1}. Complementary-like inverters based on chlorinated polymers were also demonstrated, exhibiting a sharp signal switching with high gain values due to balanced carrier transport. For the first time, both ambient-stable and balanced carrier transport are fulfilled in polymer ambipolar FETs and inverters with high performance.

Furthermore, GIXD investigation showed that the introduction of fluorine and chlorine atoms and selenophene not only modulated the polymer energy levels, but also affected the interchain interactions and led to different polymer packing in the solid state. Recently, fluorinated isoindigo polymers were also used for solar cells to enhance the open circuit voltage and power conversion efficiency [12, 34], thus demonstrating the broad applications of core functionalized isoindigo derivatives.

3.5 Experimental Details and Characterization

3.5.1 Device Fabrication and Characterization

Top-gate/bottom-contact FET devices and complementary inverters were fabricated using n^{++}-Si/SiO_2 (300 nm) substrates. The gold source and drain bottom electrodes (with Ti as the adhesion layer) were patterned by photolithography on the SiO_2 surface. The substrates were subjected to cleaning using ultrasonication in acetone, cleaning agent, deionized water (twice), and *iso*-propanol. The cleaned substrates were dried under vacuum at 80 °C. The substrates were used directly under ambient conditions or transferred into a glovebox. A thin film of the polymer was deposited on the treated substrates by spin-coating at 1,500 rpm for 60 s using a polymer solution (6 mg/mL), optionally followed by thermal annealing at 140, 160, 180 or 200 °C under ambient conditions or in a glovebox. After polymer thin film deposition, a CYTOP solution (CYTOP CTL809 M:CT-solv180 = 3:1) was spin-coated onto the semiconducting layer at 2,000 rpm for 60 s resulting in a dielectric layer of 500 nm thick. The CYTOP layer was then baked at 100 °C for 1 h under ambient conditions or in a glovebox. Gate electrodes comprising a layer of Al (50 nm) were then evaporated through a shadow mask onto the dielectric layer by thermal evaporation. The OTFT devices had a channel length (L) of 50 μm and a channel width (W) of 1,000 μm.

The evaluations of the FETs and inverters were carried out in atmosphere (humidity 50–60 %) on a probe stage using a Keithley 4200 SCS as parameter analyzer. The carrier mobility, μ, was calculated from the data in the saturated regime according to the equation $I_{SD} = (W/2L)\ C_i\mu(V_G - V_T)^2$, where I_{SD} is the drain current in the saturated regime. W and L are, respectively, the semiconductor channel width and length, C_i ($C_i = 3.7$ nF cm^{-2}) is the capacitance per unit area of the gate dielectric layer, and V_G and V_T are the gate voltage and threshold voltage.

3.5.2 Synthetic Procedures and Characterization

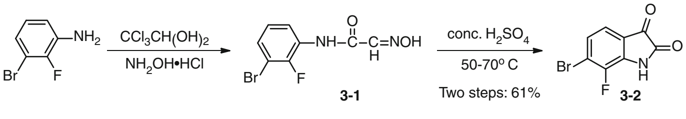

6-Bromo-7-fluoroisatin (**3-2**). To a solution of chloral hydrate (9.55 g, 57.89 mmol) in deionized water (150 mL), Na_2SO_4 (100 g, 684.19 mmol), 3-bromo-2-fluoroaniline (10 g, 52.63 mmol), H_2SO_4 (40 mL, 1 M) and hydroxylamine hydrochloride (10.97 g, 157.89 mmol) was added. The mixture was heated to 130 °C and refluxed for 30 min. The mixture was then cooled to 80 °C and filtered to collect the product. The product was washed with deionized water and dried under reduced pressure to afford **3-1** as a yellowish solid, which was directly used for the next step without further purification.

To a concentrated H_2SO_4 (100 mL) in 250 mL round-bottom flask kept at 50 °C, compound **1** was added portionwise with stirring. The mixture was heated to 70 °C for 1 h before pouring into ice water. The precipitate was collected by filtration and the filtrate was extract with ethyl acetate (EA). The precipitate and the extraction were combined and subject to column chromatography (silica gel; eluent: PE: EA = 8:1) to afforded **3-2** as an orange solid (7.80 g, 61 %). ^{1}H NMR (DMSO-d_6, 400 MHz, ppm): δ 11.74 (s, 1H), 7.40–7.37 (dd, $J_{H\text{–}H}$ = 8.0 Hz, $J_{H\text{–}F}$ = 5.6 Hz, 1H), 7.32–7.30 (d, $J_{H\text{–}H}$ = 8.0 Hz, 1H). ^{13}C NMR (DMSO-d_6, 100 MHz, ppm): δ 182.3–182.2 (d, $J^4_{F\text{–}C}$ = 3.9 Hz), 159.2, 145.2–142.8 (d, $J^1_{F\text{–}C}$ = 246 Hz), 138.2–138.1 (d, $J^2_{F\text{–}C}$ = 14.0 Hz), 126.5–126.4 (d, $J^4_{F\text{–}C}$ = 1.7 Hz), 121.4–121.3 (d, $J^3_{F\text{–}C}$ = 3.8 Hz), 119.9–119.8 (d, $J^3_{F\text{–}C}$ = 3.7 Hz), 118.4–118.3 (d, $J^2_{F\text{–}C}$ = 17.3 Hz). EI-MS calcd. for $[M + H]^+$: 243. Found: 243. Elemental Anal. calcd. for $C_8H_3BrFNO_2$: C, 39.38; H, 1.24; N, 5.74. Found: C, 39.39; H, 1.40; N, 5.74.

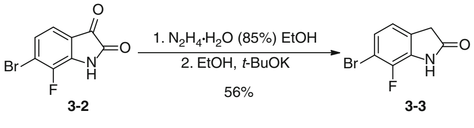

6-Bromo-7-fluoroindolin-2-one (**3-3**). To a solution of **3-2** (2.80 g, 11.48 mmol) in ethanol (50 mL), hydrazine hydrate (85 %, 0.5 mL) was added under nitrogen. After the mixture was refluxed for 30 min, a yellow participate was formed and collected by filtration. The yellow precipitate was then dissolved in anhydrous ethanol (50 mL), and *t*-BuOK (4.03 g, 35.90 mmol) was added. The mixture was refluxed under nitrogen for 2 h before pouring into water. The mixture was acidified with dilute HCl to pH = 2 and extracted with EA. The combined organic phase was washed with water, brine, dried with Na_2SO_4, and concentrated under reduced pressure. The residue was purified by column chromatography (silica gel; eluent: PE: EA = 5:1) to provide **3-3** as a light-yellow solid (1.49 g, 56 %). ^{1}H NMR (DMSO-d_6, 400 MHz, ppm): δ 11.04 (s, 1H), 7.26–7.15 (dd, $J_{\mathrm{H-H}} = 7.9$ Hz, $J_{\mathrm{F-H}} = 6.2$ Hz, 1H), 7.06–6.95 (d, $J = 7.9$ Hz, 1H), 3.54 (s, 1H).^{13}C NMR (DMSO-d_6, 100 MHz, ppm): δ 175.9, 143.8–141.4 (d, $J^1_{\mathrm{F-C}} = 242$ Hz), 132.0–131.9 (d, $J^2_{\mathrm{F-C}} = 12.6$ Hz), 128.6–128.5 (d, $J^3_{\mathrm{F-C}} = 4.1$ Hz), 124.7, 121.7–121.6 (d, $J^3_{\mathrm{F-C}} = 3.6$ Hz), 106.70–106.5 (d, $J^2_{\mathrm{F-C}} = 17.0$ Hz), 35.9–35.8 (d, $J^4_{\mathrm{F-C}} = 2.4$ Hz). EI-MS: calcd. for $[M + H]^+$: 229. Found: 229. Elemental Anal. calcd. for C_8H_5BrFNO: C, 41.77; H, 2.19; N, 6.09. Found: C, 41.52; H, 2.27; N, 6.22.

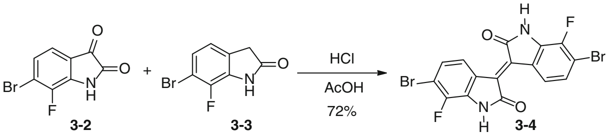

6,6′-Dibromo-7,7′-difluoroisoindigo (**3-4**). To a suspension of **3-2** (1.58 g, 6.48 mmol) and **3-3** (1.49 g, 6.48 mmol) in AcOH (75 mL) was added conc. HCl (37 %) solution (0.4 mL). The mixture was refluxed for 24 h. The mixture was allowed to cool and filtered. The solid material was washed with water, ethanol, and ether. After drying under vacuum, deep red 6,6′-Dibromo-7,7′-difluoroisoindigo (2.13 g, 72 %) was obtained. ^{1}H NMR (DMSO-d_6, 400 MHz, ppm): δ 11.68 (s, 2H), 8.83–8.81 (d, $J_{\mathrm{H-H}} = 8.7$ Hz, 2H), 7.31–7.27 (dd, $J = 8.7$ Hz, $J_{\mathrm{F-H}} = 6.7$ Hz, 2H). ^{13}C NMR (DMSO-d_6, 100 MHz, ppm): δ 168.5, 151.7, 144.0–141.6 (d, $J^1_{\mathrm{F-C}} = 242$ Hz), 133.1–133.0 (d, $J^3_{\mathrm{F-C}} = 3.9$ Hz), 132.6–132.5 (d, $J^2_{\mathrm{F-C}} = 13.6$ Hz), 126.3, 124.5, 123.4–123.3 (d, $J^3_{\mathrm{F-C}} = 4.6$ Hz), 112.47–112.3 (d, $J^2_{\mathrm{F-C}} = 16.8$ Hz). EI-MS: calcd. for $[M + H]^+$: 456. Found: 456. Elemental Anal. calcd. for $C_{16}H_6Br_2F_2N_2O_2$: C, 42.14; H, 1.33; N, 6.14. Found: C, 42.13; H, 1.40; N, 6.15.

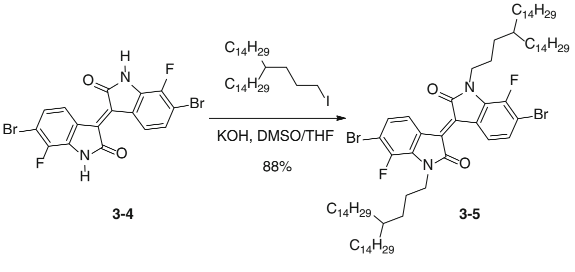

Compound 3-5. To a solution of 6,6′-dibromo-7,7′-difluoroisoindigo (**3-4**) (150 mg, 0.33 mmol) and freshly powered KOH (1.68 g, 12.1 mmol) in dimethyl sulfoxide (DMSO) (20 mL), 15-(3-iodopropyl)nonacosane (478 mg, 0.83 mmol) in THF (20 mL) was added under nitrogen. The mixture was stirred for 24 h at 25 °C before pouring into water. The residues were dissolved in $CHCl_3$ (100 mL) and washed with water (3 × 50 mL). The combined organic phase was washed with brine and dried (Na_2SO_4) and concentrated under reduced pressure. The residue was purified by silica gel chromatography with eluting ($PE:CH_2Cl_2$ = 5:1) to give **3-5** as a deep-red solid. (390 mg, 88 %). H NMR ($CDCl_3$, 400 MHz, ppm): δ 8.90–8.88 (d, J = 8.7 Hz, 2H), 7.26–7.17 (dd, $J_{\mathrm{H-H}}$ = 8.7 Hz, $J_{\mathrm{F-H}}$ = 6.3 Hz, 2H), 3.91–3.88 (t, J = 7.4 Hz 4H), 1.68–1.65 (m, 4H), 1.33–1.21 (m, 110H), 0.89–0.86 (t, J = 6.8 Hz, 12H). ^{13}C NMR ($CDCl_3$, 100 MHz, ppm): δ 167.1, 144.9–142.5 (d, $J^1_{\mathrm{F-C}}$ = 243 Hz), 133.2–133.1 (d, $J^3_{\mathrm{F-C}}$ = 3.3 Hz), 132.4–132.3 (d, $J^2_{\mathrm{F-C}}$ = 9.5 Hz), 126.5–126.4 (d, $J^3_{\mathrm{F-C}}$ = 3.4 Hz), 125.8, 123.2–123.1 (d, $J^3_{\mathrm{F-C}}$ = 3.3 Hz), 114.9–114.7 (d, $J^2_{\mathrm{F-C}}$ = 19.4 Hz), 42.8, 42.7, 37.1, 33.5, 31.9, 30.5, 30.1, 29.7, 29.7, 29.4, 26.6, 26.1, 22.7, 14.1. Elemental Anal. calcd. for $C_{80}H_{134}Br_2F_2N_2O_2$: C, 70.98; H, 9.98; N, 2.07. Found: C, 70.90; H, 9.61; N, 2.06. ESI-HRMS: calcd. for $[M + H]^+$: 1351.88529. Found: 1351.88157.

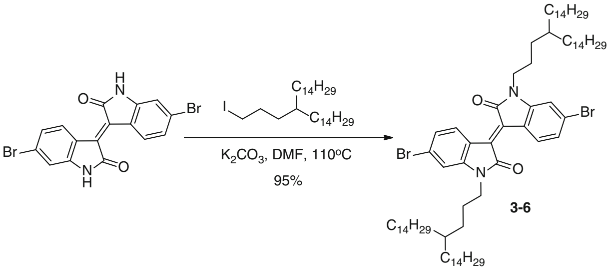

Compound 3-6. To a solution of 6,6′-dibromoisoindigo (2.00 g, 4.76 mmol) and potassium carbonate (1.97 g, 14.3 mmol) in *N*,*N*′-dimethylformamide (DMF) (100 mL), 15-(3-iodopropyl)nonacosane (6.0 g, 10.4 mmol) was added under nitrogen. The mixture was stirred for 15 h at 100 °C and then the solvent was removed under reduced pressure. The residue was dissolved in $CHCl_3$ (100 mL) and washed with water. The combined organic phase was washed with brine and dried over with Na_2SO_4, and then concentrated under reduced pressure. The residue was purified by silica gel chromatography with eluent ($PE:CH_2Cl_2$ = 5:1) to give **3-6** as a deep-red solid. (6.0 g, 95 %). ^1H NMR ($CDCl_3$, 400 MHz, ppm) δ 9.09–9.07 (d, J = 8.6 Hz, 2H), 7.16–7.14 (dd, J_1 = 8.6 Hz, J_2 = 1.8 Hz, 2H), 6.90–6.89 (d, J = 1.8 Hz, 2H), 3.71–3.67 (t, J = 7.5 Hz, 4H), 1.67–1.57 (m, 4H), 1.42–1.26 (m, 110H), 0.89–0.86 (t, J = 6.6 Hz, 12H). ^{13}C NMR ($CDCl_3$, 100 MHz, ppm): δ 167.6, 145.7, 132. 6, 131.2, 126.7, 125.1, 120.4, 111.3, 40.6, 37.1, 33.5, 31.9, 30.8, 30.1, 29.7, 29.7, 29.4, 26.7, 24.5, 22.7, 14.1. Elemental Anal. calcd. for $C_{80}H_{136}Br_2N_2O_2$: C, 72.92; H, 10.40; N, 2.13; Found: C, 72.75; H, 10.27; N, 2.06. ESI-HRMS calcd. for $[M + H]^+$: 1315.9041; Found: 1315.9067.

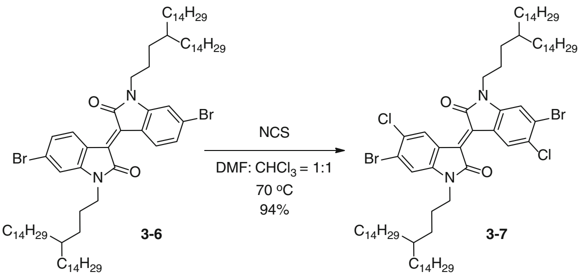

Compound 3-7. To a solution of **3-6** (2.00 g, 1.52 mmol) in the mixed solvent of $CHCl_3$ (70 mL) and *N*,*N*′-dimethylformamide (DMF) (70 mL), *N*-Chlorosuccinimide (1.00 g, 7.59 mmol) was added at 70 °C under nitrogen. The mixture was stirred at 70 °C for 3 h and then the solvent was removed under reduced pressure. The residue was dissolved in $CHCl_3$ (100 mL) and washed with water. The combined organic phase was washed with brine and dried over with Na_2SO_4, and then concentrated under reduced pressure. The residue was purified by silica gel chromatography with eluent (PE:CH_2Cl_2 = 5:1) to give **3** as a dark-red solid. (1.82 g, 87 %). ^{1}H NMR ($CDCl_3$, 400 MHz, ppm) δ 9.43 (s, 2H), 7.02 (s, 2H), 3.73–3.69 (t, $J = 7.4$ Hz, 4H), 1.69–1.55 (m, 4H), 1.30–1.22 (m, 110H), 0.89–0.86 (t, $J = 6.6$ Hz, 12H). ^{13}C NMR ($CDCl_3$, 100 MHz, ppm): δ 167.2, 144.0, 132.6, 131.4, 127.8, 126.7, 121.5, 112.7, 40.8, 37.1, 33.5, 31.9, 30.7, 30.1, 29.7, 29.7, 29.4, 26.7, 24.4, 22.7, 14.1. Elemental Anal. calcd. for $C_{80}H_{134}Br_2Cl_2N_2O_2$: C, 69.29; H, 9.74; N, 2.02; Found: C, 69.34; H, 9.42; N, 1.96. ESI-HRMS calcd. for $[M + H]^+$: 1383.8262; Found: 1383.8282.

General Procedures for Stille Polymerization and Polymer Purification:

PFII2T 3-5. (100 mg, 0.0739 mmol), 5,5′-bis(trimethylstannyl)-2,2′-bithiophene (36.3 mg, 0.0739 mmol), $Pd_2(dba)_3$ (1.4 mg, 2 mol%.), P(*o*-tol)$_3$ (1.8 mg, 8 mol%), and 10 mL of toluene were added to a Schlenk tube. The tube was charged with nitrogen through a *freeze-pump-thaw* cycle for three times. The mixture was stirred for 48 h at 120 °C. *N*,*N*′-Diethylphenylazothioformamide (10 mg) was then added and then the mixture was stirred for 1 h to remove any residual catalyst before being precipitated into methanol (200 mL). The precipitate was filtered through a nylon filter and purified via Soxhlet extraction for 8 h with acetone, 12 h with hexane, and finally was collected with chloroform. The chloroform solution was then concentrated by evaporation and precipitated into methanol (200 mL) and filtered off to afford a dark brown solid (99.1 mg, yield 99 %). Elemental Anal. calcd: for $(C_{88}H_{138}F_2N_2O_2S_2)_n$: C, 77.82; H, 10.24; N, 2.06. Found: C, 76.92; H, 9.79; N, 2.02.

PII2T: The synthetic procedure is similar as described for **PFII2T** (yield 94 %). Elemental Anal. calcd. for $(C_{88}H_{140}N_2O_2S_2)_n$: C, 79.94; H, 10.67; N, 2.12. Found: C, 78.88; H, 10.12; N, 2.07.

PCII2T: The synthetic procedure is similar as described for **PFII2T** (yield 97 %). Elemental Anal. calcd for $(C_{88}H_{138}Cl_2N_2O_2S_2)_n$: C, 75.98; H, 10.00; N, 2.01. Found: C, 75.22; H, 9.91; N, 1.93.

PCII2Se: The synthetic procedure is similar as described for **PFII2T** (yield 98 %). Elemental Anal. calcd. for $(C_{88}H_{138}Cl_2N_2O_2Se_2)_n$: C, 71.13; H, 9.43; N, 1.89. found: C, 70.09; H, 9.14; N, 1.81.

References

1. Zaumseil J, Sirringhaus H (2007) Electron and ambipolar transport in organic field-effect transistors. Chem Rev 107:1296–1323
2. Yuen JD, Wudl F (2013) Strong acceptors in donor-acceptor polymers for high performance thin film transistors. Energy Environ Sci 6:392–406
3. Fan J, Yuen JD, Wang M, Seifter J, Seo J-H, Mohebbi AR, Zakhidov D, Heeger A, Wudl F (2012) High-performance ambipolar transistors and inverters from an ultralow bandgap polymer. Adv Mater 24:2186–2190
4. Chen Z, Lee MJ, Shahid Ashraf R, Gu Y, Albert-Seifried S, Meedom Nielsen M, Schroeder B, Anthopoulos TD, Heeney M, McCulloch I, Sirringhaus H (2012) High-performance ambipolar diketopyrrolopyrrole-thieno[3,2-b]thiophene copolymer field-effect transistors with balanced hole and electron mobilities. Adv Mater 24:647–652
5. Shahid M, McCarthy-Ward T, Labram J, Rossbauer S, Domingo EB, Watkins SE, Stingelin N, Anthopoulos TD, Heeney M (2012) Low band gap selenophene-diketopyrrolopyrrole polymers exhibiting high and balanced ambipolar performance in bottom-gate transistors. Chem Sci 3:181–185
6. Liu Y-Y, Song C-L, Zeng W-J, Zhou K-G, Shi Z-F, Ma C-B, Yang F, Zhang H-L, Gong X (2010) High and balanced hole and electron mobilities from ambipolar thin-film transistors based on nitrogen-containing oligoacences. J Am Chem Soc 132:16349–16351
7. Usta H, Newman C, Chen Z, Facchetti A (2012) Dithienocoronenediimide-based copolymers as novel ambipolar semiconductors for organic thin-film transistors. Adv Mater 24:3678–3684
8. Chen Z, Lee MJ, Shahid Ashraf R, Gu Y, Albert-Seifried S, Meedom Nielsen M, Schroeder B, Anthopoulos TD, Heeney M, McCulloch I, Sirringhaus H (2012) High-performance ambipolar diketopyrrolopyrrole-thieno[3,2-b]thiophene copolymer field-effect transistors with balanced hole and electron mobilities. Adv Mater 24:647–652
9. Lei T, Cao Y, Fan Y, Liu C-J, Yuan S-C, Pei J (2011) High-performance air-stable organic field-effect transistors: isoindigo-based conjugated polymers. J Am Chem Soc 133:6099–6101
10. Lei T, Dou J-H, Pei J (2012) Influence of alkyl chain branching positions on the hole mobilities of polymer thin-film transistors. Adv Mater 24:6457–6461
11. Wang E, Ma Z, Zhang Z, Vandewal K, Henriksson P, Inganäs O, Zhang F, Andersson MR (2011) An easily accessible isoindigo-based polymer for high-performance polymer solar cells. J Am Chem Soc 133:14244–14247
12. Deng Y, Liu J, Wang J, Liu L, Li W, Tian H, Zhang X, Xie Z, Geng Y, Wang F (2014) Dithienocarbazole and isoindigo based amorphous low bandgap conjugated polymers for efficient polymer solar cells. Adv Mater 26:471–476
13. Stalder R, Mei J, Subbiah J, Grand C, Estrada LA, So F, Reynolds JR (2011) N-type conjugated polyisoindigos. Macromolecules 44:6303–6310
14. Lei T, Cao Y, Zhou X, Peng Y, Bian J, Pei J (2012) Systematic investigation of isoindigo-based polymeric field-effect transistors: design strategy and impact of polymer symmetry and backbone curvature. Chem Mater 24:1762–1770
15. Yan H, Chen Z, Zheng Y, Newman C, Quinn JR, Dotz F, Kastler M, Facchetti A (2009) A high-mobility electron-transporting polymer for printed transistors. Nature 457:679–686
16. Zhou E, Cong J, Wei Q, Tajima K, Yang C, Hashimoto K (2011) All-polymer solar cells from perylene diimide based copolymers: material design and phase separation control. Angew Chem Int Ed 50:2799–2803

17. Zhan X, Tan Z, Domercq B, An Z, Zhang X, Barlow S, Li Y, Zhu D, Kippelen B, Marder SR (2007) A high-mobility electron-transport polymer with broad absorption and its use in field-effect transistors and all-polymer solar cells. J Am Chem Soc 129:7246–7247
18. Zhou H, Yang L, Stuart AC, Price SC, Liu S, You W (2011) Development of fluorinated benzothiadiazole as a structural unit for a polymer solar cell of 7 % efficiency. Angew Chem Int Ed 50:2995–2998
19. Chen H-Y, Hou J, Zhang S, Liang Y, Yang G, Yang Y, Yu L, Wu Y, Li G (2009) Polymer solar cells with enhanced open-circuit voltage and efficiency. Nat Photon 3:649–653
20. Lei T, Dou J-H, Ma Z-J, Yao C-H, Liu C-J, Wang J-Y, Pei J (2012) Ambipolar polymer field-effect transistors based on fluorinated isoindigo: high performance and improved ambient stability. J Am Chem Soc 134:20025–20028
21. Rowland RS, Taylor R (1996) Intermolecular nonbonded contact distances in organic crystal structures: comparison with distances expected from van der Waals radii. J Phys Chem 100:7384–7391
22. Chen Z, Zheng Y, Yan H, Facchetti A (2009) Naphthalenedicarboximide- vs perylenedicarboximide-based copolymers. Synthesis and semiconducting properties in bottom-gate n-channel organic transistors. J Am Chem Soc 131:8–9
23. Kronemeijer AJ, Gili E, Shahid M, Rivnay J, Salleo A, Heeney M, Sirringhaus H (2012) A selenophene-based low-bandgap donor-acceptor polymer leading to fast ambipolar logic. Adv Mater 24:1558–1565
24. Wen Y, Liu Y, Guo Y, Yu G, Hu W (2011) Experimental techniques for the fabrication and characterization of organic thin films for field-effect transistors. Chem Rev 111:3358–3406
25. Katz HE, Lovinger AJ, Johnson J, Kloc C, Siegrist T, Li W, Lin YY, Dodabalapur A (2000) A soluble and air-stable organic semiconductor with high electron mobility. Nature 404:478–481
26. Tang ML, Bao Z (2011) Halogenated materials as organic semiconductors. Chem Mater 23:446–455
27. Tang ML, Oh JH, Reichardt AD, Bao Z (2009) Chlorination: a general route toward electron transport in organic semiconductors. J Am Chem Soc 131:3733–3740
28. Gsänger M, Oh JH, Könemann M, Höffken HW, Krause A-M, Bao Z, Würthner F (2010) A crystal-engineered hydrogen-bonded octachloroperylene diimide with a twisted core: an n-channel organic semiconductor. Angew Chem Int Ed 49:740–743
29. Lei T, Dou J-H, Ma Z-J, Liu C-J, Wang J-Y, Pei J (2013) Chlorination as a useful method to modulate conjugated polymers: balanced and ambient-stable ambipolar high-performance field-effect transistors and inverters based on chlorinated isoindigo polymers. Chem Sci 4:2447–2452
30. Ha JS, Kim KH, Choi DH (2011) 2,5-Bis(2-octyldodecyl)pyrrolo[3,4-c]pyrrole-1,4-(2H,5H)-dione-based donor–acceptor alternating copolymer bearing 5,5′-di(thiophen-2-yl)-2,2′-biselenophene exhibiting 1.5 $cm^2 V^{-1} s^{-1}$ hole mobility in thin-film transistors. J Am Chem Soc 133:10364–10367
31. Kang I, An TK, Hong J-A, Yun H-J, Kim R, Chung DS, Park CE, Kim Y-H, Kwon S-K (2013) Effect of selenophene in a DPP copolymer incorporating a vinyl group for high-performance organic field-effect transistors. Adv Mater 25:524–528
32. Nielsen KT, Bechgaard K, Krebs FC (2005) Removal of palladium nanoparticles from polymer materials. Macromolecules 38:658–659
33. Kang S-M, Leblebici Y (2003) CMOS digital integrated circuits: analysis and design, 3rd edn. McGraw-Hill, New York
34. Yang Y, Wu R, Wang X, Xu X, Li Z, Li K, Peng Q (2014) Isoindigo fluorination to enhance photovoltaic performance of donor-acceptor conjugated copolymers. Chem Commun 50:439–441

Chapter 4
BDOPV—A Strong Electron-Deficient Building Block for Polymer Field-Effect Transistors

4.1 Core Extension to Buildup New Systems

To further modulate the electronic properties of isoindigo, we designed three novel structures based on isoindigo by breaking the double bond between two lactam rings and inserting different π-conjugated skeletons (Fig. 4.1a). The third structure, benzodifurandione-based oligo(*p*-phenylene vinylene) (**BDOPV**), was successfully obtained, probably due to its four intramolecular hydrogen bonds that provide extra stability. Thus, **BDOPV** is a derivative of isoindigo. On the other hand, **BDOPV** is also a derivative of oligo(*p*-phenylene vinylene) (OPV). On the basis of **BDOPV**, a poly(*p*-phenylene vinylene) (**PPV**) derivative **BDPPV** was developed for n-type conjugated polymer FETs (Fig. 4.1b). In this chapter, our works on development of **BDOPV**-based conjugated polymers will be described.

4.2 BDPPV—The First High-Performance n-type PPV Derivative

In the organic electronics field, poly(*p*-phenylene vinylene) derivatives (**PPV**s) are among the earliest and the most widely investigated polymers [1]. **PPV**s have been used to fabricate the first polymer light-emitting diode (PLED) [2], the first bulk heterojunction (BHJ) solar cell [3], and the first optically pumped solid-state laser [4, 5]. In PLED field, considerable efforts have been devoted to improving the emission color, efficiency, and life time of **PPV**s [6, 7]. In solar cell field, **PPV**s have been widely researched to improve the power conversion efficiency [8, 9]. Nonetheless, **PPV**s were seldom applied in field-effect transistors (FETs) due to their low hole mobilities (10^{-5} to 10^{-2} cm^2 V^{-1} s^{-1}) [10, 11]. As typical p-type polymers [12, 13], the electron mobilities of **PPV**s are lower (10^{-5} to 10^{-4} cm^2 V^{-1} s^{-1}), even when low-work-function metal (Ca) and hydroxyl-free gate dielectric

T. Lei, *Design, Synthesis, and Structure-Property Relationship Study of Polymer Field-Effect Transistors*, Springer Theses, DOI 10.1007/978-3-662-45667-5_4

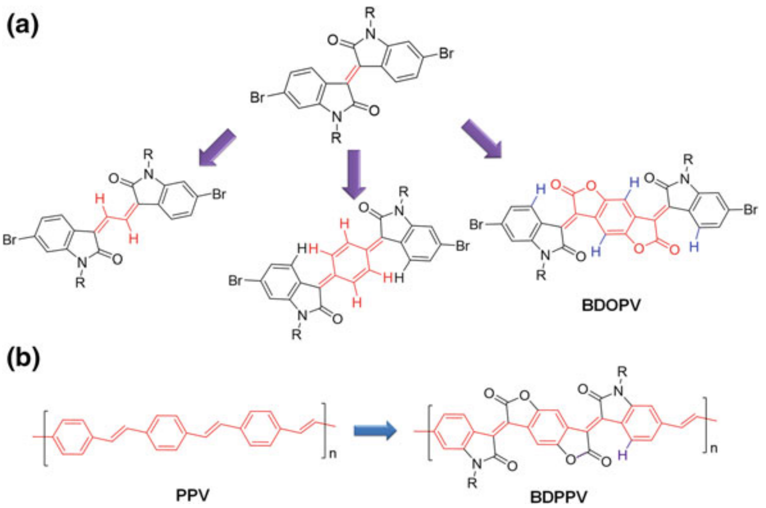

Fig. 4.1 **a** Proposed core extension strategy for isoindigo. **b** Electron-deficient **BDPPV** was constructed based on **BDOPV**

were used to fabricate the device and all operations were performed under inert atmosphere [14]. Hence, one may ask, can high carrier mobility be achieved in **PPV**-based polymers?

Recent development of several electron-deficient dyes, such as diketopyrrolopyrrole (DPP) [15–17], isoindigo (II) [18, 19], naphthalene diimide (NDI) [20], and benzobisthiadiazole (BBT) [21, 22] in polymer FETs afforded high hole mobilities under ambient conditions and high electron mobilities in nitrogen. Nevertheless, high electron mobilities over 1 cm^2 V^{-1} s^{-1} under ambient conditions has not yet been reported, although polymers with high electron mobilities under ambient conditions are important for both fundamental understanding of carrier transport and advancing practical applications. The current scenario of new polymer design mainly focuses on thiophene-based donor–acceptor copolymers (third-generation polymer named by Heeger), and **PPV**s (second-generation polymer named by Heeger) are almost neglected [23, 24].

We have discussed the transport mechanism of carrier in conjugated polymer in Chap. 1. Carrier mobility in a conjugated polymer is determined by intrachain and interchain transport [25]. Increasing the effective conjugation length and reducing torsional disorder along the polymer backbone improve the intrachain transport [26]. Good π–π stacking and ordered polymer packing, on the other hand, increase the interchain transport. Previously, we proved that the backbone curvature of polymers has a significant influence on their carrier mobility, and polymers with linear backbones have mobilities several orders of magnitude higher than those with wave-like backbones [27, 28]. Thus, the low mobility of **PPV**s is presumably caused by the following issues:

(1) The double bonds in **PPV**s readily undergo *trans* to *cis* conformational transformation under UV light both in solution and in solid state (Fig. 4.2a) [29, 30].
(2) Even for all-trans backbones, the single bonds in **PPV**s rotate freely at room temperature, creating many conformational isomers (Fig. 4.2b).
(3) **PPV**s generally have weak interchain interactions and are amorphous in the solid state [31], thus resulting in slow interchain carrier transport.
(4) The LUMO levels of **PPV**s (−2.7 to −3.2 eV) [14] are too high to achieve stable electron transport under ambient conditions.

The first two issues not only limit the intrachain carrier mobilities in **PPV**s but also weaken the interchain π–π interactions, thus further prohibiting the interchain carrier transport. Currently, the most effective approach to obtain high electron mobility in polymers, especially under ambient conditions, is introducing electron-withdrawing groups to lower their LUMO levels [32, 33].

In this section, we try to tackle these problems in traditional **PPV**s by synthesizing a novel **PPV** derivative, a benzodifurandione-based **PPV** (**BDPPV**) (Fig. 4.2c). First, strong electron-withdrawing carbonyl groups was introduced on the double bonds of **PPV** to lower its LUMO level. Second, the carbonyl groups can form intramolecular hydrogen bonds to prevent the conformational transformation of the double bonds, affording a giant “locked” aromatic plane. The enlarged aromatic backbone of **BDPPV** may help the overlaps of intermolecular frontier orbitals, thus facilitating interchain transport. Third, 4-octadecyldocosyl groups were used as side chains because we have demonstrated that a more distant branching position of side chains can enhance interchain π–π stacking and thereby improve carrier mobilities [34]. Using **BDPPV** as an active layer, FETs with electron mobilities up to 1.1 $cm^2 V^{-1} s^{-1}$ were obtained under ambient conditions, 4 orders of magnitude higher than those of other **PPV**s. To our knowledge, this result is among the highest in n-type polymer FETs, and **BDPPV** represents the first polymer that can transport electrons over 1 $cm^2 V^{-1} s^{-1}$ under ambient conditions [35].

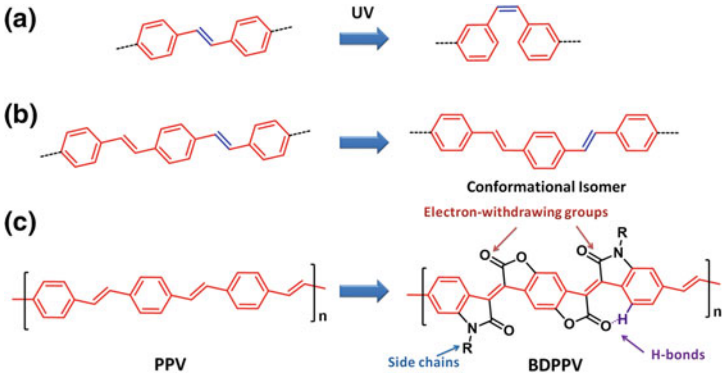

Fig. 4.2 **a** Double bond isomerization of the **PPV** segment under UV irradiation. **b** Conformational isomers in **PPV** after single bond rotation. **c** Design strategy for the electron-deficient **PPV** derivative—**BDPPV**

Scheme 4.1 illustrates the synthetic route to polymer **BDPPV**. The synthesis started from the alkylation of commercially available 6-bromoisatin (4-1), giving compound 4-3 in 80 % yield. 2,2′-(2,5-Dihydroxy-1,4-phenylene)diacetic acid (compound 4-4) was synthesized from 1,4-benzoquinone in over 10-g scale [36]. 4-4 was subjected to dehydration reaction using acetic anhydride to afford dilactone 4-5. Lithium 2,2,6,6-tetramethylpiperidine (LTMP) was used to generate intermediate 4-6 and react with 4-3, providing the desired benzodifurandione-based oligo (*p*-phenylene vinylene) (**BDOPV**) in moderate yield (67 %). A Stille coupling polymerization between **BDOPV** and (*E*)-1,2-bis(tributylstannyl)ethene gave polymer **BDPPV** in 83 % yield. The molecular weight of **BDPPV** was evaluated by high temperature gel permeation chromatography at 140 °C using 1,2,4-trichlorobenzene as eluent. The polymer displayed high molecular weight with M_n of 37.6 kDa and PDI of 2.38. The large PDI of **BDPPV** may be caused by its strong aggregation tendency. The polymer showed excellent thermal stability with decomposition temperature over 390 °C.

Figure 4.3 compares the ^{1}H NMR spectra of compounds 4-3, 4-5, and **BDOPV**. After the basic condensation reaction, the signal of H_a of compound 4-3 obviously shifted from 7.46 to 8.92 ppm (H_h in **BDOPV**). The signal of methylene (H_f) in reactant 4-5 disappeared, and another signal of H_e on benzene ring significantly shifted from 7.07 to 9.09 ppm (H_a in **BDOPV**). The ^{1}H NMR spectrum of **BDOPV** displayed clearly four signals in aromatic region, agreeing well with its chemical structure and chemical environment. The optimized structure of **BDOPV** displayed almost planar backbone with small dihedral angles about 7.6° (Fig. 4.3d). The C–H_a–O and C–H_b–O angles are approximately linear and the C–O bond distances (ca. 2.8 Å) are shorter than the combined van der Waals radii (3.3 Å) [37]. These results indicate that four intramolecular hydrogen bonds are formed [38], which may contribute to the planarity and shape-persistency of **BDOPV**.

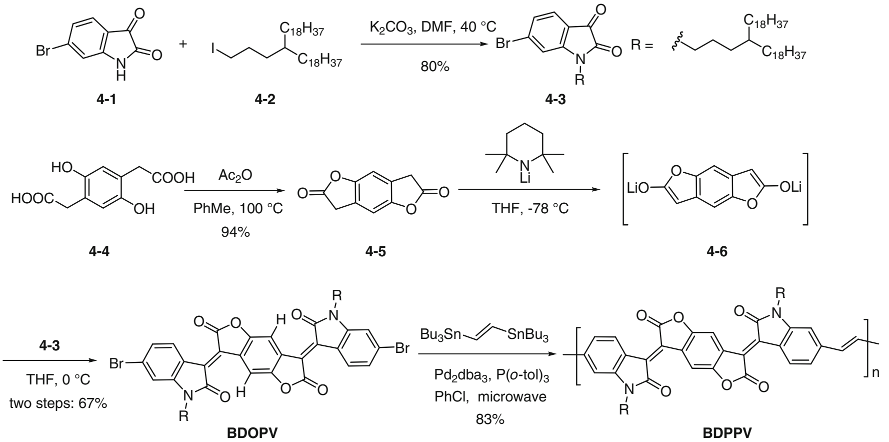

Scheme 4.1 Synthetic approach to polymer **BDPPV**

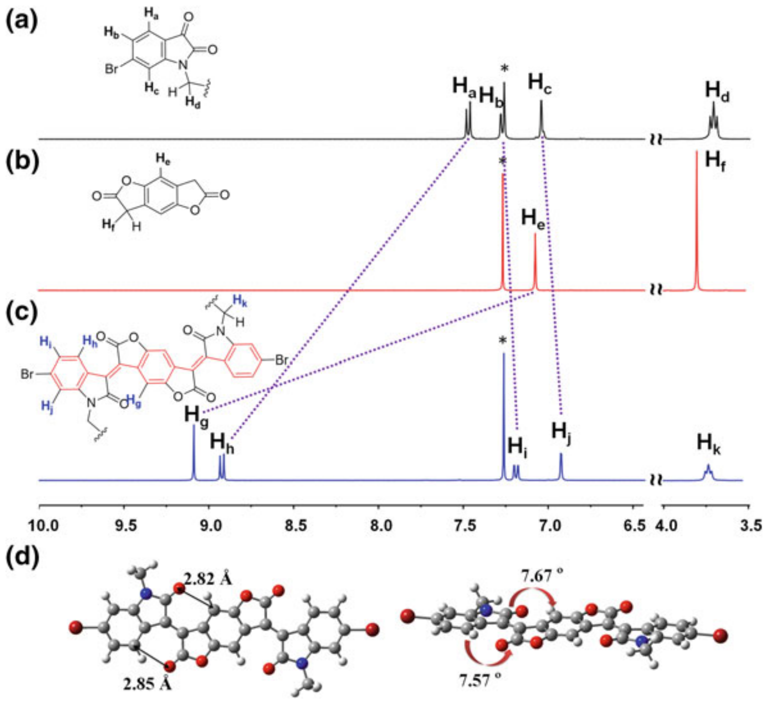

Fig. 4.3 ^{1}H NMR spectra of **a** 4-3, **b** 4-5, and **c** **BDOPV** in $CDCl_3$ (*: solvent peak). **d** The optimized molecular structure of **BDOPV** (B3LYP/6-311+G(d,p))

Under UV light irradiation (365 nm), the double bonds in **PPV**s usually undergo *trans* to *cis* conformational change [29, 30]. Figure 4.4a displays the spectra change of a commercially available model compound 1,4-bis((*E*)-2-methylstyryl)benzene under UV irradiation. Clearly, the compound showed decreased long-wavelength and increased short-wavelength absorption, indicating a conformational change from *trans* to *cis* happened under UV irradiation. In contrast, **BDOPV** showed no spectra change under UV or visible light irradiation (Fig. 4.4b), which may largely due to its "locked skeleton". More importantly, both the solution and the film of polymer **BDPPV** showed excellent stability under UV or visible light exposure. Although one third of the double bonds in **BDPPV** are not locked by intramolecular hydrogen bonds, conformational change in **BDPPV** was not observed. This phenomenon might be attributed to largely conjugated **BDOPV** core, which has strong tendency to undergo intermolecular stacking, thus creating large steric hindrance to prevent the double bond adopting *cis*-conformation in **BDPPV**.

Absorption spectra of **BDOPV** in solution and polymer **BDPPV** in solution, thin film and annealed film are shown in Fig. 4.5a. **BDOPV** displayed two absorption peaks with an onset at 700 nm and a bandgap of 1.80 eV. After polymerization, the new double bond in **BDPPV** further extended the conjugation length, leading to

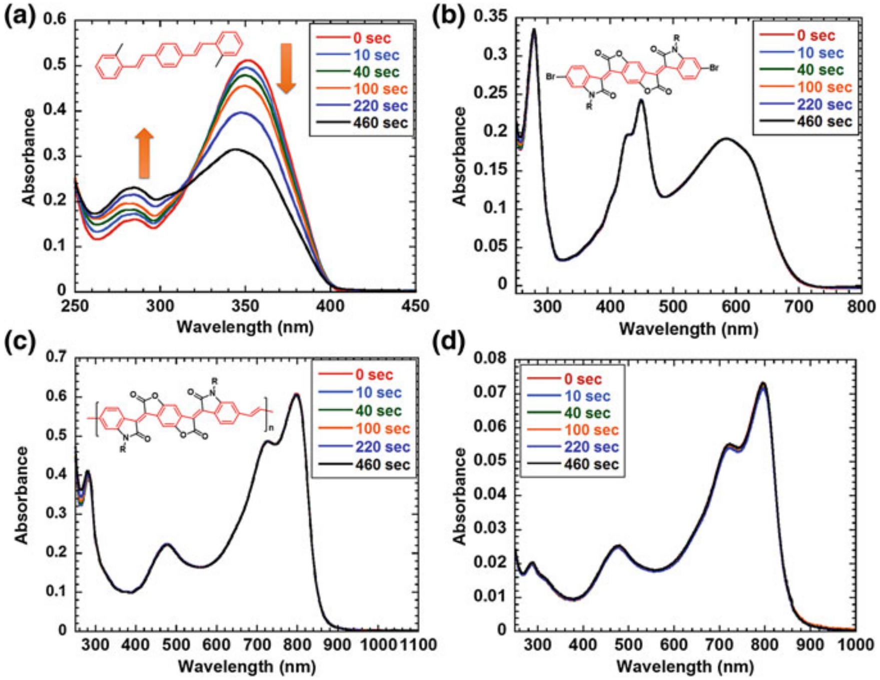

Fig. 4.4 Absorption spectra changes of **a** an OPV model compound, **b** **BDOPV** in solution, **c** **BDPPV** in solution, and **d** **BDPPV** in film under different UV irradiation times. Samples are all irradiated with an Xe lamp (365 nm, 1.0 mW cm^{-2}) in quartz cells

strong near-infrared absorption with a bandgap of 1.42 eV. The main absorption peak of **BDPPV** in film only showed a little red-shift compared to those in solution, and an obvious increase of the intensity of 0–0 vibrational peak was observed. Annealing the film led to a further increase of the intensity of 0–0 peak. These results indicate that the polymer backbone became more planar in film and annealing was helpful for further adjustment. For conjugated polymers, intermolecular stacking and conformational change may significantly shift the absorption spectra [39] which is common for most **PPV**s [31, 40]. However, no significant change was observed for **BDPPV** from solution to film. The absence of bathochromic effects indicates that the polymers probably formed some pre-aggregates in solution due to strong intermolecular interactions [41].

In cyclic voltammetry (CV) measurement, **BDOPV** displayed low HOMO/LUMO level of –6.21/–4.24 eV. Compared with the HOMO/LUMO level of **PPV** (–5.2/–2.7 eV) [14], **BDPPV** exhibited significantly lowered HOMO/LUMO level (–6.12/–4.10 eV), which is also consistent with the HOMO/LUMO level (–5.83/–4.41 eV) estimated from the photoelectron spectroscopy (PES) and optical bandgap. Note that this LUMO level is also lower than those of several ambient-stable n-type polymers, including NDI and PDI-based polymers [42]. Computational

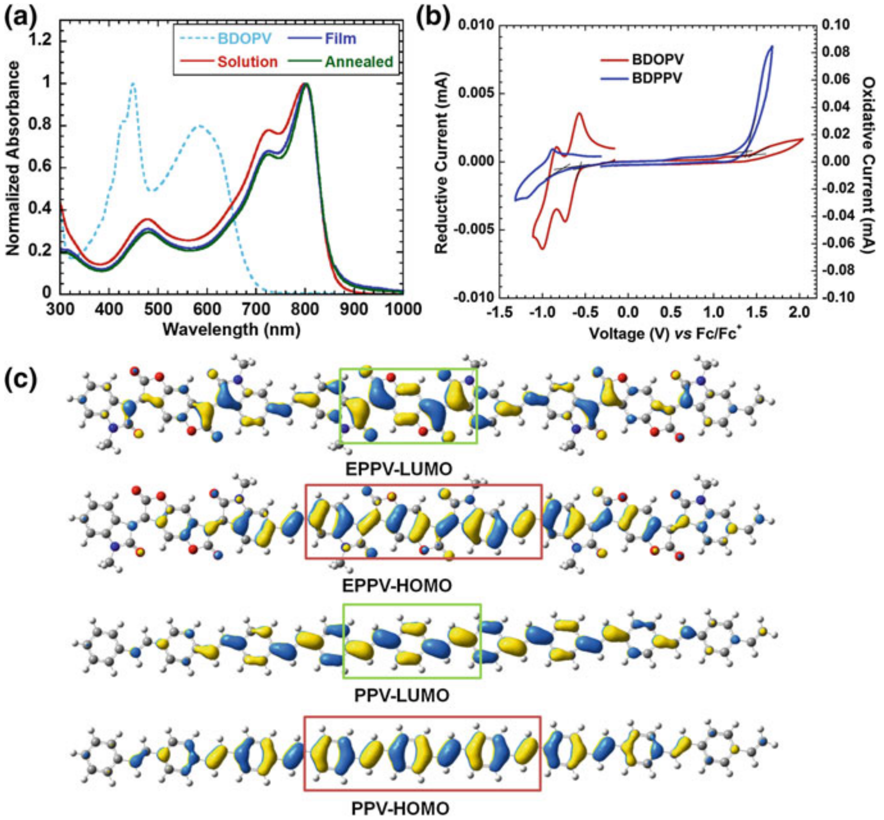

Fig. 4.5 **a** Normalized absorption spectra of **BDOPV** in $CHCl_3$ (1×10^{-5} M, *dashed line*) and **BDPPV** in $CHCl_3$ (1×10^{-5} M), in film and in annealed film (*solid line*). **b** Cyclic voltammograms of **BDOPV** in DCB solution (5 mg/mL) and **BDPPV** in drop-casted film. **c** Calculated molecular orbitals of the trimers of **BDPPV** and **PPV** (B3LYP/6-311G(d,p)). Both trimers display similar frontier orbital distributions as indicated by the *color boxes*

analysis of the oligomer of **BDPPV** showed that the HOMO and LUMO are well delocalized along the polymer backbone, and the HOMO and LUMO distributions of **BDPPV** are similar to those of **PPV**, due to their identical alternative phenylene vinylene skeletons (Fig. 4.5c).

PPVs generally form amorphous films with weak X-ray scattering, due to their weak interchain interactions and disordered packing [31]. To investigate the molecular packing of **BDPPV** in thin film, GIXD and tapping-mode AFM were used (Fig. 4.6). The polymer film of **BDPPV** showed a strong out-of-plane diffraction peak (100) at 2θ of 2.20°, corresponding to a *d*-spacing of 32.3 Å (λ = 1.24 Å). Another three diffraction peaks corresponding to (*h*00) were also observed, suggesting that a good lamellar edge-on packing was formed in the film. An in-plane (010) peak attributed to the interchain π–π stacking was also observed with a distance of 3.45 Å, comparable to those of other semiconducting polymers.

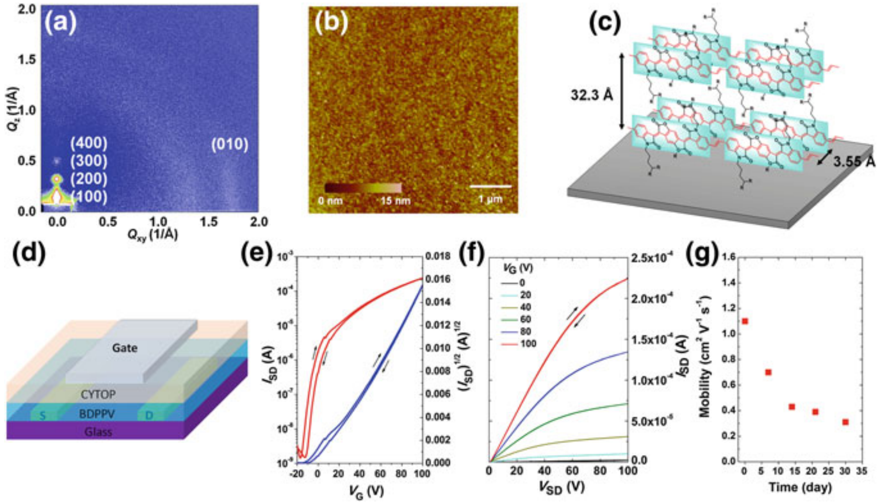

Fig. 4.6 **a** 2D-GIXD pattern and **b** AFM height images of polymer **BDPPV** film fabricated by spin-coating its DCB solution (3 mg/mL). **c** Proposed polymer packing model in thin film. **d** Top-gate/bottom-contact device configuration used to fabricate **BDPPV** FETs. **e** Transfer and **f** output characteristics of a **BDPPV** device in ambient (L = 10 μm, W = 200 μm, C_i = 3.7 nF cm^{-2}), measured V_T = 5 V. **g** Time-dependent decay of electron mobility under ambient conditions

The AFM height image of **BDPPV** showed crystalline fiber-like intercalating networks with a root-mean-square (RMS) deviation of 1.30 nm. Such crystalline networks are presumably caused by strong interchain interactions. Unlike other **PPV**s, **BDPPV** showed clearly much stronger aggregation tendency and more ordered packing. Thus, better interchain carrier transport is expected.

The low-lying LUMO of **BDPPV** indicates that it could be suitable for ambient-stable electron transport. TG/BC device configuration was used to fabricate polymer FETs. The semiconducting layer was deposited by spin-coating a polymer solution (3 mg/mL in 1,2-dichlorobenzene (DCB)) on patterned Au/SiO_2/Si substrate. After thermal annealing the film for 10 min, a CYTOP solution was spin-coated as the dielectric layer, and an aluminum layer was thermally evaporated as the gate electrode. FET devices of **BDPPV** showed clearly n-type transport characteristics under ambient conditions (Fig. 4.6e, f). Several annealing temperatures were tried, and annealing at 200 °C gave the best device performance. The polymer showed the highest electron mobilities up to 1.1 cm^2 V^{-1} s^{-1} with an average mobility of 0.84 cm^2 V^{-1} s^{-1}. This result represents the first polymer FET that can transport electrons over 1 cm^2 V^{-1} s^{-1} under ambient conditions. Note that the transfer and output characteristics showed negligible hysteresis at high gate voltages, indicating that there are only a few traps for electrons, presumably due to the significantly lowered LUMO level. No contact resistance is observed in output curves, indicating the ohmic contact between the polymer and gold electrode. Furthermore, time-dependent decay of the **BDPPV** device was also performed by storing the devices under room light and ambient conditions. The device could function effectively after being stored for 30 days, affording an electron mobility of 0.31 $cm^2\ V^{-1}\ s^{-1}$ (Fig. 4.6g), comparable to those of other high-performance n-type polymer FETs [35].

4.3 BDOPV-Based Donor–Acceptor Polymer and Oxygen-Doping Effect

A powerful strategy to achieve high carrier mobilities in semiconducting polymers is the development of an alternating conjugated polymer containing electron-rich (donor) and electron-deficient (acceptor) units. Because of their successful application in high-performance organic field-effect transistors (OFETs) and organic photovoltaics (OPVs), these donor–acceptor polymers were named as the third-generation polymers by Heeger. In the last section, we have developed a new electron-deficient building block **BDOPV**, regarded as a derivative of oligo(*p*-phenylene vinylene). In **BDOPV**, four carbonyl groups were introduced to give a low LUMO level of –4.24 eV, much lower than current best electron-deficient building blocks (Fig. 1.6 in Chap. 1). Furthermore, these carbonyl groups formed four intramolecular hydrogen bonds with the neighboring phenyl protons, maintaining good planarity and shape-persistency of **BDOPV**, which may facilitate the overlaps of intermolecular frontier orbitals of the **BDOPV** segments in polymers.

Previously, we significantly increased hole mobilities of isoindigo-based polymers by using farther branched alkyl chains or centrosymmetric donors (versus axisymmetric donors) [15]. Here we incorporate all the strategies by using the **BDOPV** unit as the acceptor, farther branched 4-octadecyldocosyl group as the side chain and a centrosymmetric 2,2′-bithiophene unit as the donor to synthesize donor–acceptor polymer **BDOPV-2T**, a typical third-generation polymer (Fig. 4.7a). To our delight, **BDOPV-2T** exhibited n-type transport behavior with high electron mobilities up to 1.74 $cm^2\ V^{-1}\ s^{-1}$ under ambient conditions. Upon oxygen exposure, this polymer displays interesting ambipolar transporting behavior, which maintains high electron mobilities up to 1.45 $cm^2\ V^{-1}\ s^{-1}$, along with significantly increased hole mobilities up to 0.47 $cm^2\ V^{-1}\ s^{-1}$.

As shown in Fig. 4.7a, a Stille coupling polymerization between **BDOPV** and 5,5′-bis(trimethylstannyl)-2,2′-bithiophene gave polymer **BDOPV-2T** in 94 % yield after standard purification. Molecular weight of **BDOPV-2T** was evaluated by high-temperature gel permeation chromatography at 140 °C using 1,2,4-trichlorobenzene as the eluent. The polymer displayed high molecular weight with an M_n of 77.2 kDa and a PDI of 3.00, and excellent thermal stability with decomposition temperature over 390 °C. We observed a phase transition of the polymer at 29 °C in DSC scan. Similar phase transition was also observed in isoindigo-based polymers with longer alkyl chains and in **BDPPV**. We observed that the transition temperature was mainly determined by the type of the alkyl side chains regardless of the

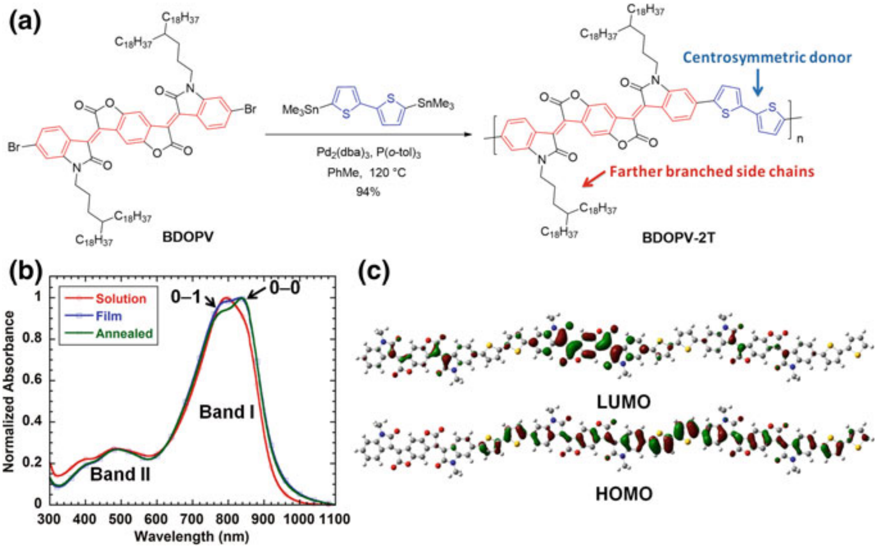

Fig. 4.7 **a** Design and synthesis of D-A polymer **BDOPV-2T**. **b** Normalized absorption spectra of **BDOPV-2T** in $CHCl_3$ (1×10^{-5} M), thin film, and annealed film (200 °C for 5 min). **c** Calculated molecular orbitals of the trimer of **BDOPV-2T** (B3LYP/6-311G(d,p))

polymer backbone, and longer alkyl chains lead to higher transition temperature. Thus, the phase transition was largely caused by the crystallization of the long alkyl chains.

The absorption spectra of polymer **BDOPV-2T** in dilute solution, thin film and annealed film are shown in Fig. 4.7b. **BDOPV-2T** showed typical dual-band absorption, where Band I is a typical charge transfer absorption from the thiophene unit to the **BDOPV** core, because computational results showed that the polymer's HOMO was well delocalized along the polymer chain, whereas its LUMO was mostly localized on the **BDOPV** cores (Fig. 4.7c). The absorption maximum of **BDOPV-2T** in film only showed a minimal red shift in comparison to that in the solution, and a slightly increase of 0–0 vibrational peak was observed. Annealing the film led to a further increase of the 0–0 peak. These results indicate that the polymer backbone in film become more planar and annealing is helpful for a further adjustment of the polymer backbone. The bandgap of **BDOPV-2T** is calculated to be 1.31 eV using the onset of its thin-film absorption spectrum. The cyclic voltammetry (CV) measurement of **BDOPV-2T** gave HOMO/LUMO levels of –5.72/–4.15 eV, in consistent with the HOMO/LUMO levels (–5.66/–4.35 eV) estimated from the photoelectron spectroscopy and the optical bandgap. Note that this LUMO level is significantly lower than those of many previously reported donor–acceptor polymers [15, 24], due to the strong electron-withdrawing ability of **BDOPV** moiety.

The low-lying LUMO level of polymer **BDOPV-2T** indicates that it is perhaps suitable for ambient-stable electron transport. To achieve this goal, a top-gate/bottom-contact (TG/BC) device configuration was used to fabricate polymer FETs, because this device configuration has better injection characteristics and encapsulation effects [43]. The semiconducting layer was deposited by spin-coating the polymer solution (3 mg/mL in DCB) on patterned n^{++}-Si/SiO$_2$/Au (source-drain) substrate. After thermal annealing the film for 5 min, a CYTOP solution was spin-coated as the dielectric layer, and an aluminum layer was thermally evaporated as the gate electrode. Except that the aluminum layer was deposited in high vacuum, we fabricated the devices either in glovebox or under ambient conditions. Several annealing temperatures were tried, and annealing at 200 °C gave the best device performance. All devices were tested under ambient conditions (R_H = 40–50 %). For devices fabricated in a glovebox, **BDOPV-2T** displayed clearly n-type transport characteristics (Fig. 4.8a, b), with high electron mobilities up to 1.74 cm^2 V^{-1} s^{-1} and an average mobility of 1.42 cm^2 V^{-1} s^{-1}, which is the highest electron mobility for polymer FETs tested under ambient conditions.

For the devices fabricated under ambient conditions, the hole mobilities of **BDOPV-2T** significantly increased. The highest hole mobility of 0.47 cm^2 V^{-1} s^{-1} and an average mobility of 0.20 cm^2 V^{-1} s^{-1} were obtained. In contrast, the highest electron mobility of **BDOPV-2T** only slightly decreased to 1.45 cm^2 V^{-1} s^{-1}

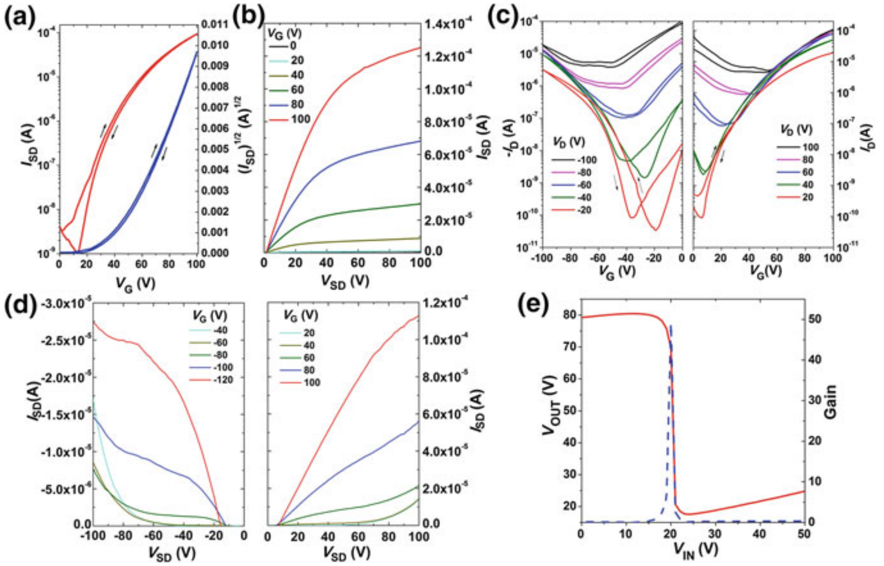

Fig. 4.8 **a** Transfer and **b** output characteristics of a **BDOPV-2T** device fabricated in a glovebox and tested under ambient conditions. **c** Transfer and **d** output characteristics of a **BDOPV-2T** device both fabricated and tested under ambient conditions. *Device configuration* TG/BC, L = 5 μm, W = 100 μm, C_i = 3.7 nF cm^{-2}. **e** The voltage transfer characteristic and gain of a complementary-like inverter fabricated with **BDOPV-2T** under ambient conditions

(average: 1.20 cm^2 V^{-1} s^{-1}) (Fig. 4.8c, d). The transfer characteristics of electron transport showed negligible hysteresis even at a low drain voltage (V_D = +20 V), presumably due to the much lowered LUMO level of **BDOPV-2T**. Moreover, devices fabricated under ambient conditions displayed larger threshold voltage in *n*-channel operation, suggesting some kind of shallow traps were formed in film. To further explore the application of this ambipolar FET, we also fabricated complementary-like inverters based on polymer **BDOPV-2T** under ambient conditions. The inverter consisted of two connected TG/BC ambipolar transistors with a common gate as input (V_{IN}) and a common drain as output (V_{OUT}). Obviously inverting functionality was observed for the inverter based on **BDOPV-2T**, and the highest gain value up to 49 was obtained (Fig. 4.8e). This gain value is also among the highest in ambipolar field-effect transistors [44, 45].

Time-dependent decay of the polymer devices was performed by exposing the devices to air in a desiccator or under ambient conditions (RH = 40–50 %). Devices under both conditions did not show obvious difference, suggesting that water has negligible effects on the device performance. For devices fabricated in glovebox, we observed a gradual decay of electron mobilities and an increase of hole mobilities (Fig. 4.9a). After one day exposure, the electron mobilities dropped to around 1 cm^2 V^{-1} s^{-1} and the hole mobilities increased from 10^{-2} to around 0.1 cm^2 V^{-1} s^{-1}. The device performance is comparable to those of the devices fabricated under ambient conditions. Prolonged storage in air led to a further decrease of electron mobilities. After 15 days, an electron mobility of 0.35 cm^2 V^{-1}

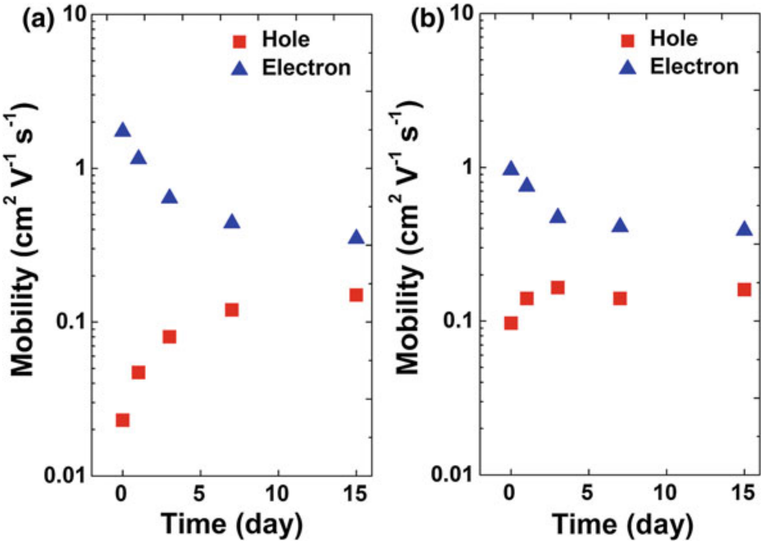

Fig. 4.9 Time-dependent decay of the device performance of **BDOPV-2T** for devices stored in dry air: **a** devices fabricated in glove box; **b** devices fabricated under ambient conditions. The devices are stored under ambient conditions (R_H = 40–50 %) did not show obvious difference from those stored in dry air

s^{-1} and a hole mobility of 0.15 $cm^2\ V^{-1}\ s^{-1}$ were obtained (Fig. 4.9b). Hence, we propose that the significantly increased hole mobilities for **BDOPV-2T** devices fabricated under ambient conditions were largely attributed to the oxygen doping in the polymer film.

Oxygen doping has been widely investigated in inorganic materials, which has a strong influence on their electrical characteristics [46, 47]. Recently, a p-type small molecule, picene, was reported to have much higher hole mobility in air than in vacuum [48]. In this system, the energy levels of the three highest occupied molecular orbitals apparently increased after exposing to oxygen, leading to the inactivation of hole traps and the reduction of the hole injection barrier [49]. To understand the oxygen doping from molecular level, we performed density functional theory (DFT) calculations to model the interaction between oxygen and **BDOPV-2T** (Fig. 4.10a). We found that the oxygen and **BDOPV-2T** formed stable complex through van der Waals interactions. Oxygen decreased the LUMO level and the LUMO clearly delocalized onto the oxygen. These results are in agreement with the device performance that some shallow traps were formed in the polymer film. Furthermore, oxygen also caused the increase of the HOMO level, which would reduce the hole injection barrier from the Au electrode, and therefore increase the hole mobility. Very recently, Sirringhaus et al. found that the HOMO level of polymers slightly increased upon interacting with molecular oxygen, which resulted in hole accumulation in the electrical characteristics [50]. Their results are consistent

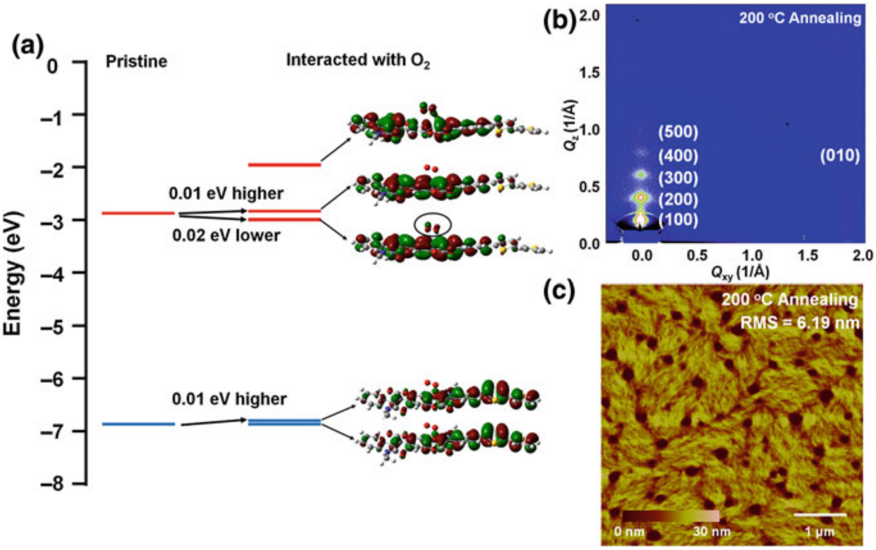

Fig. 4.10 a Calculated energy levels and frontier orbitals for the monomer and for the monomer–oxygen complex. Calculations were performed at the M06-2X/6-311G(d,p) level. **b** 2D-GIXD pattern and **c** AFM height image of polymer **BDOPV-2T** film fabricated under the same condition as the FET device (200 °C annealing)

with our findings and support our hypothesis that the significantly increased hole mobilities were caused by oxygen doping of the polymer in solid state.

To investigate the film microstructure and morphology, GIXD and AFM were used (Fig. 4.10b and c). The film of **BDOPV-2T** showed a strong out-of-plane diffraction peak (100) at 2θ of 2.48°, corresponding to a d-spacing of 28.6 Å. Another four orders of diffraction peaks attributed to (*h*00) diffractions were also observed, suggesting that a good lamellar edge-on packing was formed in film. Interestingly, the lamellar distance of 28.6 Å is smaller than those of the molecular modeling of the alkyl chains, suggesting that the long alkyl chains were not fully extended in film. In-plane (010) peak was also observed, which was attributed to the π-π stacking distance. The measured π–π stacking distance was 3.55 Å, slightly smaller than those of polymers with similar branched alkyl chains [34]. The AFM height image of **BDOPV-2T** film showed a crystalline fiber-like intercalating network with relatively high root-mean-square (RMS) deviation of 6.19 nm, presumably due to the strong interchain interactions.

4.4 Conformation-Locked BDPPV-Based Polymers and Effect of Fluorine Substitution Positions

Compared to many high-mobility p-type polymers, high-mobility n-type polymers are rare, and few can be operated under ambient conditions [35, 51–54]. Developing ambient-stable n-type semiconductors becomes a critical issue in organic electronics, because both n-type and p-type semiconductors are necessary to achieve low power complementary circuits [55]. To date, the development of strong electron-deficient building blocks remains essential to advancing n-type polymer semiconductors [51, 56]. Introducing electron-withdrawing groups can effectively lower the LUMO levels of a known building block [33, 57]. For example, fluorination of polymer backbones can improve the performance of organic photovoltaics [58, 59] and increase the electron mobility of ambipolar polymer FETs [32, 60]. Obviously, fluorination can modulate the energy-level of conjugated polymers, nonetheless, it must have other influences on polymer properties, which are important yet seldom investigated.

As discussed in Chap. 1, charge transport in conjugated polymer films generally contains intrachain transport and interchain transport. Using shape-persistent backbones increase intrachain transport through increasing effective conjugation length [26]. Shape-persistent polymer backbones and well-ordered backbone conformation increase interchain transport through enhancing π–π interactions and ordered polymer packing [61]. **BDPPV** has been prepared for n-type conjugated polymers, which exhibited high electron mobilities of up to 1.1 cm^2 V^{-1} s^{-1}, because it overcomes common defects in poly(*p*-phenylene vinylene) derivatives (**PPV**s), such as conformational disorder (freely rotating double-bonds), weak interchain interaction, and high LUMO level. Nonetheless, only two thirds of the double bonds in this polymer are "locked" by intramolecular hydrogen bonds, thus the polymer backbone still undergoes conformational disorder in solid state. Moreover, although this polymer exhibited outstanding stability in n-type polymer FETs, its device performance still deteriorates under ambient conditions.

Here we attempt to “lock” the rest one of the double bonds in the **BDPPV** polymer by introducing fluorine atoms to form intramolecular hydrogen bonds. Two new building blocks, **FBDOPV-1** and **FBDOPV-2**, with fluorine atoms at different positions of **BDOPV** are prepared. These two building blocks have perhaps the lowest LUMO levels (down to –4.38 eV). These two building blocks are used to prepare two new **PPV** derivatives, **FBDPPV-1** and **FBDPPV-2** (Scheme 4.2). Fluorine atoms can lower the LUMO level and “lock” the conformation of polymer backbones through intramolecular hydrogen bonds. **FBDPPV-1** exhibits an electron mobility up to 1.70 $cm^2\ V^{-1}\ s^{-1}$ under ambient conditions. In addition, when the fluorine atoms are substituted in different positions of the

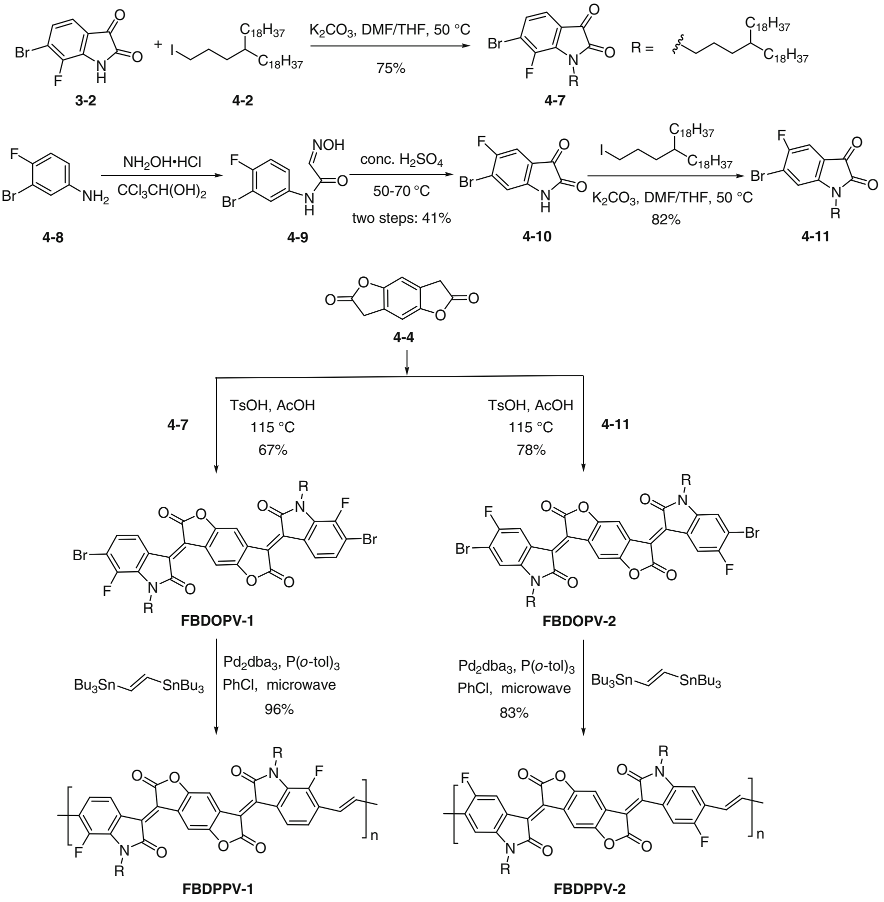

Scheme 4.2 Synthesis of fluorinated **BDOPV** derivatives and fluorinated **BDPPV** polymers

polymer backbone, different conformations are created, which eventually leads to different device performance.

Although donor–acceptor polymers can achieve high carrier mobilities [23, 24], we did not use this strategy in the design of the backbone of a “pure” n-type transporting system, because this strategy usually increases the HOMO levels of conjugated polymers and results in hole injection, low on/off ratio, or ambipolar transport [62, 63]. Moreover, electron-rich donors also increase the LUMO levels of conjugated polymers, thus making electron transport more susceptible to oxygen and moisture [64]. Alternatively, a double bond was used to link the **BDOPV** units due to its weak electron-donating property. Furthermore, we and other groups have demonstrated that carrier mobilities of conjugated polymers could be significantly increased by using farther branched alkyl chains [19, 34, 65, 66]. Thus, long and farther branched 4-octadecyldocosyl groups were used as polymer side chains to guarantee both better interchain interactions and good solubility. To understand how fluorination influences the conjugated polymers, we prepared two similar polymers with different fluorinated positions (Scheme 4.2).

Scheme 4.2 illustrates the synthetic route to **FBDOPV-1** and **FBDOPV-2**. The synthesis of fluorinated **BDOPV** started from the construction of fluorinated 6-bromoisatin. 6-bromo-7-fluoroisatin (3-2) was synthesized in Chap. 3 for fluorinated isoindigo polymers. 6-Bromo-5-fluoroisatin (4-10) was synthesized from commercially available 3-bromo-4-fluoroaniline by the condensation reaction with chloral hydrate and hydroxylamine hydrochloride, followed by catalyzed cyclization using sulfuric acid. Both fluorinated isatins (3-2 and 4-10) were then alkylated with 19-(3-iodopropyl)heptatriacontane (4-2) in the presence of K_2CO_3, affording compounds 4-7 and 4-11 in good yields. **FBDOPV-1** or **FBDOPV-2** can be readily obtained with 67 or 78 % yield by using an acidic condensation condition between 4-7 or 4-11 and 2,2′-(2,5-dihydroxy-1,4-phenylene)diacetic acid (4-4), respectively [62]. Microwave-assisted Stille coupling polymerizations between **FBDOPV-1** or **FBDOPV-2** and (*E*)-1,2-bis(tributylstannyl)ethene gave polymer **FBDPPV-1** and **FBDPPV-2** in 96 and 83 % yield, respectively. The molecular weights of both polymers were evaluated by high-temperature gel permeation chromatography (GPC) at 140 °C using 1,2,4-tricholorobenzene (TCB) as eluent. Both polymers displayed comparable molecular weights (**FBDOPV-1**: M_w = 128.9 kDa, M_n = 66. 3 kDa, PDI = 1.94; **FBDPPV-2**: M_w = 164.7 kDa, M_n = 53.8 kDa, PDI = 3.06) and showed excellent thermal stability with decomposition temperature over 370 °C.

The absorption spectra of **FBDOPV-1** and **FBDOPV-2** are similar to that of **BDOPV** (with bromine on the same position as FBDOPV) due to their identical conjugated backbones. After introducing fluorine atoms, both HOMO and LUMO levels of **FBDOPV-1** and **FBDOPV-2** are lowered. LUMO levels are lowered by 0.14 and 0.12 eV for **FBDOPV-1** and **FBDOPV-2**, respectively (Table 4.1). The LUMO level of **FBDOPV-1** reaches –4.38 eV, suggesting that **FBDOPV-1** is one of the most electron-deficient building blocks for conjugated polymers [24, 67]. Note that all three monomers display two reversible reductive peaks in solution (Fig. 4.11a), indicating their good stability in the anionic state.

Table 4.1 Optical and electrochemical properties of **BDOPV**, **FBDOPV-1** and **FBDOPV-2**

Compounds	λ_{max}^{sol} (nm)[a]	E_g^{Opt} (eV)[b]	E_{HOMO}^{CV} (eV)[c]	E_{LUMO}^{CV} (eV)[c]	E_{HOMO}^{Calc} (eV)[d]	E_{LUMO}^{Calc} (eV)[d]	E_g^{Calc} (eV)[d]
BDOPV	448, 584	1.80	–6.21	–4.24	–6.25	–3.98	2.27
FBDOPV-1	460, 569	1.81	–6.31	–4.38	–6.40	–4.13	2.27
FBDOPV-2	448, 585	1.75	–6.30	–4.36	–6.38	–4.14	2.24

[a] 10^{-5} M in chloroform

[b] Estimated from the onset of the absorption spectra of solution

[c] Cyclic voltammetry determined with Fc/Fc^+ (E_{HOMO} = –4.80 eV) as external reference

[d] Calculated at B3LYP/6-311G+(d,p) level

Three polymers show similar absorption spectra, and all of them have two absorption bands (Band I: 600–900 nm; Band II: 400–600 nm) and low bandgaps around 1.4 eV (Fig. 4.11b and Table 4.2). All polymers have structured vibrational absorption peaks in the Band I region, which agrees well with their shape-persistent conjugated backbones. Compared with **BDPPV**, **FBDPPV-1** exhibits a blue-shifted absorption spectrum, whereas **FBDPPV-2** exhibits obviously red-shifted spectrum. In addition, three polymers show different oscillator strength of the vibrational absorption peaks. The main absorption peak of **FBDPPV-1** in film only shows very little red-shift compared to those in solution, and an obvious increase of the relative intensity of their 0–0 vibrational peaks is observed (Fig. 4.11c). Annealing the film results in a further increase of the relative intensity of 0–0 peak, indicating that the polymer backbone becomes more planar in film and annealing is helpful for further adjustment. For conjugated polymers, intermolecular stacking and conformational change may significantly shift the absorption spectra [39]. However, no significant change is observed from solution to thin film, suggesting that the polymer probably formed some pre-aggregates in solution due to strong interchain interactions [41, 68]. Compared with **FBDPPV-1**, **FBDPPV-2** shows more obviously red-shifted absorption from solution to film, suggesting that both polymers might take different molecular conformations and supramolecular organizations in solid state, though they have very similar conjugated backbones [39] (Table 4.3).

Electrochemical properties of three polymers were explored by cyclic voltammetry measurement (Fig. 4.11d). After introducing fluorine atoms, the reductive currents of both fluorinated polymers increase obviously and the reductive doping processes appear to be more reversible than those of **BDPPV**. Both HOMO and LUMO levels of **FBDOPV-1** and **FBDOPV-2** are lowered, but clearly the LUMO levels are more easily affected (Table 4.2). The LUMO levels of **FBDOPV-1** and **FBDOPV-2** reach –4.26 and –4.30, 0.16 and 0.20 eV lower than that of **BDPPV**. Computational results reveal that both fluorinated polymers exhibit almost planar conjugated backbones and their HOMOs and LUMOs are well delocalized along polymer backbones (Fig. 4.11e). This contrasts with many donor–acceptor polymers, in which the LUMOs are mostly localized on the electron-deficient units of polymer backbones [27, 63].

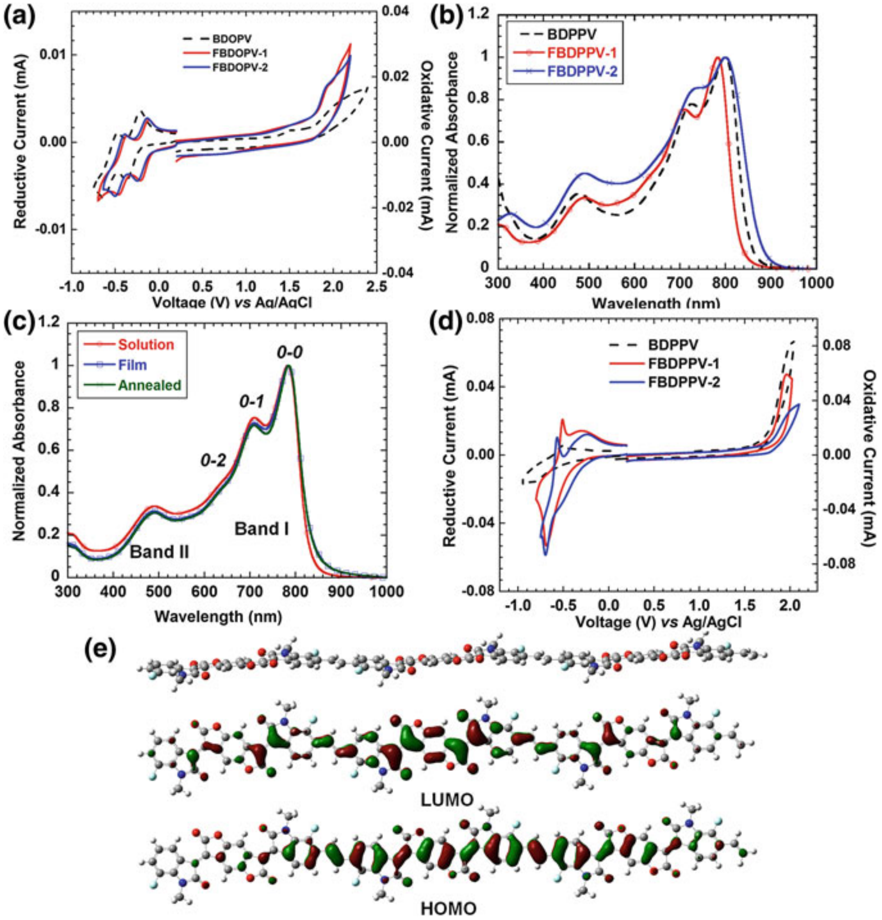

Fig. 4.11 **a** Cyclic voltammograms of **BDOPV**, **FBDOPV-1** and **FBDOPV-2** in DCB solution (5 mg/mL). **b** Normalized absorption spectra of three polymers in $CHCl_3$ (10^{-5} M). **c** Normalized absorption spectra of **FBDOPV-1** in $CHCl_3$ (10^{-5} M), thin film and annealed film (180 °C for 30 min). **d** Cyclic voltammograms of three polymers in drop-casted film prepared using their chloroform solutions (5 mg/mL). **e** Molecular frontier orbitals of the **FBDOPV-1** trimer (B3LYP/6-311G(d,p))

The molecular packing and surface morphologies of three polymer films were investigated by GIXD and tapping-mode AFM (Fig. 4.12). Three polymers display strong out-of-plane diffractions (*h*00), indicating that good edge-on lamellar packing is formed in film. Fluorinated polymers show five out-of-plane diffraction peaks, whereas **BDPPV** only shows four out-of-plane peaks. However, three polymers exhibit similar lamellar distances around 32 Å due to their similar backbones and identical side chains. (010) Peaks attributed to π–π stacking were also observed. Clearly, both fluorinated polymers exhibit a stronger (010) peak with

Table 4.2 Optical and electrochemical properties of **BDPPV**, **FBDPPV-1** and **FBDPPV-2**

Polymers	$\lambda_{\max}^{\text{sol}}$ (nm)[a]	$\lambda_{\max}^{\text{film}}$ (nm)	E_g^{Opt} (eV)[b]	$E_{\text{HOMO}}^{\text{CV}}$ (eV)[c]	$E_{\text{LUMO}}^{\text{CV}}$ (eV)[c]	$E_{\text{HOMO}}^{\text{Calc}}$ (eV)[d]	$E_{\text{LUMO}}^{\text{Calc}}$ (eV)[d]	E_g^{Calc} (eV)
BDPPV	799, 728	803, 724	1.42	–6.12	– 4.10	– 5.61	–4.07	1.54
FBDPPV-1	786, 710	784, 710	1.46	–6.19	–4.26	–5.76	–4.21	1.55
FBDPPV-2	800, 740	808, 743	1.39	–6.22	–4.30	–5.74	–4.25	1.49

[a] 10^{-5} M in chloroform

[b] Estimated from the onset of the absorption spectra of thin film

[c] Cyclic voltammetry determined with Fc/Fc$^+$ (E_{HOMO} = –4.80 eV) as external reference

[d] HOMO and LUMO energy levels were calculated by extrapolating from the values computed for their oligomers (n = 1, 2, and 3) (B3LYP/6-311G(d,p) level)

Table 4.3 OFET device performance and GIXD results of three polymers

Polymers	μ (cm^2 V^{-1} s^{-1})[a]	V_T (V)	log(I$_{\text{on}}$/I_{off})	d (Å)[b]	
				L	π
BDPPV	1.10 (0.84)	+5	5–6	32.3	3.45
FBDPPV-1	1.70 (1.39)	+18	5–6	32.9	3.42
FBDPPV-2	0.81 (0.62)	+1	4–5	32.7	3.42

[a] Electron mobility measured under ambient conditions (R_H = 50–60 %). Maximum values of electron mobilities and the average values are in parentheses

[b] Lamellar (L) and π–π stacking (π) distances determined by GIXD experiments

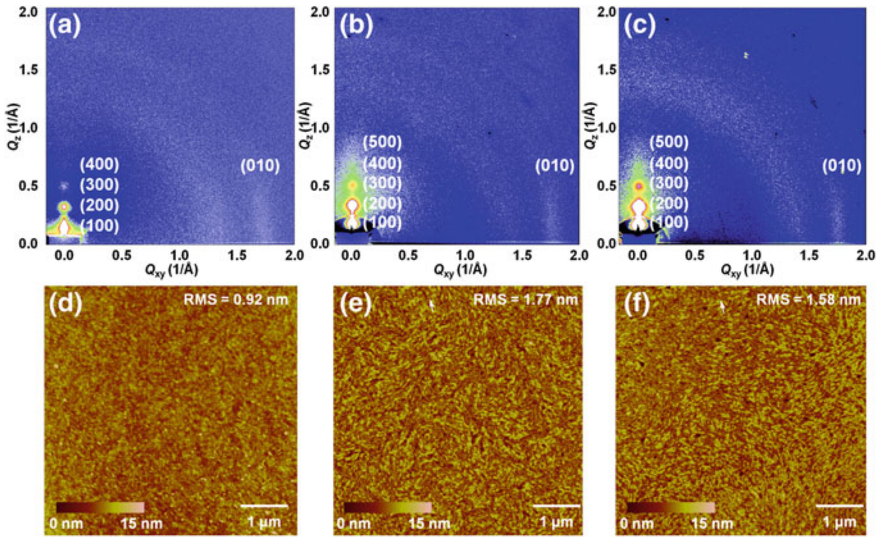

Fig. 4.12 2D-GIXD patterns and AFM height images of **a**, **d BDPPV**, **b**, **e FBDPPV-1**, and **c**, **f FBDPPV-2** films. Films were prepared by spin-coating their DCB solutions (3 mg/mL) and annealed at 180 °C for 30 min

a shorter π–π stacking distance of 3.42 Å, slightly shorter than that of **BDPPV** (3.45 Å). These results suggest that after introducing fluorine atoms, **FBDPPV-1** and **FBDPPV-2** exhibit more ordered lamellar packing and stronger interchain interactions in solid state. This is also supported by the AFM observation that both fluorinated polymers display fiber-like intercalating networks with obviously crystallized zones. Root-mean-square (RMS) analysis of the height data shows that the films of fluorinated polymers display larger roughness, presumably due to their stronger crystallinity. Therefore, the introduction of fluorine atoms not only modulates the energy levels of polymers, but also influences the interchain interactions and polymer packing in solid state.

TG/BC device configuration was used to evaluate the carrier transport of both fluorinated polymers. The semiconducting layer was deposited by spin-coating a polymer solution (3 mg/mL in DCB) on Au (source-drain)/SiO_2/Si substrate. After thermal annealing the film (180 °C for 30 min), a CYTOP solution was spin-coated on the top of the semiconducting layer and cross-linked under 100 °C for 1 h, providing the dielectric layer (500 nm thick). Then, an aluminum layer was thermally evaporated as the gate electrode. All devices were fabricated in glovebox and tested under ambient conditions (R_H = 50–60 %). Both fluorinated polymers show typical *n*-type transport characteristics under ambient conditions (Fig. 4.13a, b). The maximum mobility of the **FBDPPV-1** devices was determined to be as high as 1.70 $cm^2\ V^{-1}\ s^{-1}$. **FBDPPV-1** showed typical transfer and output characteristics with negligible hysteresis, which is seldom observed for n-type organic materials, largely due to its significantly lowered LUMO level. Besides, no contact resistance was observed in output curves, suggesting a good contact between the polymer and gold electrode. However, **FBDPPV-2** only gave the highest electron mobility of 0.81 $cm^2\ V^{-1}\ s^{-1}$ and an average mobility of 0.62 $cm^2\ V^{-1}\ s^{-1}$, unexpectedly lower than that of non-fluorinated **BDPPV** (highest: 1.1 $cm^2\ V^{-1}\ s^{-1}$ and average: 0.84 $cm^2\ V^{-1}\ s^{-1}$).

Time-dependent decays of three polymer devices were tested by storing the devices under ambient conditions (R_H = 50–60 %). All the polymers showed good stability with a slow decay of electron mobility (Fig. 4.13c). Fluorinated polymers showed obviously better stability than non-fluorinated **BDPPV**. After 30 days, the mobility of **FBDPPV-1** device decreased from 1.61 to 1.13 $cm^2\ V^{-1}\ s^{-1}$, whereas that of **BDPPV** decreased from 1.10 to 0.31 $cm^2\ V^{-1}\ s^{-1}$. The decay of the electron mobility may be caused by the further diffusion of the oxygen or moisture into the semiconducting layer [64]. Although these devices are not long-term stable under ambient conditions, these results are outstanding among n-type conjugated polymers, because few reported n-type polymers can be operated under ambient conditions [35, 51–54].

Both fluorinated polymers have considerably different device performance despite their similar physical and electrochemical properties, including molecular weight, thin-film packing, and morphology. We propose that this difference originates from their different polymer backbone conformations in solid state. To give a better understanding, a model compound (*E*)-1,2-bis(2-fluorophenyl)ethane was used to investigate the double bond conformations of the fluorinated polymers.

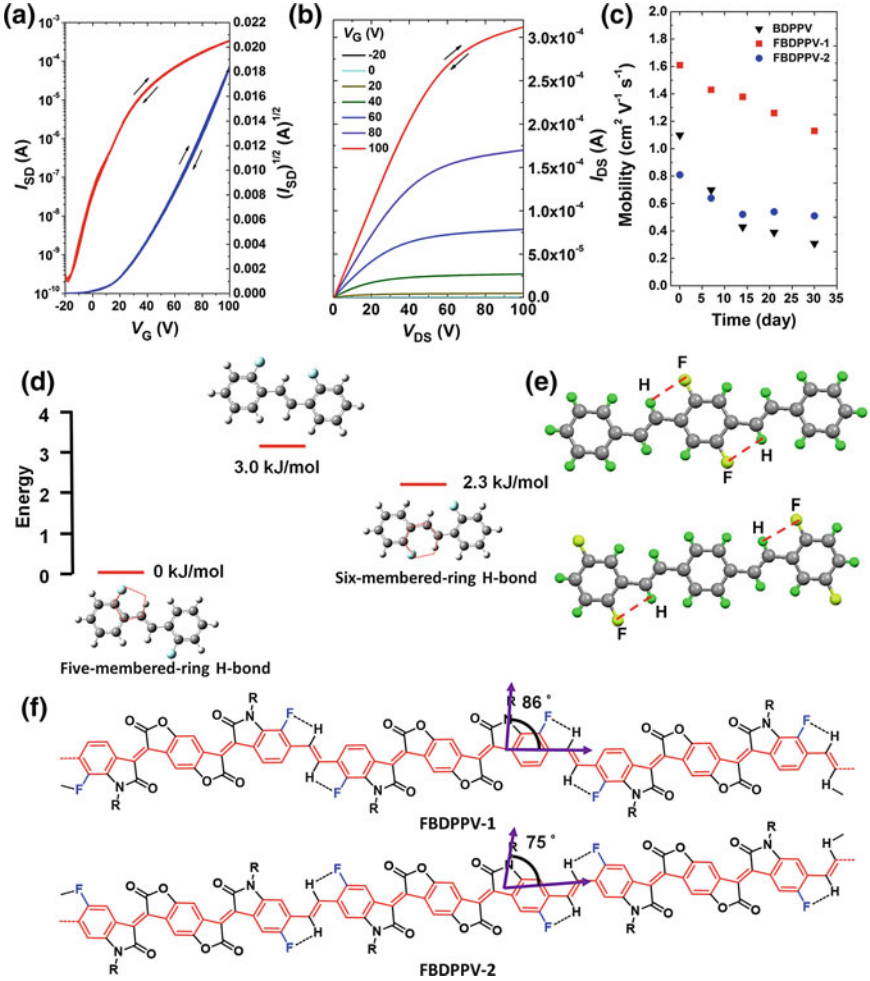

Fig. 4.13 **a** Transfer and **b** output characteristics of a **FBDPPV-1** device measured under ambient conditions. **c** Time-dependent decay of the device performance under ambient conditions. FET devices (L = 5 μm, W = 100 μm,) were fabricated with CYTOP around 500 nm thick (capacitance C_i = 3.7 nF cm^{-2}). **d** Energy diagram of different planar conformations of model compound (E)-1,2-bis(2-fluorophenyl)ethane. Optimized and calculated at B3LYP/6-311+G(d,p) level. **e** Single crystal structures of two fluorinated OPV derivatives. Both of them have five-membered-ring intramolecular hydrogen bonds. **f** Proposed intramolecular hydrogen bonds and backbone conformations of **FBDPPV-1** and **FBDPPV-2**

Figure 4.13d displays three possible conformations of the model compound. After introducing fluorine atoms, intramolecular hydrogen bonds are formed between fluorine and hydrogen atoms, thus locking the molecular conformation. The five-membered-ring hydrogen bonding is preferred, providing obviously lower energy than the six-membered-ring hydrogen bonding. This computational analysis is supported by single crystal structures of several fluorinated OPV derivatives [69], in which all the fluorine atoms formed five-membered-ring hydrogen bonds with neighboring phenyl protons (Fig. 4.13e). These results indicate that both **FBDPPV-1** and **FBDPPV-2** may have “locked” conformations and intramolecular five-membered-ring hydrogen bonds in solid state. Because of the different substitution position of fluorine, the backbone conformations of both polymers are different. Calculations on the oligomers of **FBDPPV-1** also showed that the five-membered-ring hydrogen-bonding conformation is more stable than other conformations.

Using computational method, Beljonne et al. demonstrated that interchain charge transport correlates with the supramolecular organization of conjugated polymers [70]. For example, even under the same π–π stacking distance, different polymer packing conformations can lead to greatly different interchain carrier transport. This is mainly caused by the different charge transfer integrals between polymer chains [25]. Furthermore, increasing experimental results suggest that polymer backbone conformations indeed exert their influences on carrier transport through adopting various interchain molecular packings [28, 71]. Figure 4.13f shows the proposed intramolecular hydrogen bonds in **FBDPPV-1** and **FBDPPV-2** and their polymer backbone conformations in film. The purple arrows indicate the included angles between the alkyl chain extending directions and the polymer backbone extending directions. Clearly, the double bond orientations are different for both polymers, and the included angle of **FBDPPV-1** is close to 90°, obviously larger than that of **FBDPPV-2**. This analysis agrees with the absorption spectra result that both polymers might have different molecular conformations and supramolecular organization in solid state. Because intermolecular packing and carrier mobility are sensitive to molecular conformations and the orientation of side chains [25, 72, 73], the different backbone conformations of **FBDPPV-1** and **FBDPPV-2** might lead to different interchain organization and thereby influence interchain carrier transport. Similarly, because of the ineffective interchain charge transport, **FBDPPV-2** exhibits lower electron mobility than **BDPPV** even though it has locked conformations, lower LUMO level and stronger crystallinity. However, further investigations are needed to better understand the myriad factors influencing the electron transport of these polymers.

4.5 Conclusions

In this chapter, we have developed a new electron-deficient building block **BDOPV** based on the concept of π-extended isoindigo. **BDOPV** has four carbonyl groups and exhibits a low LUMO level of –4.24 eV. The carbonyl groups form four intramolecular hydrogen bonds with the neighboring phenyl protons, maintaining good planarity and shape-persistency of **BDOPV**, which may facilitate the overlaps of intermolecular frontier orbitals of conjugated polymers.

We have demonstrated that molecular engineering of **PPV** skeleton can overcome factors that limit the electron mobility in **PPV**s, such as conformational disorder, weak interchain interactions, and high LUMO levels. The novel designed electron-deficient **BDPPV** "lock" the polymer backbone by intramolecular hydrogen bonds, endowing itself with excellent UV and visible light stability, stronger aggregation tendency, better crystallinity, lower LUMO level, and above all higher electron mobilities up to 1.1 $cm^2 V^{-1} s^{-1}$ under ambient conditions. Our molecular engineering strategy effectively avoids the defects of other **PPV**s and increases the electron mobility of **PPV**s from 10^{-4} $cm^2 V^{-1} s^{-1}$ to over 1 $cm^2 V^{-1} s^{-1}$.

BDOPV was then used to construct a D-A polymer **BDOPV-2T**, which showed a high electron mobility of 1.74 $cm^2 V^{-1} s^{-1}$. Upon oxygen exposure, **BDOPV-2T** displayed interesting ambipolar transporting behavior, which maintained high electron mobilities up to 1.45 $cm^2 V^{-1} s^{-1}$, along with significantly increased hole mobilities up to 0.47 $cm^2 V^{-1} s^{-1}$. Furthermore, inverters based on the oxygen-doped devices with high gain values up to 49 are also demonstrated, suggesting the potential application of the polymer in complex logic circuits. Li et al. independently synthesized two structurally similar BDOPV-based polymers. Nonetheless, one polymer was insoluble, and another showed hole and electron mobilities around 0.01 $cm^2 V^{-1} s^{-1}$ [62]. The low mobility is probably caused by the axisymmetric donor and the close branching position of the side chains, thereby further demonstrating that the synergy of polymer backbone and side chain engineering is essential to achieve high performance in conjugated polymers.

In the third part, we attempt to "lock" the rest one third of the double bonds in **BDPPV** by introducing fluorine atoms to form more intramolecular hydrogen bonds. We have developed two novel strong electron-deficient building blocks, **FBDOPV-1** and **FBDOPV-2**. These two building blocks have extremely low LUMO levels down to –4.38 eV. Using the building blocks, two **PPV** derivatives, **FBDPPV-1** and **FBDPPV-2**, are developed for ambient-stable n-type polymer FETs. Both polymers exhibit improved device stability under ambient conditions due to their low-lying LUMO levels. **FBDPPV-1** has increased electron mobility up to 1.70 $cm^2 V^{-1} s^{-1}$ under ambient conditions, whereas **FBDPPV-2** has decreased electron mobility. This work demonstrated that fluorination is more than lowering the energy level of the polymers, it can also influence backbone conformations (hence interchain interactions and film microstructures), which is critical to the device performance.

4.6 Experimental Details and Characterization

4.6.1 Device Fabrication and Characterization

Top-gate/bottom-contact FET devices and complementary inverters were fabricated using n^{++}-Si/SiO_2 (300 nm) substrates. The gold source and drain bottom electrodes (with Ti as the adhesion layer) were patterned by photolithography on the SiO_2 surface. The substrates were subjected to cleaning using ultrasonication in acetone, cleaning agent, deionized water (twice), and isopropanol. The cleaned substrates were dried under vacuum at 80 °C. The substrates were transferred into a glovebox. A thin film of the polymer was deposited on the treated substrates by spin-coating at 1,500 rpm for 60 s using a polymer solution (6 mg/mL), optionally followed by thermal annealing at 160, 180, 200 or 220 °C for 5 min. After polymer thin film deposition, a CYTOP solution (CTL809 M:CT-solv180 = 3:1) was spin-coated onto the semiconducting layer at 2,000 rpm for 60 s resulting in a dielectric layer of 500 nm thick. The CYTOP layer was then baked at 100 °C for 1 h. Gate electrodes comprising a layer of Al (50 nm) were then evaporated through a shadow mask onto the dielectric layer by thermal evaporation.

The evaluations of the FETs and inverters were carried out in atmosphere (humidity 50–60 %) on a probe stage using a Keithley 4200 SCS as parameter analyzer. The carrier mobility, μ, was calculated from the data in the saturated regime according to the equation $I_{SD} = (W/2L)C_i\mu(V_G - V_T)^2$, where I_{SD} is the drain current in the saturated regime. W and L are, respectively, the semiconductor channel width and length, C_i (C_i = 3.7 nF cm^{-2}) is the capacitance per unit area of the gate dielectric layer, and V_G and V_T are the gate voltage and threshold voltage.

4.6.2 Synthetic Procedures and Characterization

Alkyl chain **4-2** is commercial available from Lyn (Beijing) Science & Technology Co., Ltd. Compound **4-4** was synthesized according to literature [36].

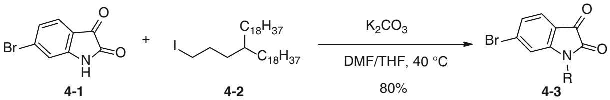

Compound 4-3. To a solution of **2** (2.13 g, 3.1 mmol) in a mixure of THF (30 mL) and *N*,*N*′-dimethylformamide (DMF) (30 mL), 6-bromoisatin (**1**, 700 mg, 3.1 mmol) and K_2CO_3 (856 mg, 6.2 mmol) was added. The mixture was stirred at 50 °C for 8 h and then the solvent was removed under reduced pressure. The residues were dissolved in $CHCl_3$ (100 mL) and then washed with water and brine, and dried over with Na_2SO_4. After removal of the solvents under reduced pressure, the residue was purified by silica gel chromatography with eluent (PE: CH_2Cl_2 = 1:1) to give **4-3** as an orange solid (1.94 g, 80 %). ^{1}H NMR ($CDCl_3$, 400 MHz, ppm): δ 7.47–7.45 (d, J = 7.9 Hz, 2H), 7.29–7.26 (dd, J_1 = 7.9 Hz, J_2 = 1.2 Hz, 2H), 7.07–7.05 (d, J = 1.2 Hz 2H), 3.69–3.66 (t, J = 7.4 Hz 2H), 1.69–1.62 (m, 2H), 1.40–1.22 (m, 71H), 0.90–0.86 (t, J = 6.8 Hz, 6H). ^{13}C NMR ($CDCl_3$, 100 MHz, ppm): δ 182.3, 157.9, 151.8, 133.5, 126.8, 126.3, 116.2, 113.7, 40.8, 37.0, 33.4, 31.9, 30.6, 30.1, 30.0, 29.7, 29.7, 29.8, 29.4, 26.6, 24.3, 22.7, 14.1. Elemental Anal. calcd. for $C_{48}H_{84}BrNO_2$: C, 73.25; H, 10.76; N, 1.78; Found:

C, 73.21; H, 10.71; N, 1.80. ESI-HRMS calcd. for $[M + H]^+$: 786.5758; Found: 786.5754.

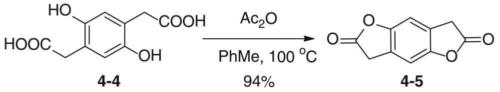

Compound 4-5. To a suspension of **4-4** (1.0 g, 4.4 mmol) in anhydrous toluene (50 mL), Ac_2O (10 mL) was added. The mixture was stirred at 100 °C for 5 h and then the solvent was removed under reduced pressure. The residue was purified by silica gel chromatography with eluent ($CHCl_3$), and recrystallized from toluene to give **4-5** as a white crystal (0.79 g, 94 %). ^1H NMR ($CDCl_3$, 400 MHz, ppm): δ 7.07 (s, 2H), 3.78 (s, 4H). ^{13}C NMR ($CDCl_3$, 100 MHz, ppm): δ 173.3, 150.9, 123.3, 107.7, 33.5. Elemental Anal. calcd. for $C_{48}H_{84}BrNO_2$: C, 63.16; H, 3.18; Found: C, 62.91; H, 3.35. EI-MS: 190 (M^+).

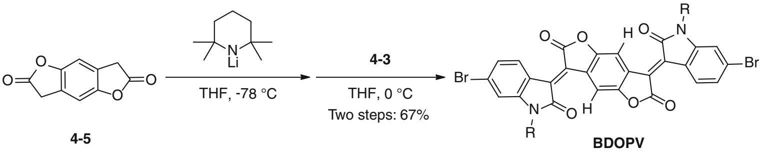

BDOPV: To a solution of 2,2,6,6-tetramethylpiperidine (446 mg, 3.16 mmol) in anhydrous THF (10 mL), *n*-BuLi (2.4 M in pentane, 1.05 mL, 2.53 mmol) was add at 0 °C. The mixture was cooled to −78 °C, and **4-5** (200 mg, 1.05 mmol) in anhydrous THF (20 mL) was added. After stirring at −78 °C for 30 min, the mixture was directly transferred to a solution of **3** (1.99 g, 2.53 mmol) in anhydrous THF (20 mL) at 0 °C. After stirring at room temperature for 5 h, the mixture was quenched with water and extracted with $CHCl_3$. The combined organic phase was washed with brine and then dried over with Na_2SO_4. After removal of the solvents under reduced pressure, the residue was purified by silica gel chromatography with eluent (PE:CH_2Cl_2 = 1:1) to give **BDOPV** as a dark solid (1.21 g, 67 %). ^1H NMR ($CDCl_3$, 400 MHz, ppm): δ 9.09 (s, 2H), 8.93–8.91 (d, $J = 8.6$ Hz, 2H), 7.20–7.18 (dd, $J_1 = 8.6$, $J_2 = 1.6$ Hz, 2H), 6.93–6.92 (d, $J = 1.6$ Hz, 2H), 3.74–3.70 (t, $J = 7.3$ Hz, 4H), 1.71–1.68 (m, 4H), 1.34–1.24 (m, 142H), 0.89–0.86 (t, $J = 6.8$ Hz, 12H). ^{13}C NMR ($CDCl_3$, 100 MHz, ppm): δ 167.0, 166.8, 151.7, 146.8, 135.6, 131.6, 129.0, 126.8, 126.4, 125.6, 119.7, 111.7, 111.0, 40.7, 37.1, 33.5, 31.9, 30.8, 30.1, 29.7, 29.4, 26.7, 24.4, 22.7, 14.1. Elemental Anal. Calcd. for $C_{48}H_{84}BrNO_2$: C, 73.66; H, 9.91; N, 1.62; Found: C, 73.66; H, 10.01; N, 1.57. MALDI-TOF MS: 1729.2 $[M + H]^+$, 1751.2; $[M + Na]^+$.

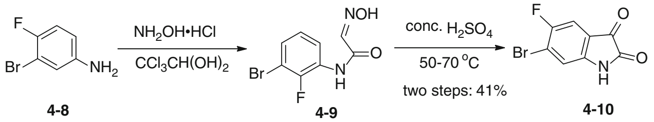

6-Bromo-5-fluoroisatin (**4-9**). To a solution of chloral hydrate (12.9 g, 78 mmol) in deionized water (180 mL), Na_2SO_4 (142 g, 923 mmol), 3-bromo-4-fluoroaniline (13.5 g, 71 mmol), H_2SO_4 (45 mL, 1 M) and hydroxylamine hydrochloride (14.8 g, 213 mmol) were added. The mixture was heated to 130 °C and refluxed for 30 min. The mixture was then cooled to 80 °C and filtered to collect the product. The product was washed with deionized water and dried in vacuum to afford **4-8** as a yellowish solid, which was directly used for the next step without further purification.

To a concentrated H_2SO_4 (150 mL) in 250 mL round-bottom flask kept at 50 °C, compound **6** was added portionwise with stirring. The mixture was heated to 70 °C for 1 h before pouring into ice water. The precipitate was collected by filtration and the filtrate was extract with ethyl acetate (EA). The precipitate and the extraction were combined and subject to column chromatography (silica gel; eluent: petroleum ester PE:EA = 8:1) to afforded **4-9** as an orange solid (7.10 g, 41 %). ^{1}H NMR (DMSO-d_6, 400 MHz, ppm): δ 11.13 (s, 1H), 7.60–7.58 (d, $J^3_{\text{F–H}}$ = 7.59 Hz, 1H), 7.19–7.18 (d, $J^4_{\text{F–H}}$ = 7.18 Hz, 1H). ^{13}C NMR (DMSO-d_6, 100 MHz, ppm): δ 182.95–182.93 (d, $J^4_{\text{F–C}}$ = 2.0 Hz), 159.34–159.32 (d, $J^5_{\text{F–C}}$ = 1.6 Hz), 155.70–153.31 (d, $J^1_{\text{F–C}}$ = 241.2 Hz), 147.21–147.18 (d, $J^4_{\text{F–C}}$ = 2.2 Hz), 118.15–118.04 (d, $J^2_{\text{F–C}}$ = 10.2 Hz), 117.98–117.92 (d, $J^3_{\text{F–C}}$ = 6.6 Hz), 116.28 (s), 112.44–112.19 (d, $J^2_{\text{F–C}}$ = 25.1 Hz). EI-MS calcd. for M$^+$: 243; found: 243. Elemental Anal. calcd. for $C_8H_3BrFNO_2$: C, 39.38; H, 1.24; N, 5.74; found: C, 39.33; H, 1.48; N, 5.73.

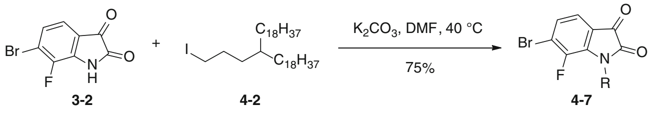

Compound 4-7: To a solution of **4-2** (2.20 g, 3.22 mmol) in a mixture of THF (30 mL) and *N,N'*-dimethylformamide (DMF) (30 mL), 6-bromo-7-fluoroisatin (**3-2**, 750 mg, 3.07 mmol) and K_2CO_3 (635 mg, 4.61 mmol) were added. The mixture was stirred at 50 °C for 8 h and then the solvents were removed under reduced pressure. The residue was dissolved in $CHCl_3$ (100 mL) and then washed with water and brine, and dried over with Na_2SO_4. After removal of the solvents under reduced pressure, the residue was purified by silica gel chromatography with eluent (PE:CH_2Cl_2 = 1:1) to give **4-7** as an orange solid (1.84 g, 75 %). ^{1}H NMR ($CDCl_3$, 400 MHz, ppm): δ 7.34–7.29 (m, 2H), 3.86–3.82 (t, J = 7.4 Hz, 2H),

1.69–1.62 (m, 2H), 1.30–1.22 (m, 71H), 0.90–0.86 (t, J = 6.8 Hz, 6H). ^{13}C NMR (CDCl$_3$, 100 MHz, ppm): δ 181.7 (s), 157.6 (s), 146.09–143.62 (d, $J_{\text{F--C}}^1$ = 248.5 Hz), 137.88–137.78 (d, $J^2_{\text{F–C}}$ = 9.7 Hz), 128.19 (s), 122.02–121.83 (d, $J^2_{\text{F–C}}$ = 19.6 Hz), 121.60–121.56 (d, $J^3_{\text{F–C}}$ = 3.9 Hz), 119.28–119.25 (d, $J_{\text{F--C}}^3$ = 2.5 Hz), 43.1, 43.1, 42.8, 42.8, 37.3, 37.0, 33.6, 33.5, 33.3, 31.9, 30.4, 30.1, 30.1, 29.7, 29.7, 29.4, 29.2, 29.2, 26.7, 26.6, 25.9, 25.9, 23.9, 22.7, 14.1. Elemental Anal. calcd. for $C_{48}H_{83}BrFNO_2$: C, 71.61; H, 10.39; N, 1.74; Found: C, 71.48; H, 10.36; N, 1.82. ESI-HRMS calcd. for $[C_{48}H_{83}BrFNO_2 + H]^+$: 804.5664; Found: 804.5693.

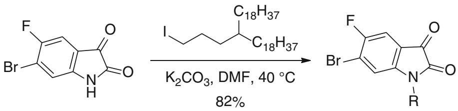

4-10 **4-11**

Compound 4-11: The synthetic procedure is similar to that of compound **4-7**. Yield: 82 %, orange solid. ^{1}H NMR (CDCl$_3$, 400 MHz, ppm): δ 7.36–7.35 (d, $J^3_{\text{F–H}}$ = 6.3 Hz, 1H), 7.10–7.09 (d, $J^4_{\text{F–H}}$ = 4.8 Hz, 1H), 3.69–3.66 (t, J = 7.4 Hz, 2H), 1.69–1.62 (m, 2H), 1.32–1.22 (m, 71H), 0.90–0.86 (t, J = 6.8 Hz, 6H). ^{13}C NMR (CDCl$_3$, 100 MHz, ppm): δ 182.0 (s), 157.64–157.62 (d, $J^5_{\text{F–C}}$ = 1.6 Hz), 157.14–154.68(d, $J^1_{\text{F–C}}$ = 247.0 Hz), 147.27–147.25 (d, $J^4_{\text{F–C}}$ = 2.5 Hz), 120.22–119.99 (d, $J^2_{\text{F–C}}$ = 23.4 Hz), 117.20–117.14 (d, $J^3_{\text{F–C}}$ = 6.1 Hz), 115.07 (s), 112.96–112.71 (d, $J^2_{\text{F–C}}$ = 25.2 Hz), 40.9, 37.0, 33.5, 31.9, 30.7, 30.1, 29.7, 29.6, 29.3, 26.9, 26.6, 26.5, 26.3, 24.3, 22.7, 14.1. Anal. calcd. for $C_{48}H_{83}BrFNO_2$: C, 71.61; H, 10.39; N, 1.74; Found: C, 71.29; H, 10.30; N, 1.49. ESI-HRMS calcd. for $[C_{48}H_{83}BrFNO_2 + H]^+$: 804.5660; Found: 804.5700.

General Procedure for the Synthesis of Fluorinated **BDOPV**:

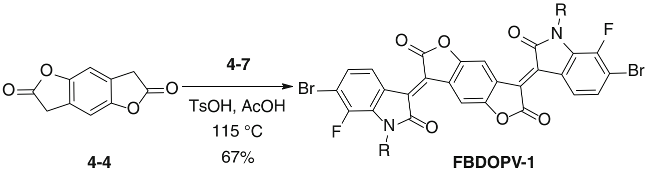

4-4 **FBDOPV-1**

FBDOPV-1: To a solution of **4-7** (508 mg, 0.631 mmol) in acetic acid (15 mL), **4-4** (50 mg, 0.263 mmol) and *p*-toluenesulfonic acid monohydrate (12.6 mg, 0.073 mmol) were add under nitrogen atmosphere. The mixture was stirred at 115 °C under nitrogen for 17 h. The mixture was then cooled to room temperature and filtered. The solid was washed with acetic acid and then methanol. The residue was purified by silica gel chromatography with eluent (PE:CH$_2$Cl$_2$ = 1:1) to give **FBDOPV-1** as a black solid (312 mg, 67 %). ^{1}H NMR (CDCl$_3$, 400 MHz, ppm): δ 9.09 (s, 2H), 8.79–8.77 (d, $J^3_{\text{H–H}}$ = 8.7 Hz, 2H), 7.26–7.21 (dd, $J^3_{\text{H–H}}$ = 8.7 Hz,

$J^4_{\text{F–H}}$ = 6.4 Hz, 2H), 3.94–3.90 (t, J = 7.1 Hz, 4H), 1.70–1.68 (m, 2H), 1.34–1.24 (m, 152H), 0.89–0.86 (t, J = 6.8 Hz, 12H). ^{13}C NMR (126 MHz, $C_2D_2Cl_4$, 100 °C, ppm) δ 166.41, 166.37, 151.9, 144.7, 142.8, 135.3, 135.3, 133.5, 133.4, 127.3, 127.03, 126.51, 126.48, 126.2, 122.7, 122.7, 116.6, 116.4, 111.0, 42.9, 42.8, 37.1, 33.7, 31.7, 30.7, 29.9, 29.43, 29.38, 29.0, 26.6, 26.0, 22.4, 13.8. Elemental Anal. Calcd. for $C_{106}H_{168}Br_2F_2N_2O_6$: C, 72.16; H, 9.60; N, 1.59; Found: C, 71.83; H, 9.59; N, 1.52. MALDI-TOF MS: calcd. for $C_{106}H_{168}Br_2F_2N_2O_6^+$: 1764.1; Found: 1764.4.

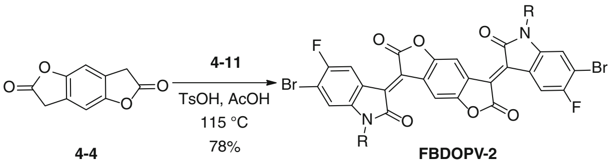

FBDOPV-2: The synthetic procedure is similar to that of **FBDOPV-1**. Yield: 78 %, black solid. ^{1}H NMR ($CDCl_3$, 400 MHz, ppm): δ 9.05 (s, 2H), 8.87–8.84 (d, $J^3_{\text{F–H}}$ = 10.3 Hz, 2H), 6.87–6.85 (d, $J^4_{\text{F–H}}$ = 5.6 Hz, 2H), 3.72–3.68 (t, J = 7.2 Hz, 4H), 1.69–1.65 (m, 4H), 1.46–1.12 (m, 152H), 0.89–0.86 (t, J = 6.8 Hz, 12H). ^{13}C NMR (126 MHz, $C_2D_2Cl_4$, 100 °C, ppm) δ 166.5, 166.4, 155.7, 153.8, 152.0, 142.8, 135.43, 135.40, 127.1, 126.8, 120.7, 120.6, 118.0, 117.8, 115.4, 115.2, 112.3, 111.2, 40.9, 37.2, 33.7, 31.7, 31.0, 29.9, 29.4, 29.4, 29.0, 26.6, 24.3, 22.4, 13.8. Elemental Anal. Calcd. for $C_{106}H_{168}Br_2F_2N_2O_6$: C, 72.16; H, 9.60; N, 1.59; Found: C, 71.79; H, 9.56; N, 1.54. MALDI-TOF MS: calcd. for $C_{106}H_{168}Br_2F_2N_2O_6^+$: 1764.1; found: 1764.4.

General Procedure for Microwave-Assisted Stille Polymerization:

BDPPV: To a microwave vessel, **BDOPV** (50 mg, 0.0289 mmol), (*E*)-1,2-bis (tributylstannyl)ethene (17.5 mg, 0.0289 mmol), $Pd_2(dba)_3$ (1 mg, 4 mol%.), P(*o*-tol)$_3$ (1.4 mg, 16 mol%), and 4 mL of chlorobenzene were added under nitrogen atmosphere. The vessel was then sealed with a snap cap under nitrogen atmosphere, and subjected to the following reaction conditions in a microwave reactor (120 °C, 5 min; 140 °C, 5 min; 160 °C, 5 min; 180 °C, 30 min). After completion, diethylphenylazothioformamide (5 mg) was added and then the mixture was stirred for 1 h to remove any residual catalyst before being precipitated into methanol (200 mL). The precipitate was filtered through a nylon filter and purified via Soxhlet extraction for 8 h with acetone, 12 h with hexane, and finally was collected with chloroform. The chloroform solution was then concentrated by evaporation and precipitated into methanol (200 mL) and filtered off to afford a dark solid (38 mg, yield 83 %). Elemental Anal. Calcd: for $(C_{108}H_{174}N_2O_6)_n$: C, 81.35; H, 10.87; N, 1.76; Found: C, 79.65; H, 10.42; N, 1.75.

FBDPPV-1: The synthetic procedure is similar to that of **BDPPV**, Yield: 96 %. Elemental Anal. Calcd: for $(C_{108}H_{170}F_2N_2O_6)_n$: C, 79.56; H, 10.51; N, 1.72; Found: C, 78.36; H, 10.42; N, 1.75.

FBDPPV-2: The synthetic procedure is similar to that of **BDPPV**, Yield: 83 %. Elemental Anal. Calcd: for $(C_{108}H_{170}F_2N_2O_6)_n$: C, 79.56; H, 10.51; N, 1.72; Found: C, 78.94; H, 10.40; N, 1.68.

BDOPV-2T: **BDOPV** (50 mg, 0.0289 mmol), 5,5′-bis(trimethylstannyl)-2,2′-bithiophene (14.2 mg, 0.0289 mmol), $Pd_2(dba)_3$ (0.5 mg, 2 mol%.), $P(o\text{-tol})_3$ (0.7 mg, 8 mol%), and 10 mL of toluene were added to a Schlenk tube. The tube was charged with nitrogen through a *freeze-pump-thaw* cycle for three times. The mixture was stirred for 24 h at 120 °C. *N*,*N*′-Diethylphenylazothioformamide (10 mg) was then added and then the mixture was stirred for 1 h to remove any residual catalyst before being precipitated into methanol (200 mL). The precipitate was filtered through a nylon filter and purified via Soxhlet extraction for 8 h with acetone, 12 h with hexane, and finally collected with chloroform. The chloroform solution was then concentrated by evaporation and precipitated into methanol (200 mL) and filtered off to afford a dark solid (47 mg, yield 94 %). Elemental Anal. calcd: for $(C_{114}H_{174}N_2O_6S_2)_n$: C, 79.02; H, 10.12; N, 1.62; found: C, 76.62; H, 10.02; N, 1.54.

References

1. Kraft A, Grimsdale AC, Holmes AB (1998) Electroluminescent conjugated polymers—seeing polymers in a new light. Angew Chem Int Ed 37:402–428
2. Burroughes JH, Bradley DDC, Brown AR, Marks RN, Mackay K, Friend RH, Burns PL, Holmes AB (1990) Light-emitting diodes based on conjugated polymers. Nature 347:539–541
3. Yu G, Gao J, Hummelen JC, Wudl F, Heeger AJ (1995) Polymer photovoltaic cells: enhanced efficiencies via a network of internal donor-acceptor heterojunctions. Science 270:1789–1791
4. Hide F, Díaz-García MA, Schwartz BJ, Andersson MR, Pei Q, Heeger AJ (1996) Semiconducting polymers: a new class of solid-state laser materials. Science 273:1833–1836
5. Tessler N, Denton GJ, Friend RH (1996) Lasing from conjugated-polymer microcavities. Nature 382:695–697
6. Welter S, Brunner K, Hofstraat JW, De Cola L (2003) Electroluminescent device with reversible switching between red and green emission. Nature 421:54–57
7. Akcelrud L (2003) Electroluminescent polymers. Prog Polym Sci 28:875–962
8. Chen J, Cao Y (2009) Development of novel conjugated donor polymers for high-efficiency bulk-heterojunction photovoltaic devices. Acc Chem Res 42:1709–1718
9. Wang L, Liu Y, Jiang X, Qin D, Cao Y (2007) Enhancement of photovoltaic characteristics using a suitable solvent in hybrid polymer/multiarmed Cds nanorods solar cells. J Phys Chem C 111:9538–9542
10. Wang C, Dong H, Hu W, Liu Y, Zhu D (2011) Semiconducting π-conjugated systems in field-effect transistors: a material odyssey of organic electronics. Chem Rev 112:2208–2267
11. van Breemen AJJM, Herwig PT, Chlon CHT, Sweelssen J, Schoo HFM, Benito EM, de Leeuw DM, Tanase C, Wildeman J, Blom PWM (2005) High-performance solution-processable poly(*p*-phenylene vinylene)s for air-stable organic field-effect transistors. Adv Funct Mater 15:872–876
12. Meijer EJ, de Leeuw DM, Setayesh S, van Veenendaal E, Huisman BH, Blom PWM, Hummelen JC, Scherf U, Klapwijk TM (2003) Solution-processed ambipolar organic field-effect transistors and inverters. Nat Mater 2:678–682
13. Blom PWM, de Jong MJM, van Munster MG (1997) Electric-field and temperature dependence of the hole mobility in poly(*p*-phenylene vinylene). Phys Rev B 55:R656–R659

14. Chua L-L, Zaumseil J, Chang J-F, Ou ECW, Ho PKH, Sirringhaus H, Friend RH (2005) General observation of n-type field-effect behaviour in organic semiconductors. Nature 434:194–199
15. Nielsen CB, Turbiez M, McCulloch I (2013) Recent advances in the development of semiconducting DPP-containing polymers for transistor applications. Adv Mater 25:1859–1880
16. Li J, Zhao Y, Tan HS, Guo Y, Di C-A, Yu G, Liu Y, Lin M, Lim SH, Zhou Y, Su H, Ong BS (2012) A stable solution-processed polymer semiconductor with record high-mobility for printed transistors. Sci Rep 2:754
17. Chen H, Guo Y, Yu G, Zhao Y, Zhang J, Gao D, Liu H, Liu Y (2012) Highly π-extended copolymers with diketopyrrolopyrrole moieties for high-performance field-effect transistors. Adv Mater 24:4618–4622
18. Lei T, Cao Y, Fan Y, Liu C-J, Yuan S-C, Pei J (2011) High-performance air-stable organic field-effect transistors: Isoindigo-based conjugated polymers. J Am Chem Soc 133:6099–6101
19. Mei J, Kim DH, Ayzner AL, Toney MF, Bao Z (2011) Siloxane-terminated solubilizing side chains: bringing conjugated polymer backbones closer and boosting hole mobilities in thin-film transistors. J Am Chem Soc 133:20130–20133
20. Zhan X, Facchetti A, Barlow S, Marks TJ, Ratner MA, Wasielewski MR, Marder SR (2011) Rylene and related diimides for organic electronics. Adv Mater 23:268–284
21. Fan J, Yuen JD, Cui W, Seifter J, Mohebbi AR, Wang M, Zhou H, Heeger A, Wudl F (2012) High-hole-mobility field-effect transistors based on co-benzobisthiadiazole-quaterthiophene. Adv Mater 24:6164–6168
22. Yuen JD, Fan J, Seifter J, Lim B, Hufschmid R, Heeger AJ, Wudl F (2011) High performance weak donor–acceptor polymers in thin film transistors: effect of the acceptor on electronic properties, ambipolar conductivity, mobility, and thermal stability. J Am Chem Soc 133:20799–20807
23. Heeger AJ (2010) Semiconducting polymers: the third generation. Chem Soc Rev 39:2354–2371
24. Yuen JD, Wudl F (2013) Strong acceptors in donor-acceptor polymers for high performance thin film transistors. Energy Environ Sci 6:392–406
25. Coropceanu V, Cornil J, da Silva Filho DA, Olivier Y, Silbey R, Brédas J-L (2007) Charge transport in organic semiconductors. Chem Rev 107:926–952
26. Prins P, Grozema FC, Schins JM, Patil S, Scherf U, Siebbeles LDA (2006) High intrachain hole mobility on molecular wires of ladder-type poly(*p*-phenylenes). Phys Rev Lett 96:146601
27. Lei T, Cao Y, Zhou X, Peng Y, Bian J, Pei J (2012) Systematic investigation of isoindigo-based polymeric field-effect transistors: design strategy and impact of polymer symmetry and backbone curvature. Chem Mater 24:1762–1770
28. Osaka I, Abe T, Shinamura S, Takimiya K (2011) Impact of isomeric structures on transistor performances in naphthodithiophene semiconducting polymers. J Am Chem Soc 133:6852–6860
29. Wakioka M, Ikegami M, Ozawa F (2010) Stereocontrolled synthesis and photoisomerization behavior of all-*cis* and all-*trans* poly(*m*-phenylenevinylene)s. Macromolecules 43:6980–6985
30. Moslin RM, Espino CG, Swager TM (2008) Synthesis of conjugated polymers containing *cis*-phenylenevinylenes by titanium-mediated reductions. Macromolecules 42:452–454
31. Chen SH, Su AC, Huang YF, Su CH, Peng GY, Chen SA (2002) Supramolecular aggregation in bulk poly(2-methoxy-5-(2′-ethylhexyloxy)-1,4- phenylenevinylene). Macromolecules 35:4229–4232
32. Lei T, Dou J-H, Ma Z-J, Yao C-H, Liu C-J, Wang J-Y, Pei J (2012) Ambipolar polymer field-effect transistors based on fluorinated isoindigo: high performance and improved ambient stability. J Am Chem Soc 134:20025–20028
33. Lei T, Dou J-H, Ma Z-J, Liu C-J, Wang J-Y, Pei J (2013) Chlorination as a useful method to modulate conjugated polymers: balanced and ambient-stable ambipolar high-performance field-effect transistors and inverters based on chlorinated isoindigo polymers. Chem Sci 4:2447–2452
34. Lei T, Dou J-H, Pei J (2012) Influence of alkyl chain branching positions on the hole mobilities of polymer thin-film transistors. Adv Mater 24:6457–6461
35. Yan H, Chen Z, Zheng Y, Newman C, Quinn JR, Dotz F, Kastler M, Facchetti A (2009) A high-mobility electron-transporting polymer for printed transistors. Nature 457:679–686
36. Wood JH, Cox L (1946) 2,5-dihydroxy-p-benzenediacetic acid. Org Synth 26:24

37. Rowland RS, Taylor R (1996) Intermolecular nonbonded contact distances in organic crystal structures: comparison with distances expected from van der waals radii. J Phys Chem 100:7384–7391
38. Musah RA, Jensen GM, Rosenfeld RJ, McRee DE, Goodin DB, Bunte SW (1997) Variation in strength of an unconventional C–H to O hydrogen bond in an engineered protein cavity. J Am Chem Soc 119:9083–9084
39. Kim J, Swager TM (2001) Control of conformational and interpolymer effects in conjugated polymers. Nature 411:1030–1034
40. Chen SH, Su AC, Han SR, Chen SA, Lee YZ (2003) Molecular aggregation and luminescence properties of bulk poly(2,5-di-n-octyloxy-1,4-phenylenevinylene). Macromolecules 37:181–186
41. Zhou N, Guo X, Ortiz RP, Li S, Zhang S, Chang RPH, Facchetti A, Marks TJ (2012) Bithiophene imide and benzodithiophene copolymers for efficient inverted polymer solar cells. Adv Mater 24:2242–2248
42. Chen Z, Zheng Y, Yan H, Facchetti A (2009) Naphthalenedicarboximide- vs perylenedicarboximide-based copolymers. Synthesis and semiconducting properties in bottom-gate n-channel organic transistors. J Am Chem Soc 131:8–9
43. Di C-A, Liu Y, Yu G, Zhu D (2009) Interface engineering: an effective approach toward high-performance organic field-effect transistors. Acc Chem Res 42:1573–1583
44. Chen Z, Lee MJ, Shahid Ashraf R, Gu Y, Albert-Seifried S, Meedom Nielsen M, Schroeder B, Anthopoulos TD, Heeney M, McCulloch I, Sirringhaus H (2012) High-performance ambipolar diketopyrrolopyrrole-thieno[3,2-b]thiophene copolymer field-effect transistors with balanced hole and electron mobilities. Adv Mater 24:647–652
45. Chen Z, Lemke H, Albert-Seifried S, Caironi M, Nielsen MM, Heeney M, Zhang W, McCulloch I, Sirringhaus H (2010) High mobility ambipolar charge transport in polyselenophene conjugated polymers. Adv Mater 22:2371–2375
46. Collins PG, Bradley K, Ishigami M, Zettl A (2000) Extreme oxygen sensitivity of electronic properties of carbon nanotubes. Science 287:1801–1804
47. Ryu S, Liu L, Berciaud S, Yu Y-J, Liu H, Kim P, Flynn GW, Brus LE (2010) Atmospheric oxygen binding and hole doping in deformed graphene on a SiO_2 substrate. Nano Lett 10:4944–4951
48. Okamoto H, Kawasaki N, Kaji Y, Kubozono Y, Fujiwara A, Yamaji M (2008) Air-assisted high-performance field-effect transistor with thin films of picene. J Am Chem Soc 130:10470–10471
49. Wang Y, Motta SD, Negri F, Friedlein R (2011) Effect of oxygen on the electronic structure of highly crystalline picene films. J Am Chem Soc 133:10054–10057
50. Di Pietro R, Fazzi D, Kehoe TB, Sirringhaus H (2012) Spectroscopic investigation of oxygen- and water-induced electron trapping and charge transport instabilities in n-type polymer semiconductors. J Am Chem Soc 134:14877–14889
51. Li H, Kim FS, Ren G, Jenekhe SA (2013) High-mobility n-type conjugated polymers based on electron-deficient tetraazabenzodifluoranthene diimide for organic electronics. J Am Chem Soc 135:14920–14923
52. Takeda Y, Andrew TL, Lobez JM, Mork AJ, Swager TM (2012) An air-stable low-bandgap n-type organic polymer semiconductor exhibiting selective solubility in perfluorinated solvents. Angew Chem Int Ed 51:9042–9046
53. Lee J-K, Gwinner MC, Berger R, Newby C, Zentel R, Friend RH, Sirringhaus H, Ober CK (2011) High-performance electron-transporting polymers derived from a heteroaryl bis (trifluoroborate). J Am Chem Soc 133:9949–9951
54. Babel A, Jenekhe SA (2003) High electron mobility in ladder polymer field-effect transistors. J Am Chem Soc 125:13656–13657
55. Zaumseil J, Sirringhaus H (2007) Electron and ambipolar transport in organic field-effect transistors. Chem Rev 107:1296–1323
56. Wang C, Dong H, Hu W, Liu Y, Zhu D (2012) Semiconducting π-conjugated systems in field-effect transistors: a material odyssey of organic electronics. Chem Rev 112:2208–2267

57. Tang ML, Bao Z (2011) Halogenated materials as organic semiconductors. Chem Mater 23:446–455
58. Chen H-Y, Hou J, Zhang S, Liang Y, Yang G, Yang Y, Yu L, Wu Y, Li G (2009) Polymer solar cells with enhanced open-circuit voltage and efficiency. Nat Photon 3:649–653
59. Bronstein H, Frost JM, Hadipour A, Kim Y, Nielsen CB, Ashraf RS, Rand BP, Watkins S, McCulloch I (2013) Effect of fluorination on the properties of a donor–acceptor copolymer for use in photovoltaic cells and transistors. Chem Mater 25:277–285
60. Park JH, Jung EH, Jung JW, Jo WH (2013) A fluorinated phenylene unit as a building block for high-performance n-type semiconducting polymer. Adv Mater 25:2583–2588
61. Noriega R, Rivnay J, Vandewal K, Koch FPV, Stingelin N, Smith P, Toney MF, Salleo A (2013) A general relationship between disorder, aggregation and charge transport in conjugated polymers. Nat Mater 12:1038–1044
62. Yan Z, Sun B, Li Y (2013) Novel stable (3E,7E)-3,7-bis(2-oxoindolin-3-ylidene)benzo[1,2-*b*:4,5-*b*′]difuran-2,6(3H,7H)-dione based donor-acceptor polymer semiconductors for n-type organic thin film transistors. Chem Commun 49:3790–3792
63. Lei T, Dou JH, Cao XY, Wang JY, Pei J (2013) A BDOPV-based donor-acceptor polymer for high-performance n-type and oxygen-doped ambipolar field-effect transistors. Adv Mater 25:6589–6593
64. Di Pietro R, Fazzi D, Kehoe TB, Sirringhaus H (2012) Spectroscopic investigation of oxygen- and water-induced electron trapping and charge transport instabilities in n-type polymer semiconductors. J Am Chem Soc 134:14877–14889
65. Lee J, Han AR, Yu H, Shin TJ, Yang C, Oh JH (2013) Boosting the ambipolar performance of solution-processable polymer semiconductors via hybrid side-chain engineering. J Am Chem Soc 135:9540–9547
66. Zhang F, Hu Y, Schuettfort T, Di C-A, Gao X, McNeill CR, Thomsen L, Mannsfeld SCB, Yuan W, Sirringhaus H, Zhu D (2013) Critical role of alkyl chain branching of organic semiconductors in enabling solution-processed n-channel organic thin-film transistors with mobility of up to 3.50 cm^2 V^{-1} s^{-1}. J Am Chem Soc 135:2338–2349
67. Wen Y, Liu Y, Guo Y, Yu G, Hu W (2011) Experimental techniques for the fabrication and characterization of organic thin films for field-effect transistors. Chem Rev 111:3358–3406
68. Steyrleuthner R, Schubert M, Howard I, Klaumünzer B, Schilling K, Chen Z, Saalfrank P, Laquai F, Facchetti A, Neher D (2012) Aggregation in a high-mobility n-type low-bandgap copolymer with implications on semicrystalline morphology. J Am Chem Soc 134:18303–18317
69. Renak ML, Bartholomew GP, Wang S, Ricatto PJ, Lachicotte RJ, Bazan GC (1999) Fluorinated distyrylbenzene chromophores: effect of fluorine regiochemistry on molecular properties and solid-state organization. J Am Chem Soc 121:7787–7799
70. Niedzialek D, Lemaur V, Dudenko D, Shu J, Hansen MR, Andreasen JW, Pisula W, Müllen K, Cornil J, Beljonne D (2013) Probing the relation between charge transport and supramolecular organization down to ångström resolution in a benzothiadiazole-cyclopentadithiophene copolymer. Adv Mater 25:1939–1947
71. Rieger R, Beckmann D, Mavrinskiy A, Kastler M, Müllen K (2010) Backbone curvature in polythiophenes. Chem Mater 22:5314–5318
72. Lei T, Wang J-Y, Pei J (2014) Roles of flexible chains in organic semiconducting materials. Chem Mater 26:594–603
73. Mei J, Bao Z (2014) Side chain engineering in solution-processable conjugated polymers. Chem Mater 26:604–615

Chapter 5
Summary and Outlook

Flexible and stretchable electronics may become future mainstream technologies. The performance of polymer field-effect transistors (FETs) is surpassing that of amorphous silicon and vacuum-deposited organic FETs, comparable to organic single-crystal and polycrystalline silicon FETs. Among them, conjugated polymers provide many unique advantages, such as low-cost, solution-processable, mechanically flexible, and compatible with heat-sensitive substrates. Conjugated polymer is becoming one of the most active research areas in chemistry, material science, and electronic engineering. The research works in this thesis focus on the design, synthesis, and structure-property relationship study of isoindigo-based polymer FETs.

In Chap. 2, we initialized our investigation on polymer FETs through careful analysis the influence of the alkyl chain on the interchain interaction of conjugated polymers. For the first time, isoindigo-based conjugated polymers were used as the active layer in polymer FETs, exhibiting high performance and high stability for 6 months under ambient conditions. In order to investigate the structure-property relationship in isoindigo-based polymers, we have developed ten isoindigo-based polymers and analyzed their device performances and polymer packings in thin film. Our study reveals that the symmetry and backbone curvature of conjugated polymers affected the polymer packings and interchain interactions, thus leading to significant influences on the hole mobilities in these polymers. After introducing methyl groups on donor units, the hole mobility of the polymer obviously decreased, further demonstrating our hypothesis that the improper introduction of alkyl chains could reduce interchain interactions in conjugated polymers. To further enhance the device performance of isoindigo polymers, we investigated how moving branching point away from the polymer backbone influenced the carrier mobilities. The sequential changing of the conventional branched alkyl chains resulted in a remarkably high hole mobility of 3.62 $cm^2\ V^{-1}\ s^{-1}$ in the isoindigo-based polymer. Therefore, we demonstrated that a subtle change of conventional alkyl chains can lead to significant influence on device performance.

T. Lei, *Design, Synthesis, and Structure-Property Relationship Study of Polymer Field-Effect Transistors*, Springer Theses, DOI 10.1007/978-3-662-45667-5_5

In Chap. 3, in order to improve the electron mobility and device stability in isoindigo-based polymers, we have introduced fluorine atoms on the isoindigo core and lowered the LUMO level of an isoindigo polymer. After introducing fluorine atoms, ambipolar transport behaviors in isoindigo-based conjugated polymers were observed for the first time. Fluorination on the isoindigo unit significantly increased the electron mobility from 10^{-2} to 0.43 $cm^2\ V^{-1}\ s^{-1}$ while maintaining high hole mobility of up to 1.85 $cm^2\ V^{-1}\ s^{-1}$ for devices fabricated under ambient conditions. Furthermore, we chlorinated isoindigo-based polymers through an efficient chlorination reaction. Balanced charge carrier transport with hole mobilities of up to 0.81 $cm^2\ V^{-1}\ s^{-1}$ and electron mobilities of up to 0.66 $cm^2\ V^{-1}\ s^{-1}$ were obtained for devices fabricated under ambient conditions. This work represents the first chlorination on semiconducting polymers, and the chlorinated isoindigo polymers are the first ambipolar polymers that can transport carriers both in balance and in ambient.

In Chap. 4, encouraged by the research in isoindigo-based polymers, we have developed a new electron-deficient building block **BDOPV** for high electron mobility conjugated polymers. We have analyzed the factors that limited the carrier transport in poly(*p*-phenylene vinylene) and its derivatives (**PPV**s) and designed a novel **PPV**-based polymer **BDPPV** by using **BDOPV**. This polymer displayed high electron mobilities of up to 1.1 $cm^2\ V^{-1}\ s^{-1}$ under ambient conditions. The mobility is 4 orders of magnitude higher than other PPVs, because **BDPPV** overcame common defects in **PPV**s, such as conformational disorder, weak interchain interaction, and high LUMO level. By using the **BDOPV** unit as the acceptor, donor–acceptor polymer **BDOPV-2T**, a typical third-generation polymer have been developed. **BDOPV-2T** exhibited *n*-type transport behavior with high electron mobilities of up to 1.74 $cm^2\ V^{-1}\ s^{-1}$ under ambient conditions. Upon oxygen exposure, this polymer displayed interesting ambipolar transporting behavior and maintains high electron mobility of 1.45 $cm^2\ V^{-1}\ s^{-1}$, along with significantly increased hole mobility of 0.47 $cm^2\ V^{-1}\ s^{-1}$. Based on these results, the oxygen-doping effect and possible mechanism in **BDOPV-2T** was also investigated. The “conformation locking” strategy was used to further improve the device performance of **BDPPV**. To “lock” the rest one of the double bonds in the **BDPPV** polymer, we have introduced fluorine atoms to form intramolecular hydrogen bonds. We synthesized two new building blocks, **FBDOPV-1** and **FBDOPV-2**, with fluorine atoms at different positions of **BDOPV**. These two building blocks showed very deep LUMO levels of −4.38 eV, significantly lower than the acceptors reported in literature. The two building blocks are used to prepare two new PPV derivatives, **FBDPPV-1** and **FBDPPV-2**. Fluorine atoms can lower the LUMO level and “lock” the conformation of polymer backbones through intramolecular hydrogen bonds. **FBDPPV-1** exhibited an electron mobilities of up to 1.70 $cm^2\ V^{-1}\ s^{-1}$ under ambient conditions, which is among the highest in *n*-type conjugated polymers. The two fluorinated polymers had considerably different device performance despite their similar physical and electrochemical properties, including molecular weight, thin-film packing, and morphology. This work demonstrates that fluorination can do more than lower the energy level of the polymers, it can also influence backbone conformations, interchain interactions, molecular packings, and thereby device performance.

From the consideration of the impediment of alkyl chains to the variation of the side-chain branching positions, from the design of high-stability *p*-type FETs to the realization of ambient-stable ambipolar and *n*-type FETs, from the engineering of donor symmetry to the extension of the isoindigo core, and from the introduction of shape-persistent backbones to the locking of polymer conformations, this book describes my PhD works on developing isoindigo-based conjugated polymers and investigating the structure-property relationship of polymer FETs. These works demonstrate that a synergy of the molecular engineering strategies toward isoindigo core, donor units and side chains not only improves the device performance and broadens the application of isoindigo polymers, but also enables a better fundamental understanding of the structure-property relationship in conjugated polymers. Many results demonstrate that these developments and design strategies are also significant for other polymer systems and even small molecules. However, to advance the practical application of polymer FETs, challenges persist, especially in further enhancing both hole and electron mobilities, better controlling the molecular packing, and substantially improving the device reproducibility and stability, which call for the integrated consideration of both molecular design and process engineering and the collective efforts of scientists in multiple disciplines.